

EUROPEAN ORGANISATION FOR NUCLEAR RESEARCH (CERN)



Submitted to: Phys. Rev. D.

CERN-EP-2017-226
September 1, 2018

Measurements of $t\bar{t}$ differential cross-sections of highly boosted top quarks decaying to all-hadronic final states in pp collisions at $\sqrt{s} = 13$ TeV using the ATLAS detector

The ATLAS Collaboration

Measurements are made of differential cross-sections of highly boosted pair-produced top quarks as a function of top-quark and $t\bar{t}$ system kinematic observables using proton–proton collisions at a center-of-mass energy of $\sqrt{s} = 13$ TeV. The data set corresponds to an integrated luminosity of 36.1 fb^{-1} , recorded in 2015 and 2016 with the ATLAS detector at the CERN Large Hadron Collider. Events with two large-radius jets in the final state, one with transverse momentum $p_T > 500 \text{ GeV}$ and a second with $p_T > 350 \text{ GeV}$, are used for the measurement. The top-quark candidates are separated from the multijet background using jet substructure information and association with a b -tagged jet. The measured spectra are corrected for detector effects to a particle-level fiducial phase space and a parton-level limited phase space, and are compared to several Monte Carlo simulations by means of calculated χ^2 values. The cross-section for $t\bar{t}$ production in the fiducial phase-space region is $292 \pm 7 \text{ (stat)} \pm 76 \text{ (syst) fb}$, to be compared to the theoretical prediction of $384 \pm 36 \text{ fb}$.

1 Introduction

The large top-quark pair-production cross-section at the Large Hadron Collider (LHC) allows detailed studies of the characteristics of the production of top–antitop ($t\bar{t}$) quark pairs, providing an opportunity to further test the Standard Model (SM). Focusing on highly boosted final states probes the QCD $t\bar{t}$ production processes in the TeV scale range, a kinematic region where theoretical calculations based on the SM still present large uncertainties [1–3]. High-precision measurements, especially in kinematic regions that have not been explored extensively, are necessary to better constrain the models currently in use. Furthermore, effects beyond the SM can appear as modifications of $t\bar{t}$ differential distributions with respect to the SM predictions [4–6] that may not be detected with an inclusive cross-section measurement.

In the SM, the top quark decays almost exclusively to a W boson and a b -quark. The signature of a $t\bar{t}$ final state is therefore determined by the W boson decay modes. The ATLAS [7–14] and CMS [15–19] Collaborations have published measurements of the $t\bar{t}$ differential cross-sections at center-of-mass energies of $\sqrt{s} = 7$ TeV, $\sqrt{s} = 8$ TeV and $\sqrt{s} = 13$ TeV in pp collisions using final states containing leptons. The analysis presented here makes use of the all-hadronic $t\bar{t}$ decay mode, where only top-quark candidates with high transverse momentum (p_T) are selected. This highly boosted topology is easier to reconstruct than other final-state configurations as the top-quark decay products are collimated into a large-radius jet by the Lorentz boost of the top quarks. This analysis is performed on events with the leading top-quark jet having $p_T^{t,1} > 500$ GeV and the second-leading top-quark jet having $p_T^{t,2} > 350$ GeV. These jets are reconstructed from calorimeter energy deposits and tagged as top-quark candidates to separate the $t\bar{t}$ final state from background sources. The event selection and background estimation follows the approach used in Ref. [20], but with updated tagging methods and data-driven multijet background estimates.

These measurements are based on data collected by the ATLAS detector in 2015 and 2016 from pp collisions at $\sqrt{s} = 13$ TeV, corresponding to an integrated luminosity of 36.1 fb^{-1} . Measurements are made of the $t\bar{t}$ differential cross-sections by unfolding the detector-level distributions to a particle-level fiducial phase-space region. The goal of unfolding to a particle-level fiducial phase space and of using variables directly related to detector observables is to allow precision tests of QCD by avoiding model-dependent extrapolation of the measurements to a phase-space region outside the detector acceptance. Measurements of parton-level differential cross-sections are also presented, where the detector-level distributions are unfolded to the top quark at the parton-level in a limited phase-space region. These allow comparisons to the higher-order calculations that are currently restricted to stable top quarks [1–3].

These differential cross-sections are similar to those studied in dijet measurements at large jet transverse momentum [21, 22] and are sensitive to effects of initial- and final-state radiation (ISR and FSR), to different parton distribution functions (PDF) and to different schemes for matching matrix-element calculations to parton shower models.

Measurements are made of the differential cross-sections for the leading and second-leading top quarks as a function of $p_T^{t,1}$ and $p_T^{t,2}$, as well as the rapidities of the top quarks. The rapidities of the leading and second-leading top quarks in the laboratory frame are denoted by $y^{t,1}$ and $y^{t,2}$, respectively, while their rapidities in the $t\bar{t}$ center-of-mass frame are $y^* = 1/2(y^{t,1} - y^{t,2})$ and $-y^*$. These allow the construction of the variable $\chi^{t\bar{t}} = \exp 2|y^*|$, which is of particular interest as many processes not included in the Standard Model are predicted to peak at low values of $\chi^{t\bar{t}}$ [23]. The longitudinal motion of the $t\bar{t}$ system in the laboratory frame is described by the rapidity boost $y_B^{t\bar{t}} = 1/2(y^{t,1} + y^{t,2})$ and is sensitive to PDFs. Measurements are also made of the differential cross-sections as a function of the invariant mass, p_T and rapidity of the $t\bar{t}$ system; the absolute value of the azimuthal angle between the two top quarks, $\Delta\phi^{t\bar{t}}$; the

absolute value of the out-of-plane momentum, $|p_{\text{out}}^{t\bar{t}}|$ (i.e., the projection of the three-momentum of one of the top-quark jets onto the direction perpendicular to a plane defined by the other top quark and the beam axis (z) in the laboratory frame [22]); the cosine of the production angle in the Collins–Soper¹ reference frame, $\cos\theta^*$; and the scalar sum of the transverse momenta of the two top quarks, $H_T^{t\bar{t}}$ [24, 25]. Some of the variables (e.g. $\Delta\phi^{t\bar{t}}$ and $|p_{\text{out}}^{t\bar{t}}|$) are more sensitive to additional radiation in the main scattering process, and thus are more sensitive to effects beyond leading order (LO) in the matrix elements. All of these variables are sensitive to the kinematics of the $t\bar{t}$ production process.

The paper is organized as follows. Section 2 briefly describes the ATLAS detector, while Sec. 3 describes the data and simulation samples used in the measurements. The reconstruction of physics objects and the event selection is explained in Sec. 4 and the background estimates are discussed in Sec. 5. The procedure for unfolding to particle level and parton level are described in Sec. 6. The systematic uncertainties affecting the measurements are summarized in Sec. 7. The results of the measurements are presented in Sec. 8 and comparisons of these results with theoretical predictions are made in Sec. 9. A summary is presented in Sec. 10.

2 ATLAS detector

The ATLAS experiment [26] at the LHC uses a multi-purpose detector with a forward-backward symmetric cylindrical geometry and near 4π coverage in solid angle.² It consists of an inner tracking detector surrounded by a superconducting solenoid magnet creating a 2 T axial magnetic field, electromagnetic and hadronic calorimeters, and a muon spectrometer.

The inner tracking detector covers the pseudorapidity range $|\eta| < 2.5$. Consisting of silicon pixel, silicon microstrip and transition radiation tracking detectors, the inner tracking detector allows highly efficient reconstruction of the trajectories of the charged particles produced in the pp interactions. An additional silicon pixel layer, the insertable B-layer, was added between 3 and 4 cm from the beam line to improve b -hadron tagging [27]. Lead/liquid-argon (LAr) sampling calorimeters provide electromagnetic (EM) energy measurements with high granularity and shower-depth segmentation. A hadronic (steel/scintillator-tile) calorimeter covers the central pseudorapidity range ($|\eta| < 1.7$). The endcap and forward regions are instrumented with LAr calorimeters for EM and hadronic energy measurements up to $|\eta| = 4.9$. The muon spectrometer is located outside of the calorimeter systems and is based on three large air-core toroid superconducting magnets with eight coils each. It includes a system of precision tracking chambers and detectors with sufficient timing resolution to enable triggering of events.

A two-level trigger system is used to select events [28]. The first-level hardware-based trigger uses a subset of the detector information to reduce the rate of accepted events to a design maximum of 100 kHz. This is followed by a software-based trigger with a maximum average accepted event rate of 1 kHz.

¹ The Collins–Soper frame is the rest frame of the $t\bar{t}$ pair, wherein the two top quarks have equal and opposite momenta; thus, each makes the same angle θ^* with the beam direction.

² ATLAS uses a right-handed coordinate system with its origin at the nominal interaction point (IP) in the center of the detector and the z -axis along the beam pipe. The x -axis points from the IP to the center of the LHC ring and the y -axis points upward. Cylindrical coordinates (r, ϕ) are used in the transverse plane, ϕ being the azimuthal angle around the z -axis. The pseudorapidity is defined in terms of the polar angle θ as $\eta = -\ln \tan(\theta/2)$.

3 Data sets and Monte Carlo event generation

The data used for this analysis were recorded with the ATLAS detector at a center-of-mass energy of 13 TeV in 2015 and 2016 and correspond to an integrated luminosity of 36.1 fb^{-1} . Only the data-taking periods in which all the subdetectors were operational are considered.

The events for this analysis were collected using an inclusive anti- k_t jet trigger with radius parameter $R = 1.0$ and nominal p_T thresholds of 360 GeV and 420 GeV for the 2015 and 2016 data-taking periods, respectively. These triggers were fully efficient for jets with $p_T > 480 \text{ GeV}$ [28].

The signal and several background processes are modeled using Monte Carlo (MC) event generators. Multiple overlaid proton–proton collisions (pileup) are simulated with the soft QCD processes of PYTHIA 8.186 [29] using a set of tuned parameters called the A2 tune [30] and the MSTW2008LO [31] PDF set. The detector response is simulated using the GEANT4 framework [32, 33]. The data and MC events are reconstructed with the same software algorithms.

Several next-to-leading-order (NLO) MC calculations of the $t\bar{t}$ process are used in the analysis, and to compare with the measured differential cross-sections. The POWHEG-Box v2 [34], MADGRAPH5_aMC@NLO [35] and SHERPA [36] Monte Carlo event generators encode different approaches to the matrix element calculation and different matching schemes between the NLO QCD matrix-element calculation and the parton shower algorithm. A more detailed explanation of the differences among these event generators can be found in Ref. [37].

The nominal sample uses the POWHEG-Box v2 [34] event generator employing the NNPDF30 PDF set interfaced with the PYTHIA8 parton shower and hadronization model (hereafter also referred to as PWG+PY8). The POWHEG h_{damp} parameter, which controls the p_T of the first additional emission beyond the Born configuration, is set to 1.5 times the top-quark mass [38]. The main effect of this is to regulate the high- p_T emission against which the $t\bar{t}$ system recoils. To enhance the production of top quarks in the high- p_T region, the POWHEG parameter `bornsuppfact` is set to $p_{T,\text{supp}} = 500 \text{ GeV}$ [34, 39]. The PYTHIA8 parameters are chosen for good agreement with ATLAS Run-1 data by employing the A14 tune [40] with the NNPDF23LO PDF set [41].

Two alternative POWHEG+PYTHIA8 samples with systematic variations of the POWHEG and PYTHIA8 parameters probe the effects of the experimental tuning of the MC event generators. One sample, which primarily increases the amount of initial- and final-state radiation, uses $h_{\text{damp}} = 3m_{\text{top}}$, the factorization and renormalization scale reduced by a factor of 2 and the A14 Var3c Up tune variation [40]. The second sample, which decreases the amount of initial- and final-state radiation, uses $h_{\text{damp}} = 1.5m_{\text{top}}$, the factorization and renormalization scale increased by a factor of 2 and the A14 Var3c Down tune variation [40].

An alternative matrix element calculation and matching with the parton shower is realized with the MADGRAPH5_aMC@NLO event generator (hereafter referred to as MG5_aMC@NLO) [35] interfaced with the PYTHIA8 parton shower and hadronization model using the same tune as the nominal sample. This sample requires the leading top quark in each event to have $p_T > 300 \text{ GeV}$ to ensure that the high- p_T region is adequately populated. The effects of using alternative parton shower and hadronization models is probed by interfacing the nominal POWHEG setup with the Herwig7 parton shower and hadronization model [42] employing the H7UE tune (hereafter also referred to as PWG+H7). Another calculation using the SHERPA v2.2.1 event generator [36] with the default SHERPA parton shower and hadronization model merges the NLO $t\bar{t}$ matrix element with matrix element calculations including up to four additional jets using the MEPS@NLO setup [43].

The Wt single-top-quark processes are modeled using the POWHEG-Box v2 event generator with the CT10 PDF set [44]. For the single-top-quark process, the top quarks are decayed using MADSPIN [45]. The parton shower, fragmentation and the underlying event for these processes are simulated using the PYTHIA 6.428 event generator [46] with the CTEQ6L1 PDF sets and the corresponding Perugia 2012 tune (P2012) [47]. Electroweak t - and s -channel single-top-quark events are not explicitly modeled because of the small cross-section of these processes and the low jet multiplicity in the final state. Their contribution is accounted for in the data-driven background estimate.

The associated production of $t\bar{t}$ pairs with W , Z and Higgs bosons is modeled using the MG5_aMC@NLO event generator [35] coupled to the PYTHIA8 parton shower and hadronization model using the same PDF sets and tunes as the $t\bar{t}$ sample.

The top-quark mass is set to $m_{\text{top}} = 172.5$ GeV for all samples and the renormalization and factorization scales are set to $\mu_{\text{R/F}} = \sqrt{m_{\text{top}}^2 + \frac{1}{2}(p_{\text{T}}(t)^2 + p_{\text{T}}(\bar{t})^2)}$ for all $t\bar{t}$ samples except where explicitly noted above. The EvtGen v1.2.0 program [48] is used for modeling the properties of the bottom and charm hadron decays for all event generator setups other than for the SHERPA sample.

The $t\bar{t}$ samples are normalized using the next-to-next-to-leading-order cross-section plus next-to-next-to-leading-logarithm corrections (NNLO+NNLL) $\sigma_{t\bar{t}} = 832_{-51}^{+46}$ pb [49], where the uncertainties reflect the effect of scale and PDF variations. The single-top-quark cross-section is normalized to the NLO predictions [50]. The associated production of $t\bar{t}$ pairs with W , Z and Higgs bosons are normalized to 0.603 pb, 0.586 pb and 0.231 pb, respectively, as predicted by the MG5_aMC@NLO event generator.

4 Event reconstruction and selection

This analysis makes use of jets, electrons and muons as well as event-based measures formed from their combinations. The event reconstruction and selection are summarized in the following subsections.

4.1 Event reconstruction

Electron candidates are identified from high-quality inner detector tracks matched to calorimeter deposits consistent with an electromagnetic shower. The calorimeter deposits have to form a cluster with $E_{\text{T}} > 25$ GeV, $|\eta| < 2.47$ and be outside the transition region $1.37 \leq |\eta| \leq 1.52$ between the barrel and endcap calorimeters. A likelihood-based requirement is used to suppress misidentified jets (hereafter referred to as fakes), and calorimeter- and track-based isolation requirements are imposed [51, 52]. Overall, these criteria result in electron identification efficiencies of $\sim 90\%$ for electrons with $p_{\text{T}} > 25$ GeV and 96% for electrons with $p_{\text{T}} > 60$ GeV.

Muon candidates are reconstructed using high-quality inner detector tracks combined with tracks reconstructed in the muon spectrometer. Only muon candidates with $p_{\text{T}} > 25$ GeV and $|\eta| < 2.5$ are considered. Isolation criteria similar to those used for electrons are used [53]. To reduce the impact of non-prompt leptons, muons within $\Delta R = \sqrt{(\Delta\eta)^2 + (\Delta\phi)^2} = 0.4$ of a jet are removed.

The anti- k_t algorithm implemented in the FastJet package [54, 55] is used to define two types of jets for this analysis: small- R jets with a radius parameter of $R = 0.4$ and large- R jets with $R = 1.0$. These are reconstructed independently of each other from topological clusters in the calorimeter. The clusters

used as input to the large- R jet reconstruction are calibrated using the local calibration method described in Ref. [56]. The small- R jet energy scale is obtained by using an energy- and η -dependent calibration scheme resulting from simulation and *in situ* corrections based on data [57–60]. Only small- R jets that have $|\eta| < 2.5$ and $p_T > 25$ GeV are considered. To reduce pileup effects, an algorithm that determines whether the primary vertex is the origin of the charged-particle tracks associated with a jet candidate is used to reject jets coming from other interactions [61]. This is done only for jet candidates with $p_T < 50$ GeV and $|\eta| < 2.4$. The small- R jet closest to an electron candidate is removed if they are separated by no more than $\Delta R = 0.2$. Small- R jets containing b -hadrons are identified (b -tagged) using a multivariate discriminant that combines information about secondary vertices and impact parameters. The small- R jets are considered b -tagged if the value of the discriminant is larger than a threshold that provides 70% efficiency. The corresponding rejection factors for gluon/light-quark jets and charm-quark jets are approximately 125 and 4.5, respectively [62, 63].

The large- R jet energy scale is derived by using energy- and η -dependent calibration factors derived from simulation and *in situ* measurements [57, 58, 64]. The large- R jet candidates are required to have $|\eta| < 2.0$ and $p_T > 300$ GeV. A trimming algorithm [65] with parameters $R_{\text{sub}} = 0.2$ and $f_{\text{cut}} = 0.05$ is applied to suppress gluon radiation and further mitigate pileup effects. A top-tagging algorithm [66] is applied that consists of p_T -dependent requirements on two variables: the jet mass m_J , measured from clusters in the calorimeter, and the N -subjettiness ratio τ_{32} [67, 68]. The N -subjettiness variable τ_N expresses how well a jet can be described as containing N or fewer subjets. The ratio $\tau_{32} = \tau_3/\tau_2$ allows discrimination between jets containing a three-prong structure and jets containing a two-prong structure. The p_T -dependent requirements provide a 50% top-quark tagging efficiency independent of p_T , with a light-quark and gluon jet rejection factor of ~ 17 at $p_T = 500$ GeV and decreasing with increasing p_T to ~ 10 at $p_T = 1$ TeV. This combination of variables used with trimmed large- R jets provides the necessary rejection for this analysis, and is insensitive to the effects of pileup.

4.2 Event selection

The event selection identifies fully hadronic $t\bar{t}$ events where both top quarks have high p_T . Each event is required to have a primary vertex with five or more associated tracks with $p_T > 0.4$ GeV. In order to reject top-quark events where a top quark has decayed semileptonically, the events are required to contain no reconstructed electron or muon candidate. To identify the fully hadronic decay topology, events must have at least two large- R jets with $p_T > 350$ GeV, $|\eta| < 2.0$ and $|m_J - m_{\text{top}}| < 50$ GeV, where the top-quark mass m_{top} is set to 172.5 GeV. The leading jet is required to have $p_T > 500$ GeV and the event must contain at least two small- R jets with $p_T > 25$ GeV and $|\eta| < 2.5$. This preselection results in an event sample of 22.7 million events.

To reject multijet background events, the two highest p_T large- R jets must satisfy the top-tagging criteria described in Sec. 4.1. Furthermore, both top-tagged large- R jets are required to have an associated small- R b -tagged jet. This association, hence referred to as b -matching, is made by requiring $\Delta R < 1.0$ between the small- R and large- R jets. These two highest p_T large- R jets are the leading and second-leading top-quark candidate jets (or “top-quark jets” in what follows). The candidate $t\bar{t}$ final state is defined as the sum of the four-momenta of the two large- R top-quark jets.

This selection defines the signal region, which has 3541 events.

5 Background estimation

There are two categories of background sources: those involving one or more top quarks in the final state and those sources where no top quark is involved. The background processes involving top quarks are estimated using MC calculations. The largest background source is events where the two leading jets both arise from gluons or u , d , s , c , or b quarks (which are referred to as “multijet” events). Monte Carlo predictions of multijet events have large uncertainties coming from the relatively poorly understood higher-order contributions that produce a pair of massive jets [69, 70]. To avoid these large uncertainties the multijet background is determined using a data-driven technique. A similar method was used in previous work [20].

A POWHEG+PYTHIA8 $t\bar{t}$ sample is used to estimate the number of $t\bar{t}$ events in the sample that arise from at least one top quark decaying semileptonically. This includes contributions from decays resulting in τ leptons, as no attempt is made to identify τ lepton candidates and reject them. The rate is estimated to be only $\sim 4\%$ in the signal region, primarily due to the top-tagging requirements. However, this category of $t\bar{t}$ events contributes to control and validation regions where the top-tagging and/or b -tagging requirements are relaxed. Thus, this MC prediction is used to estimate this contamination. Single-top-quark production in the Wt -channel makes a small contribution to the signal sample, which is estimated using the MC predictions described earlier. The t -channel single-top-quark process is not included, but is partially accounted for in the multijet background estimate.

The data-driven multijet background estimate is performed using a set of control regions. Sixteen separate regions are defined by classifying each event in the preselection sample according to whether the leading and second-leading jets are top-tagged or b -tagged. Table 1 shows the 16 regions that are defined in this way, and illustrates the proportion of expected $t\bar{t}$ events in each region relative to the observed rate. Region S is the signal region, while the regions with no b -tags (A, C, E and F) and the regions with one b -tag and no top-tags (B and I) are dominated by multijet backgrounds.

After subtracting the estimated contributions of the $t\bar{t}$ signal and of the other background sources to each of the control regions, the number of events in region J divided by the number of events in region A gives

Table 1: Region labels and expected proportion of $t\bar{t}$ events used for the data-driven background prediction of multijet events. A top-quark tagged jet is defined by the tagging algorithm described in the text, and denoted “1t” in the table, while a jet that is not top-tagged is labeled “0t”. A b -match is defined as $\Delta R(J, b) < 1.0$, where J represents a large- R jet and “ b ” represents a b -tagged jet. The labels “1b” and “0b” represent large- R jets that either have or not have a b -match. Regions K, L, N and M have an expected contribution from sources involving one or more top quarks of at least 15% of the observed yield. In other regions, the expected contribution from signal and backgrounds involving top quarks is less than 15% of the observed event rate.

| | | | | | |
|------------------------|------|----------|----------|----------|---------|
| 2nd large- R jet | 1t1b | J (7.6%) | K (21%) | L (42%) | S |
| | 0t1b | B (2.2%) | D (5.8%) | H (13%) | N (47%) |
| | 1t0b | E (0.7%) | F (2.4%) | G (6.4%) | M (30%) |
| | 0t0b | A (0.2%) | C (0.8%) | I (2.2%) | O (11%) |
| | 0t0b | 1t0b | 0t1b | 1t1b | |
| Leading large- R jet | | | | | |

an estimate of the ratio of the number of multijet events in region S to the number of multijet events in region O.

Thus one can use these relationships to estimate the multijet background rate in region S, i.e. $S = O \times J/A$, where O , J and A are the number of observed events in each region, while S is the estimate of the multijet background in region S.

This “ABCD” estimate assumes that the mistagging rate of the leading jet does not depend on how the second-leading jet is tagged. This assumption is avoided by measuring the correlations in background-dominated regions, e.g. comparing the ratio of the numbers of events in regions F and E (giving the leading jet top-tagging rate when the second-leading jet is top-tagged) with the ratios of events in regions C and A (giving the leading jet top-tagging rate when the second leading jet is not top-tagged). This results in a refined data-driven estimate of the size of the multijet background given by

$$\begin{aligned} S &= \frac{J \times O}{A} \cdot \frac{D \times A}{B \times C} \cdot \frac{G \times A}{E \times I} \cdot \frac{F \times A}{E \times C} \cdot \frac{H \times A}{B \times I}, \\ &= \frac{J \times O \times H \times F \times D \times G \times A^3}{(B \times E \times C \times I)^2}, \end{aligned} \quad (1)$$

where the region name is the number of observed events in that region. The measured correlations in the tagging of background jets result in an increase of $(12 \pm 3)\%$ in the background estimate compared with the estimate assuming that the tagging rates are independent. This estimate is also valid when a variable characterizing the kinematics of the events in all the regions is further restricted to range between specific values. This provides a bin-by-bin data-driven background estimate with uncertainties that come from the number of events in the regions used in Eq. (1).

Regions L and N are estimated to consist of approximately equal numbers of $t\bar{t}$ signal events and multijet background events. They are used as validation regions to verify that the signal and background estimates are robust. In these cases, the multijet background is estimated using different combinations of control regions, namely $N = H \times D/B$ and $L = H \times G/I$.

The number of multijet events in the signal region is calculated by applying Eq. (1) to the number of events in the control regions. This results in an estimate of 810 ± 50 multijet events in the signal region, where the uncertainty takes into account the statistical uncertainties as well as the systematic uncertainties in the $t\bar{t}$ signal subtraction.

There is good agreement in the validation regions between the predicted and observed event yields, as well as in the shape of distributions that are sensitive to the proportion of $t\bar{t}$ signal and multijet background. This is illustrated in Fig. 1, which compares the large- R jet mass distributions and the highest- p_T subject mass distribution of the leading jets. A shift between the measured and predicted jet mass distributions, shown in Figs. 1(a) and 1(b), is consistent with the uncertainties arising from the calibration for large- R jets [71]. The distributions for the leading and second-leading jet p_T and rapidity in regions N and L are shown in Fig. 2, and can be compared with the signal region distributions in Fig. 3.

The level of agreement between the observed and predicted distributions in the signal region can be seen in Fig. 3, which shows the distributions of the leading top-quark p_T and absolute value of rapidity, as well as the same distributions for the second-leading jet.

The event yields are summarized in Table 2 for the simulated signal, the background sources and the data sample.

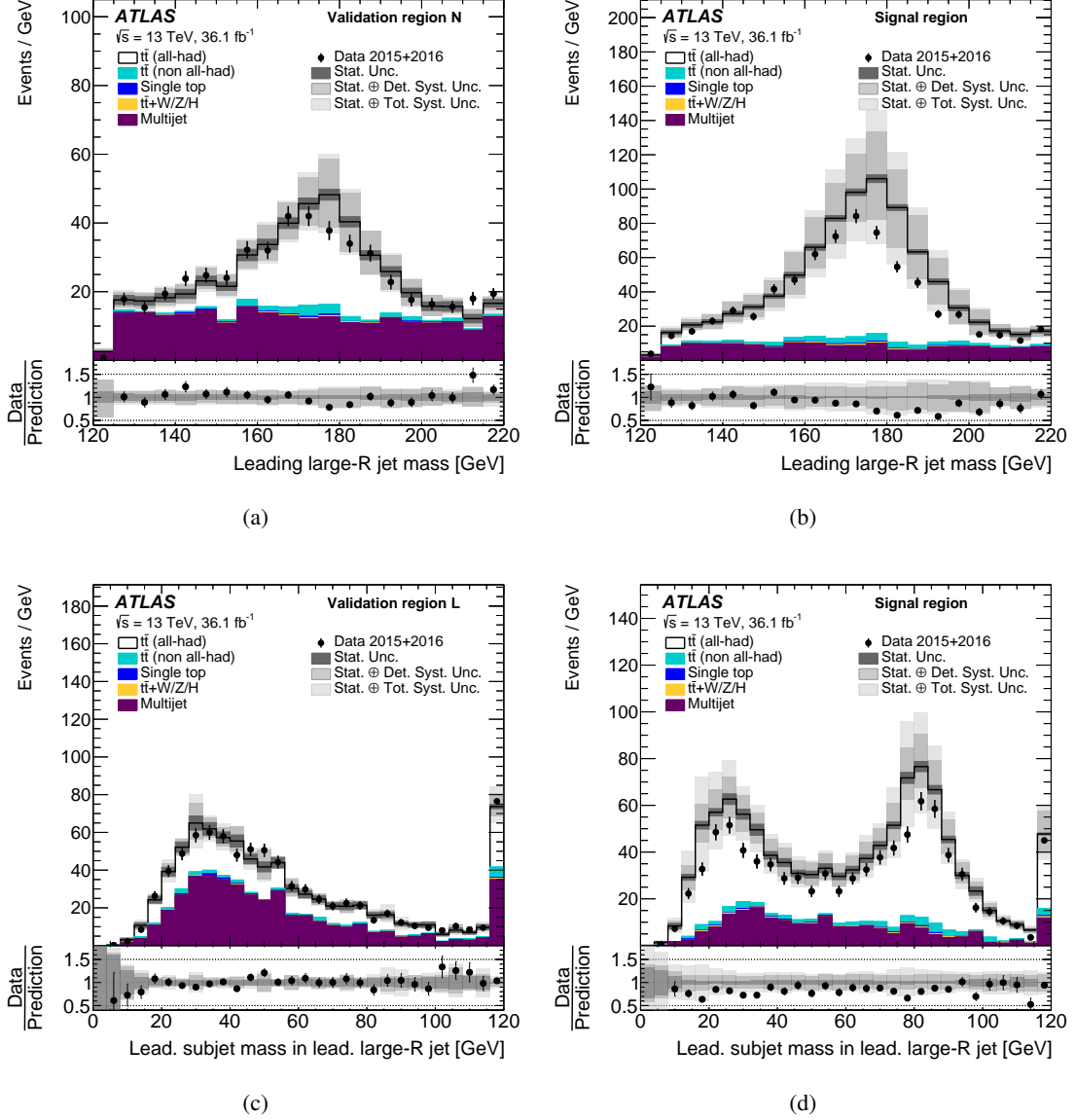


Figure 1: Kinematic distributions of top-quark candidate jets in the signal region S and in the two validation regions N and L. The leading large- R jet mass distributions for the events in the validation region N and the signal region S are shown in (a) and (b), respectively. The mass distribution of the leading small- R subject in the leading large- R jet for events in the validation region L and in the signal region are shown in (c) and (d), respectively. The signal prediction (open histogram) is based on the POWHEG+PYTHIA8 event generator normalized to the NNLO+NLL cross-section. The background is the sum of the data-driven multijet estimate (dark histogram) and the MC-based expectation for the contributions of non-all-hadronic $t\bar{t}$ and single-top-quark processes. Events beyond the x -axis range are included in the last bin. The gray area indicates the combined statistical and systematic uncertainties, including $t\bar{t}$ modeling uncertainties.

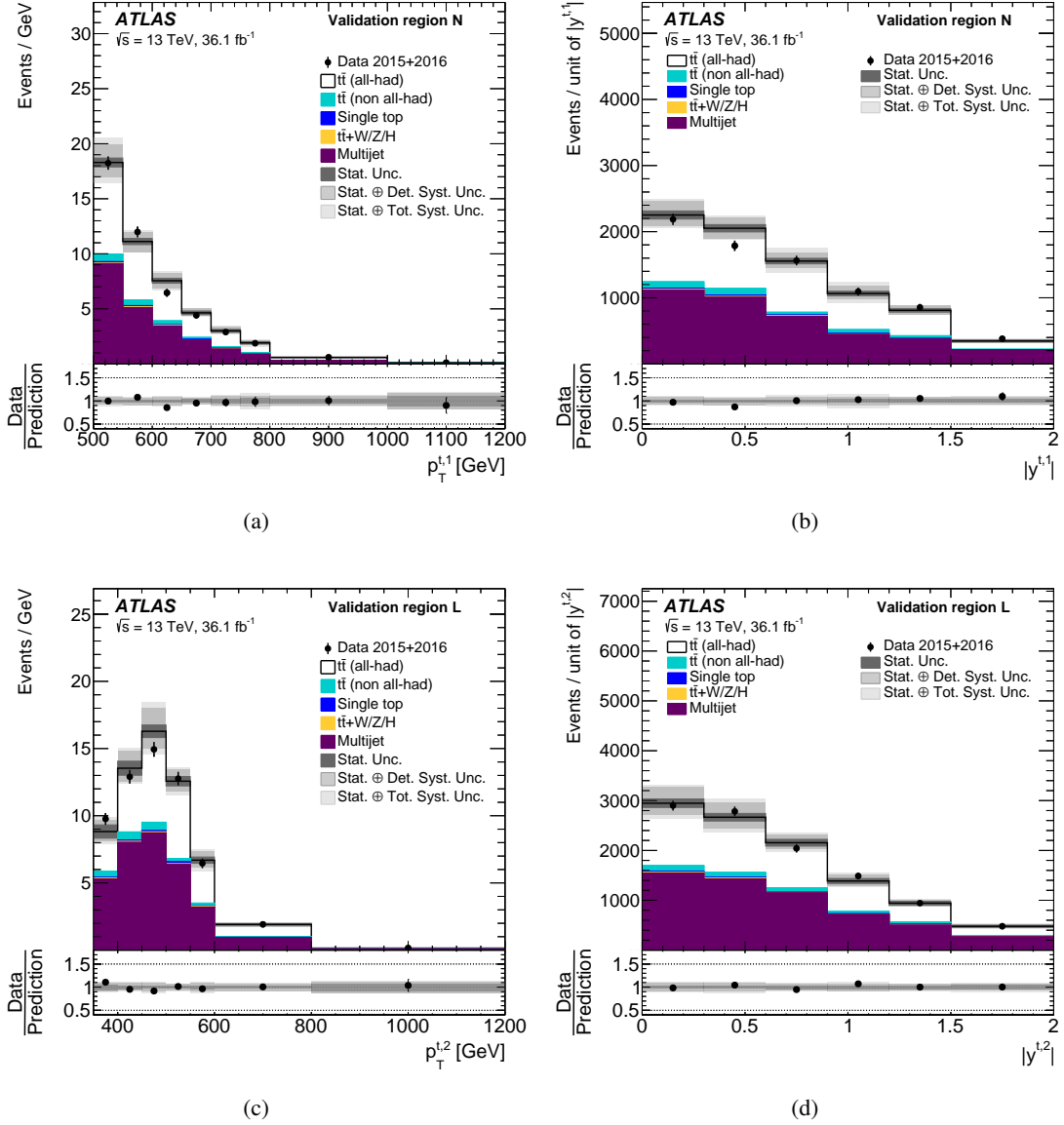


Figure 2: Kinematic distributions of top-quark candidate jets in the two validation regions N and L : (a) transverse momentum and (b) absolute value of the rapidity of the leading large- R jet, (c) transverse momentum and (d) absolute value of the rapidity of the second-leading large- R jet. The signal prediction (open histogram) is based on the POWHEG+PYTHIA8 event generator normalized to the NNLO+NLL cross-section. The background is the sum of the data-driven multijet estimate (dark histogram) and the MC-based expectation for the contributions of non-all-hadronic $t\bar{t}$ and single-top-quark processes. Events beyond the x -axis range are included in the last bin. The gray area indicates the combined statistical and systematic uncertainties, including $t\bar{t}$ modeling uncertainties.

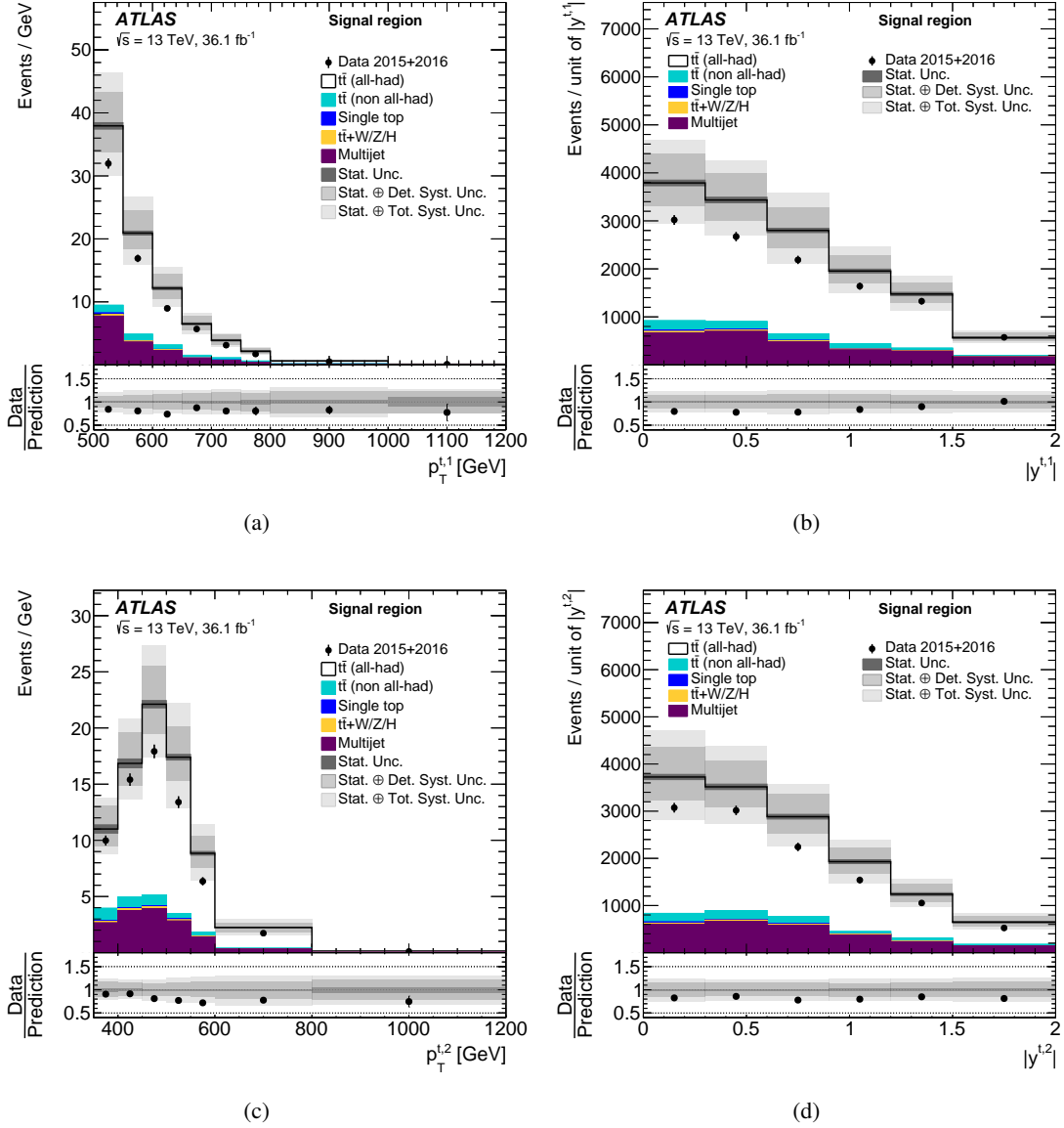


Figure 3: Kinematic distributions of top-quark candidate jets in the signal region S: (a) transverse momentum and (b) absolute value of the rapidity of the leading top-quark jet, (c) transverse momentum and (d) absolute value of the rapidity of the second-leading top-quark jet. The signal prediction (open histogram) is based on the POWHEG+PYTHIA8 simulation normalized to the NNLO+NLL cross-section. The background is the sum of the data-driven multijet estimate (dark histogram) and the MC-based expectation for the contributions of non-all-hadronic $t\bar{t}$ and single-top-quark processes. Events beyond the x -axis range are included in the last bin. The gray area indicates the combined statistical and systematic uncertainties in the total prediction, including $t\bar{t}$ modeling uncertainties.

Table 2: Event yields in the signal region for the expected $t\bar{t}$ signal process and the background processes. The sum of these are compared to the observed yield. The uncertainties represent the sum in quadrature of the statistical and systematic uncertainties in each subsample. Neither modeling uncertainties nor uncertainties in the inclusive $t\bar{t}$ cross-section are included in the systematic uncertainties. The single-top-quark background does not include the t -channel process.

| | |
|---------------------------------|----------------|
| $t\bar{t}$ (all-hadronic) | 3250 ± 470 |
| $t\bar{t}$ (non-all-hadronic) | 200 ± 40 |
| Single-top-quark | 24 ± 12 |
| $t\bar{t}+W/Z/H$ | 33 ± 10 |
| Multijet events | 810 ± 50 |
| Prediction | 4320 ± 530 |
| Data (36.1 fb^{-1}) | 3541 |

6 Unfolding procedure

The differential cross-sections are obtained from the data using an unfolding technique that corrects for detector effects such as efficiency, acceptance and resolution. This correction is made to the particle level using a fiducial phase space that is defined to match the experimental acceptance and hence avoid large MC extrapolations. The parton-level differential cross-sections are obtained using a similar procedure, but in this case the correction is made to the top-quark parton after final-state radiation effects have been included in the generation process using a limited phase-space region matched to the kinematic acceptance of the analysis.

In the following subsections, the particle-level fiducial phase space and the parton-level phase space are defined and the algorithm used for the unfolding is described.

6.1 Particle-level fiducial phase-space and parton-level phase-space regions

The particle-level fiducial phase-space definition models the kinematic requirements used to select the $t\bar{t}$ process.

In the MC signal sample, electrons and muons that do not originate from hadron decays are combined or “dressed” with any photons found in a cone of size $\Delta R = 0.1$ around the lepton direction. The four-momentum of each photon in the cone is added to the four-momentum of the lepton to produce the dressed lepton.

Jets are clustered using all stable particles except those used in the definition of dressed electrons and muons and neutrinos not from hadron decays, using the anti- k_t algorithm with a radius parameter $R = 0.4$ and $R = 1.0$ for small- R and large- R jets, respectively. The decay products of hadronically decaying τ leptons are included. These jets do not include particles from pileup events but do include those from the underlying event. Large- R jets are required to have $p_T > 350 \text{ GeV}$ and a mass within 50 GeV of the top-quark mass.

The following requirements on particle-level electrons, muons and jets in the all-hadronic $t\bar{t}$ MC events define the particle-level fiducial phase space:

- no dressed electrons or muons with $p_T > 25$ GeV and $|\eta| < 2.5$ be in the event,
- at least two anti- k_t $R = 1.0$ jets with $p_T > 350$ GeV and $|\eta| < 2.0$,
- at least one anti- k_t $R = 1.0$ jet with $p_T > 500$ GeV and $|\eta| < 2.0$,
- the masses of the two large- R jets be within 50 GeV of the top-quark mass of 172.5 GeV,
- at least two anti- k_t $R = 0.4$ jets with $p_T > 25$ GeV and $|\eta| < 2.5$ and
- the two leading $R = 1.0$ jets be matched to a b -hadron in the final state using a ghost-matching technique as described in Ref. [72] (called top-quark particle jets).

The parton-level phase space is defined by requiring that the leading top quark have $p_T > 500$ GeV and the second-leading top quark have $p_T > 350$ GeV. No rapidity or other kinematic requirements are made. This definition avoids a large extrapolation in the unfolding procedure that results in large systematic uncertainties.

6.2 Unfolding algorithm

The iterative Bayesian method [73] as implemented in RooUNFOLD [74] is used to correct the detector-level event distributions to their corresponding particle- and parton-level differential cross-sections. The unfolding starts from the detector-level event distributions after subtraction of the estimated backgrounds. An acceptance correction f_{acc} is applied that accounts for events that are generated outside the fiducial or parton phase space but pass the detector-level selection.

In order to properly account for resolution and any combinatorial effects, the detector-level and particle-level (parton-level) objects in MC events are required to be well-matched using the angular difference ΔR . At particle (parton) level, each top-quark particle-level jet (top quark) is matched to the closest detector-level jet within $\Delta R < 1.0$, a requirement that ensures high matching efficiency. The resulting acceptance corrections f_{acc}^j are illustrated in Fig. 4.

The unfolding step uses a migration matrix (\mathcal{M}) derived from simulated $t\bar{t}$ events with matching detector-level jets by binning these events in the particle-level and parton-level phase spaces. The probability for particle-level (parton-level) events to remain in the same bin is therefore represented by the elements on the diagonal, and the off-diagonal elements describe the fraction of particle-level (parton-level) events that migrate into other bins. Therefore, the elements of each row add up to unity (within rounding) as shown in Fig. 5. The efficiency corrections ϵ_{eff} correct for events that are in the fiducial particle-level (parton-level) phase space but are not reconstructed at the detector level, and are illustrated in Fig. 4. The overall efficiency is largely determined by the working points of the b -tagging (70%) and top-tagging (50%) algorithms. The reduction in efficiency at higher top-quark candidate p_T arises primarily from the b -tagging requirements. Examples of the migration matrices for several variables are shown in Fig. 5.

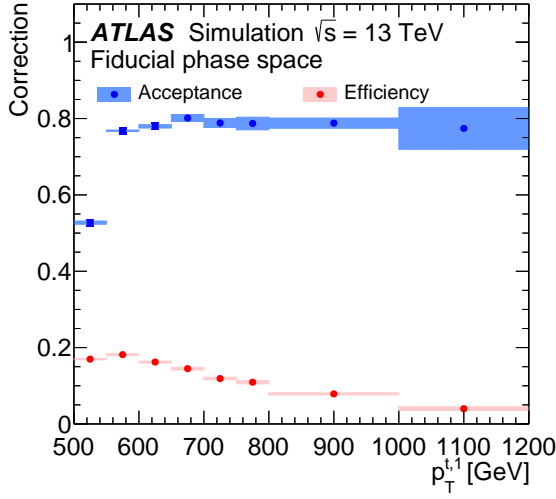
The unfolding procedure for an observable X at both particle and parton level is summarized by the expression

$$\frac{d\sigma^{\text{fid}}}{dX^i} \equiv \frac{1}{\int \mathcal{L} dt \cdot \Delta X^i} \cdot \frac{1}{\epsilon_{\text{eff}}^i} \cdot \sum_j \mathcal{M}_{ij}^{-1} \cdot f_{\text{acc}}^j \cdot (N_{\text{reco}}^j - N_{\text{bg}}^j),$$

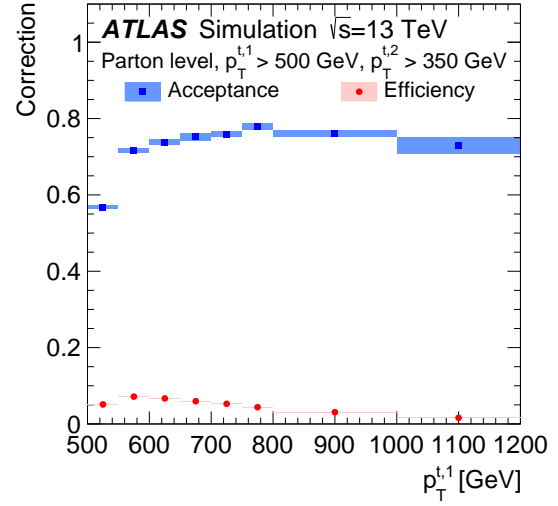
where N_{reco} and N_{bg} refer to the number of reconstructed signal and background events, respectively; the index j runs over bins of X at detector level while the index i labels bins at particle and parton level; ΔX^i is the bin width while $\int \mathcal{L} dt$ is the integrated luminosity. The Bayesian unfolding is symbolized by \mathcal{M}_{ij}^{-1} .

The inclusive cross-section for $t\bar{t}$ pairs in the fiducial (parton) phase space, obtained by integrating the absolute differential cross-section, is used to determine the normalized differential cross-section $1/\sigma^{\text{fid}} \cdot d\sigma^{\text{fid}}/dX^i$. This cross-section is not corrected for the all-hadronic $t\bar{t}$ branching fraction of 0.457 [75].

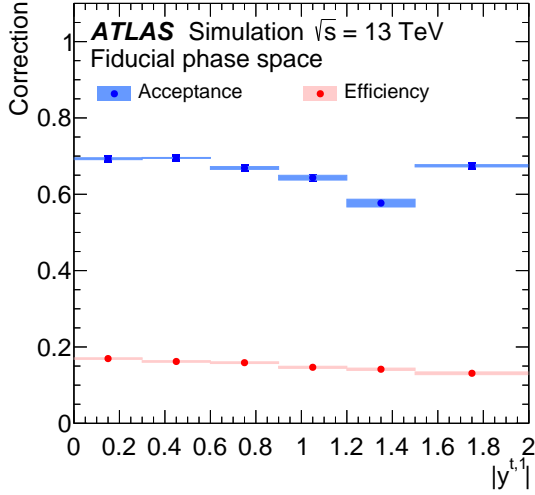
Tests are performed at both particle and parton level to verify that the unfolding procedure is able to recover the generator-level distributions for input distributions that vary from the observed distributions or nominal predictions. These closure tests show that the unfolding procedure results are unbiased so long as the features of the input distributions are consistent with the measurement resolution of the variable.



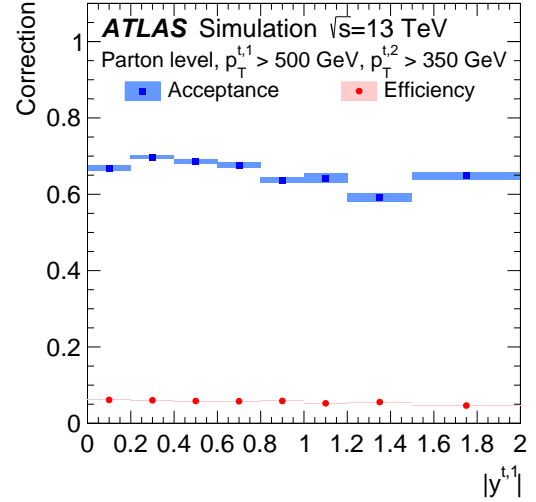
(a)



(b)



(c)



(d)

Figure 4: Acceptance and efficiency corrections as a function of p_T and $|y|$ of the leading top-quark jet for the particle-level phase space in (a) and (c) and for the parton-level phase space in (b) and (d). The POWHEG+PYTHIA8 event generator is used as the nominal prediction to correct for detector effects. The blue and red areas represent statistical uncertainties.

7 Systematic uncertainties

Systematic uncertainties resulting from electron, muon and jet reconstruction and calibration, MC event generator modeling and background estimation, are described below. The propagation of systematic uncertainties through the unfolding procedure is described in Sec. 7.2.

7.1 Estimation of systematic uncertainties

The systematic uncertainties in the measured distributions are estimated using MC data sets and the data satisfying the final selection requirements.

Estimates of large- R jet uncertainties [71] are derived by studying tracking and calorimeter-based measurements and comparing these in data and MC simulations. These uncertainties also include the energy, mass and substructure response. The uncertainty in the large- R jet mass resolution is incorporated by measuring the effect that an additional resolution degradation of 20% has on the observables [64, 76]. The total uncertainty affecting the cross-section arising from jet calibration and reconstruction ranges from 11% to 30% for jet p_T over the range 350 to 900 GeV.

The small- R jet energy scale uncertainty is derived using a combination of simulations, test-beam data and *in situ* measurements [57–59, 77]. Additional uncertainty contributions from the jet flavor composition, calorimeter response to different jet flavors and pileup are taken into account. Uncertainties in the jet energy resolution are obtained with an *in situ* measurement of the jet response asymmetry in dijet events [78]. These small- R jet uncertainties are typically below 1% for all distributions.

Uncertainties associated with pileup, the effect of additional interactions and the selection requirements used to mitigate them are estimated using comparisons of data and MC samples and are approximately 1%. The efficiency to tag jets containing b -hadrons is corrected in simulated events by applying b -tagging scale factors, extracted in $t\bar{t}$ and dijet samples, in order to account for the residual difference between data and simulation. The associated systematic uncertainties, computed by varying the b -tagging scale factors within their uncertainties [62, 63], are found to range from $\pm 8\%$ to $\pm 17\%$ for large- R jet p_T increasing from 500 to 900 GeV. The uncertainties arising from lepton energy scale and resolution [52, 53, 79] are $< 1\%$.

Systematic uncertainties affecting the multijet background estimates come from the subtraction of other background processes in the control regions and from the uncertainties in the measured tagging correlations (which are statistical in nature). The uncertainty in the subtraction of the all-hadronic $t\bar{t}$ events in the control regions arises from the uncertainties in the $t\bar{t}$ cross-section and b -matching algorithm. Together, these result in background uncertainties ranging from ± 2 to $\pm 5\%$ for large- R jet p_T ranging from 350 to 900 GeV, respectively. The uncertainty in the single-top-quark background rates comes from the uncertainties in the Wt production cross-section, the integrated luminosity, detection efficiency and the relative contribution of t -channel and Wt production, which is assigned an uncertainty of $\pm 50\%$.

Other MC event generators are employed to assess modeling systematic uncertainties. In these cases, the difference between the unfolded distribution of an alternative model and its own particle-level or parton-level distribution is used as the estimate of the corresponding systematic uncertainty in the unfolded differential cross-section.

To assess the uncertainty related to the matrix element calculation and matching to the parton shower, MG5_aMC@NLO+PYTHIA8 events are unfolded using the migration matrix and correction factors derived from the POWHEG+PYTHIA8 sample. This uncertainty is found to be in the range $\pm 10\text{--}15\%$, depending on the variable, increasing to $\pm 20\text{--}30\%$ at large p_T^t , $m^{t\bar{t}}$, $p_T^{\bar{t}}$ and $|y^{t\bar{t}}|$ where there are fewer data events. To assess the uncertainty associated with the choice of parton shower and hadronization model, a comparison is made of the unfolded and particle-level distributions of simulated events created with POWHEG interfaced to the Herwig7 parton shower and hadronization model using the nominal POWHEG+PYTHIA8 corrections and unfolding matrices. The resulting systematic uncertainties, taken as the symmetrized difference, are found to be $\pm 5\text{--}15\%$. The uncertainty related to the modeling of initial- and final-state radiation is determined using two alternative POWHEG+PYTHIA8 $t\bar{t}$ MC samples described in Sec. 3. This uncertainty is found to be in the range $\pm 10\text{--}15\%$, depending on the variable considered. The uncertainty arising from the size of the nominal MC sample is approximately 1%, scaling with the statistical uncertainty of the data as a function of the measured variables.

The uncertainty arising from parton distribution functions is assessed using the POWHEG+PYTHIA8 $t\bar{t}$ sample. An envelope of spectra is determined by reweighting the central prediction of the PDF4LHC PDF set [80] and applying the relative variation to the nominal distributions. This uncertainty is found to be less than 1%.

The uncertainty in the integrated luminosity is $\pm 2.1\%$. It is derived, following a methodology similar to that detailed in Ref. [81], from a calibration of the luminosity scale using x - y beam-separation scans performed in August 2015 and May 2016.

Other sources of systematic uncertainty (e.g., the top-quark mass) are less than 1%.

7.2 Propagation of systematic uncertainties and treatment of correlations

The statistical and systematic uncertainties are propagated and combined in the same way for both the particle-level and parton-level results using pseudoexperiments created from the nominal and alternative MC samples.

The effect of the data statistical uncertainty is incorporated by creating pseudoexperiments in which independent Poisson fluctuations in each data bin are made. The statistical uncertainty due to the size of the signal MC samples used to correct the data is incorporated into the pseudoexperiments by adding independent Poisson fluctuations for a bin corresponding to the MC population in the bin.

To evaluate the impact of each uncertainty after the unfolding, the simulated distribution is varied, then unfolded using corrections obtained with the nominal POWHEG+PYTHIA8 sample. The unfolded varied distribution is compared to the corresponding particle- or parton-level distribution. For each systematic uncertainty, the correlation between the signal and background distributions is taken into account. All detector- and background-related systematic uncertainties are estimated using the nominal POWHEG+PYTHIA8 sample. Alternative hard-scattering, parton shower and hadronization, ISR/FSR and PDF uncertainties are estimated by a comparison between the unfolded cross-section and the corresponding particle- or parton-level distribution produced using the corresponding alternative Monte Carlo event generator.

The systematic uncertainties for the particle-level fiducial phase-space total cross-section measurement described below are listed in Table 3.

Table 3: Summary of the largest systematic and statistical relative uncertainties for the absolute particle-level fiducial phase-space cross-section measurement in percent. Most of the uncertainties that are less than 1% are not listed.

| Source | Percentage |
|-------------------------------------|------------|
| Large- R jet energy scale | 5.9 |
| Large- R jet mass calibration | 1.4 |
| Large- R jet top-tagging | 12 |
| Small- R jets | 0.3 |
| Pileup | 0.6 |
| Flavor tagging | 8.3 |
| Background | 0.9 |
| Luminosity | 2.0 |
| Monte Carlo statistical uncertainty | 0.9 |
| Alternative hard-scattering model | 11 |
| Alternative parton-shower model | 14 |
| ISR/FSR + scale | 1.1 |
| Total systematic uncertainty | 24 |
| Data statistical uncertainty | 2.3 |
| Total uncertainty | 24 |

Figure 6 shows a summary of the relative size of the systematic uncertainties for the leading top-quark jet transverse momentum and rapidity at particle level and parton level.

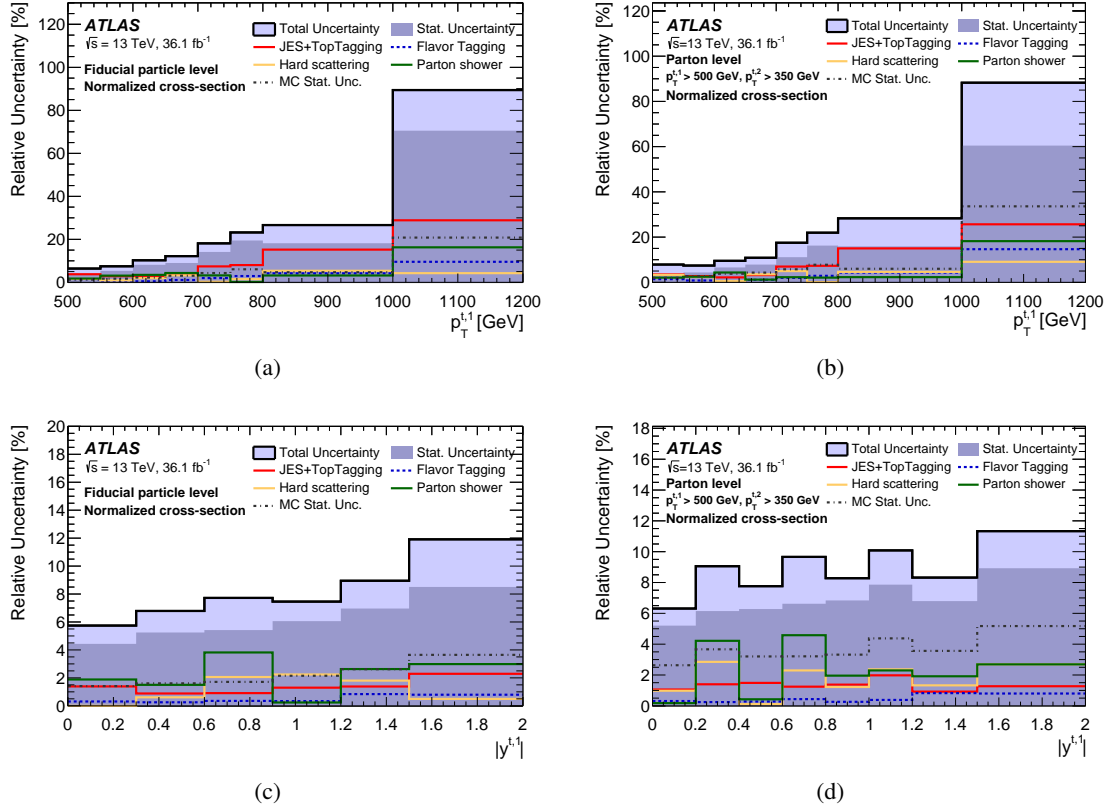


Figure 6: Relative uncertainties in the normalized differential cross-sections as a function of the leading top-quark jet transverse momentum and rapidity at particle level and parton level. The light and dark blue areas represent the total and statistical uncertainty, respectively. The POWHEG+PYTHIA8 event generator is used as the nominal prediction to correct for detector effects.

A covariance matrix is constructed for each differential cross-section to include the effect of all uncertainties to allow quantitative comparisons with theoretical predictions. This covariance matrix is derived by summing two covariance matrices following the same approach used in Refs. [10, 14].

The first covariance matrix incorporates statistical uncertainties and systematic uncertainties from detector effects and background estimation by using pseudoexperiments to convolve the sources. In each pseudoexperiment, the detector-level data distribution is varied following a Poisson distribution. For each systematic uncertainty effect, Gaussian-distributed shifts are coherently included by scaling each Poisson-fluctuated bin content with its expected relative variation from the associated systematic uncertainty. Differential cross-sections are obtained by unfolding the varied distribution with the nominal corrections, and the distribution of the resulting changes in the unfolded distributions are used to compute this first covariance matrix.

The second covariance matrix is obtained by summing four separate covariance matrices corresponding to the effects of the $t\bar{t}$ event generator, parton shower and hadronization, ISR/FSR and PDF uncertainties. The bin-to-bin correlation values are set to unity for all these matrices.

The comparison between the measured differential cross-sections and a variety of MC predictions is quantified by calculating χ^2 values employing the covariance matrix and by calculating the corresponding

p -values (probabilities that the χ^2 is larger than or equal to the observed value assuming that the measured and predicted distributions are statistically equivalent) from the χ^2 and the number of degrees of freedom (NDF). The χ^2 values are obtained using

$$\chi^2 = V_{N_b}^T \cdot \text{Cov}_{N_b}^{-1} \cdot V_{N_b},$$

where V_{N_b} is the vector of differences between measured differential cross-section values and predictions, and $\text{Cov}_{N_b}^{-1}$ is the inverse of the covariance matrix.

The normalization constraint used to derive the normalized differential cross-sections lowers the NDF to one less than the rank of the $N_b \times N_b$ covariance matrix, where N_b is the number of bins in the unfolded distribution. The χ^2 for the normalized differential cross-sections is

$$\chi^2 = V_{N_b-1}^T \cdot \text{Cov}_{N_b-1}^{-1} \cdot V_{N_b-1},$$

where V_{N_b-1} is the vector of differences between measurement and prediction obtained by discarding one of the N_b elements and Cov_{N_b-1} is the $(N_b - 1) \times (N_b - 1)$ sub-matrix derived from the covariance matrix by discarding the corresponding row and column.

8 Measurement of the differential cross-sections

The differential cross-sections are obtained from the data using the unfolding technique described above. In the following subsections, the resulting particle-level and parton-level differential cross-sections are presented.

8.1 Particle-level fiducial phase-space differential cross-section

The unfolded differential cross-sections, normalized to the total cross-section for the fiducial phase space, are shown in Fig. 7 for the p_T and rapidity of the leading and second-leading top-quark jets, and in Fig. 8 for the p_T , mass and rapidity of the $t\bar{t}$ system. The unfolded differential cross-sections are shown in Figs. 9–11 for the $t\bar{t}$ production angle in the Collins–Soper reference frame, the scalar sum of the transverse momenta of the two top quarks, $H_T^{t\bar{t}}$, the longitudinal boost, $y_B^{t\bar{t}}$, the azimuthal angle between the two top-quark jets, $\Delta\phi_{t\bar{t}}$, the variable related to the rapidity difference between the two top-quark jets, $\chi^{t\bar{t}}$, and the absolute value of the out-of-plane momentum, $p_{\text{out}}^{t\bar{t}}$. These are compared with SM predictions obtained using the NLO MC event generators described in Sec. 3.

This analysis is sensitive to top-quark jets produced with p_T up to approximately 1 TeV and to a rapidity $|y^t| < 2.0$. The differential cross-section falls by two orders of magnitude as a function of top-quark jet transverse momentum over a p_T range from 500 GeV to 1 TeV. The production cross-section decreases as a function of top-quark jet rapidity by approximately 30% from $y^t = 0$ to $y^t = \pm 1$. The differential cross-section as a function of p_T for the second-leading top-quark jet reflects the effect of the p_T requirement on the leading top-quark jet and the strong correlation in p_T of the two top-quark jets arising from the pair-production process.

The $t\bar{t}$ system is centrally produced with a transverse momentum typically below 200 GeV, an invariant mass below 1.5 TeV and a rapidity $|y^{t\bar{t}}| < 1.5$. In particular, the $m^{t\bar{t}}$ distribution falls smoothly, with a sensitivity that extends up to ~ 2 TeV.

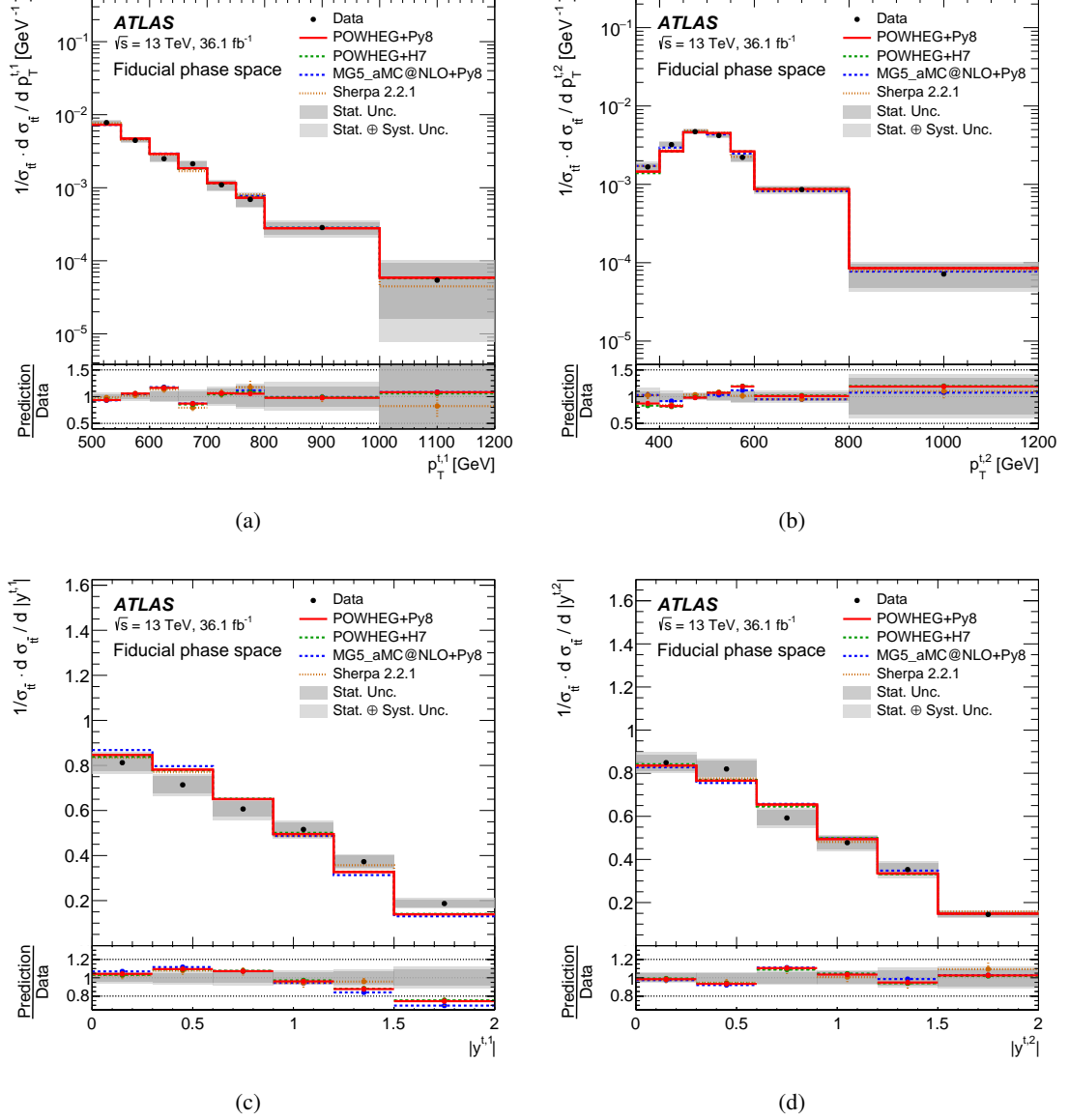


Figure 7: Normalized particle-level fiducial phase-space differential cross-sections as a function of (a) transverse momentum of the leading top-quark jet, (b) transverse momentum of the second-leading top-quark jet, (c) absolute value of the rapidity of the leading top-quark jet and (d) absolute value of the rapidity of the second-leading top-quark jet. The gray bands indicate the total uncertainty in the data in each bin. The vertical bars indicate the statistical uncertainties in the theoretical models. The POWHEG+PYTHIA8 event generator is used as the nominal prediction. Data points are placed at the center of each bin.

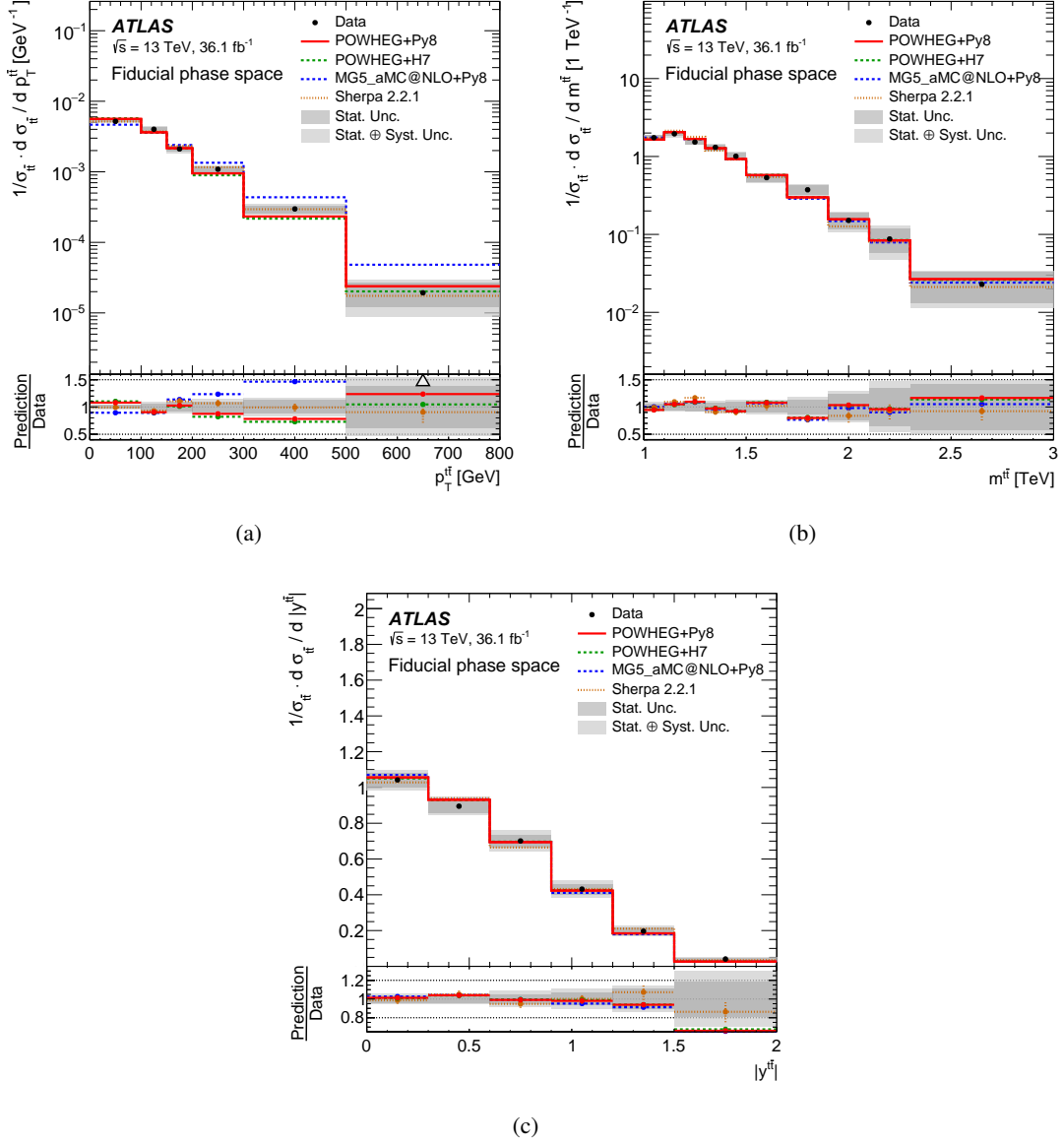


Figure 8: Normalized particle-level fiducial phase-space differential cross-sections as a function of (a) transverse momentum, (b) invariant mass and (c) absolute value of the rapidity of the $t\bar{t}$ system. The gray bands indicate the total uncertainty in the data in each bin. The vertical bars indicate the statistical uncertainties in the theoretical models. The POWHEG+PYTHIA8 event generator is used as the nominal prediction. Data points are placed at the center of each bin.

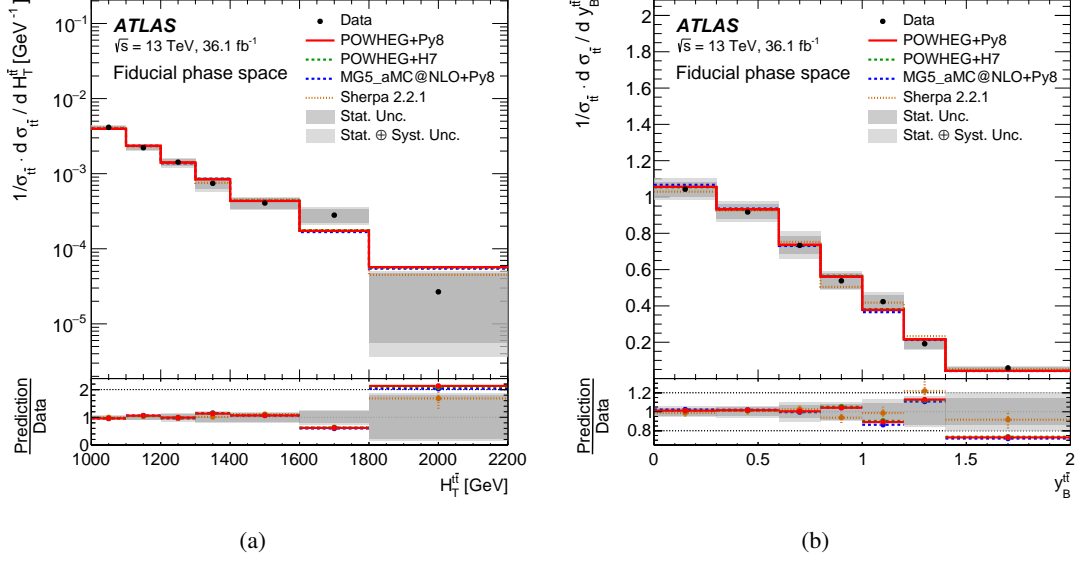


Figure 9: Normalized particle-level fiducial phase-space differential cross-sections as a function of (a) the scalar sum of the transverse momenta of the two top-quark jets and (b) the longitudinal boost y_B^{tt} . The gray bands indicate the total uncertainty in the data in each bin. The vertical bars indicate the statistical uncertainties in the theoretical models. The POWHEG+PYTHIA8 event generator is used as the nominal prediction. Data points are placed at the center of each bin.

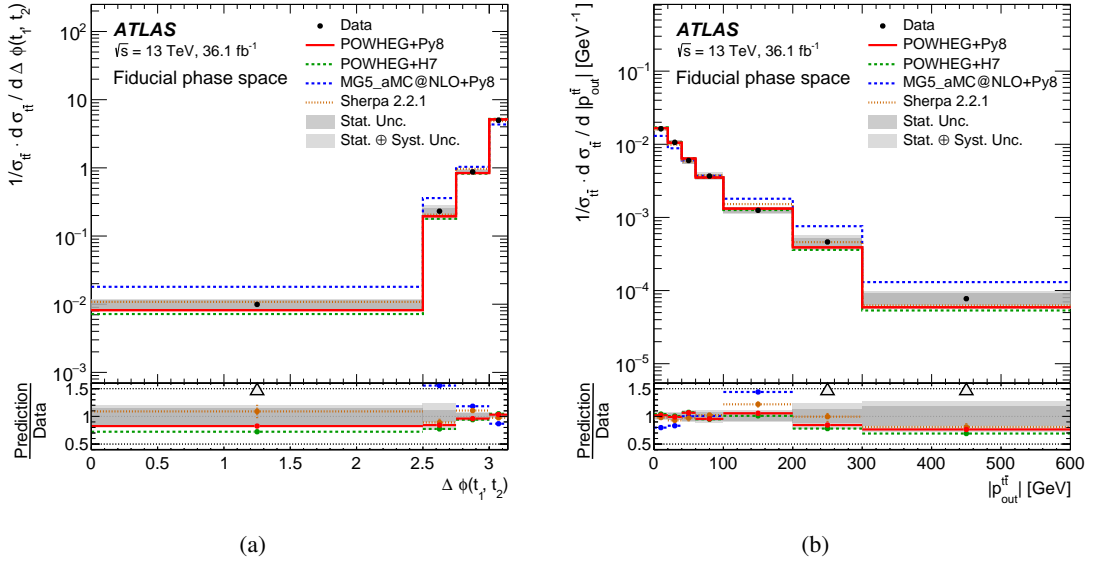


Figure 10: Normalized particle-level fiducial phase-space differential cross-sections as a function of (a) the azimuthal angle between the two top-quark jets $\Delta\phi_{t\bar{t}}$ and (b) the absolute value of the out-of-plane momentum $p_{out}^{t\bar{t}}$. The gray bands indicate the total uncertainty in the data in each bin. The vertical bars indicate the statistical uncertainties in the theoretical models. The POWHEG+PYTHIA8 event generator is used as the nominal prediction. Data points are placed at the center of each bin.

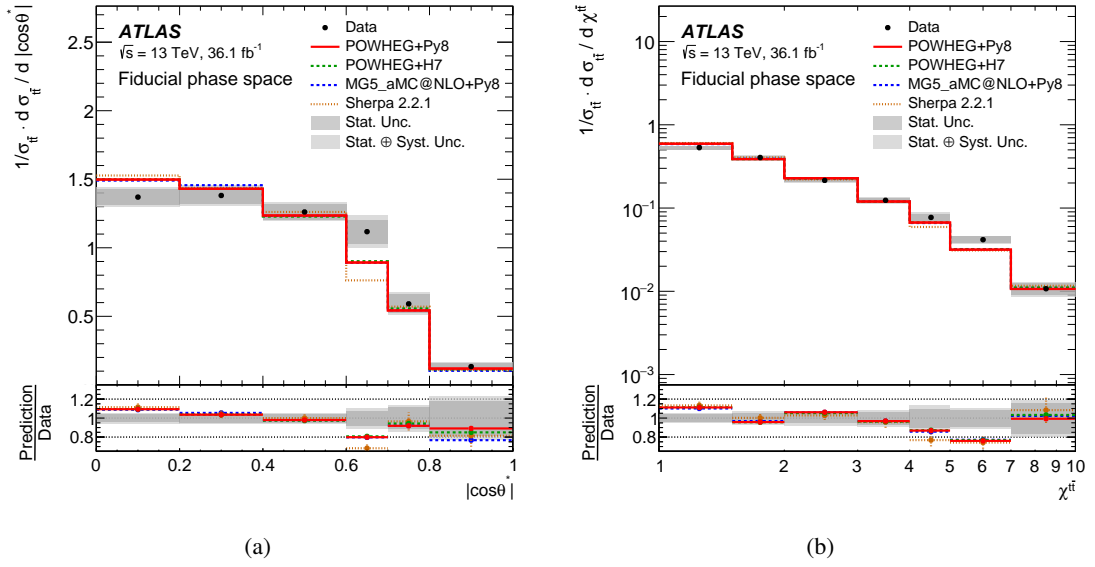


Figure 11: Normalized particle-level fiducial phase-space differential cross-sections as a function of (a) the production angle in the Collins–Soper reference frame and (b) the variable χ^{tt} . The gray bands indicate the total uncertainty in the data in each bin. The vertical bars indicate the statistical uncertainties in the theoretical models. The POWHEG+PYTHIA8 event generator is used as the nominal prediction. Data points are placed at the center of each bin.

8.2 Parton-level phase-space differential cross-sections

The unfolded parton-level phase-space differential cross-sections are shown in Figs.12–16 for the kinematical variables describing the top quark, leading top quark, second-leading top quark and the $t\bar{t}$ system.

To measure the average top-quark p_T distribution that can be compared with NNLO+NNLL calculations [1–3], the data are unfolded by randomly selecting one of the two top-quark candidates at the detector level for each event. The normalized average top-quark p_T and rapidity differential cross-sections are shown in Fig. 12(a) and Fig. 12(b), respectively.

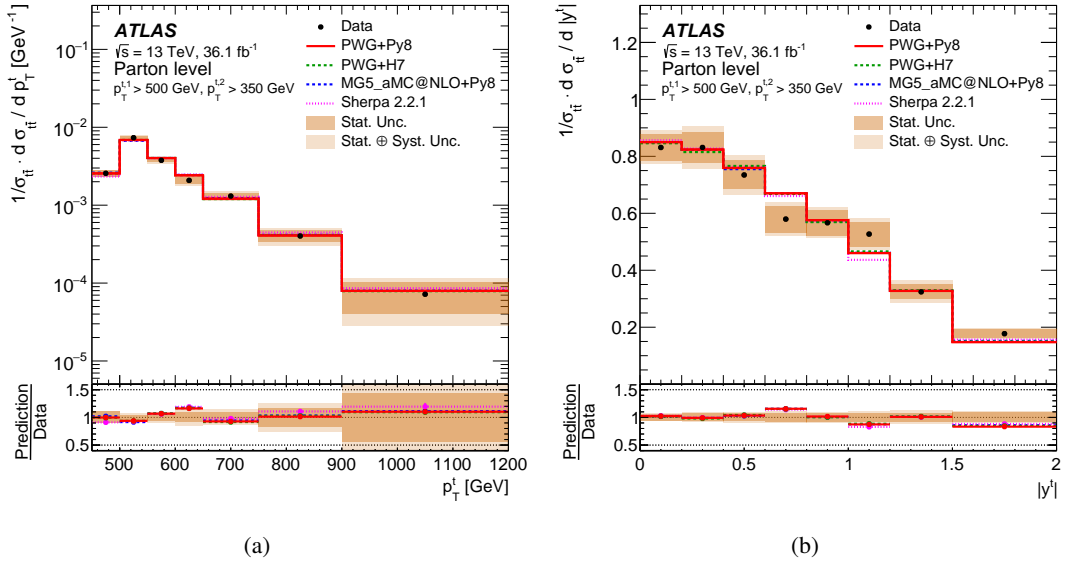


Figure 12: The normalized parton-level differential cross-sections as a function of (a) the transverse momentum and (b) the rapidity of the top quark. The orange bands indicate the total uncertainty in the data in each bin. The vertical bars indicate the statistical uncertainties in the theoretical models. The POWHEG+PYTHIA8 event generator is used as the nominal prediction to correct for detector effects, parton showering and hadronization. Data points are placed at the center of each bin. The unfolding has required the leading top-quark $p_T > 500$ GeV and the second-leading top-quark $p_T > 350$ GeV.

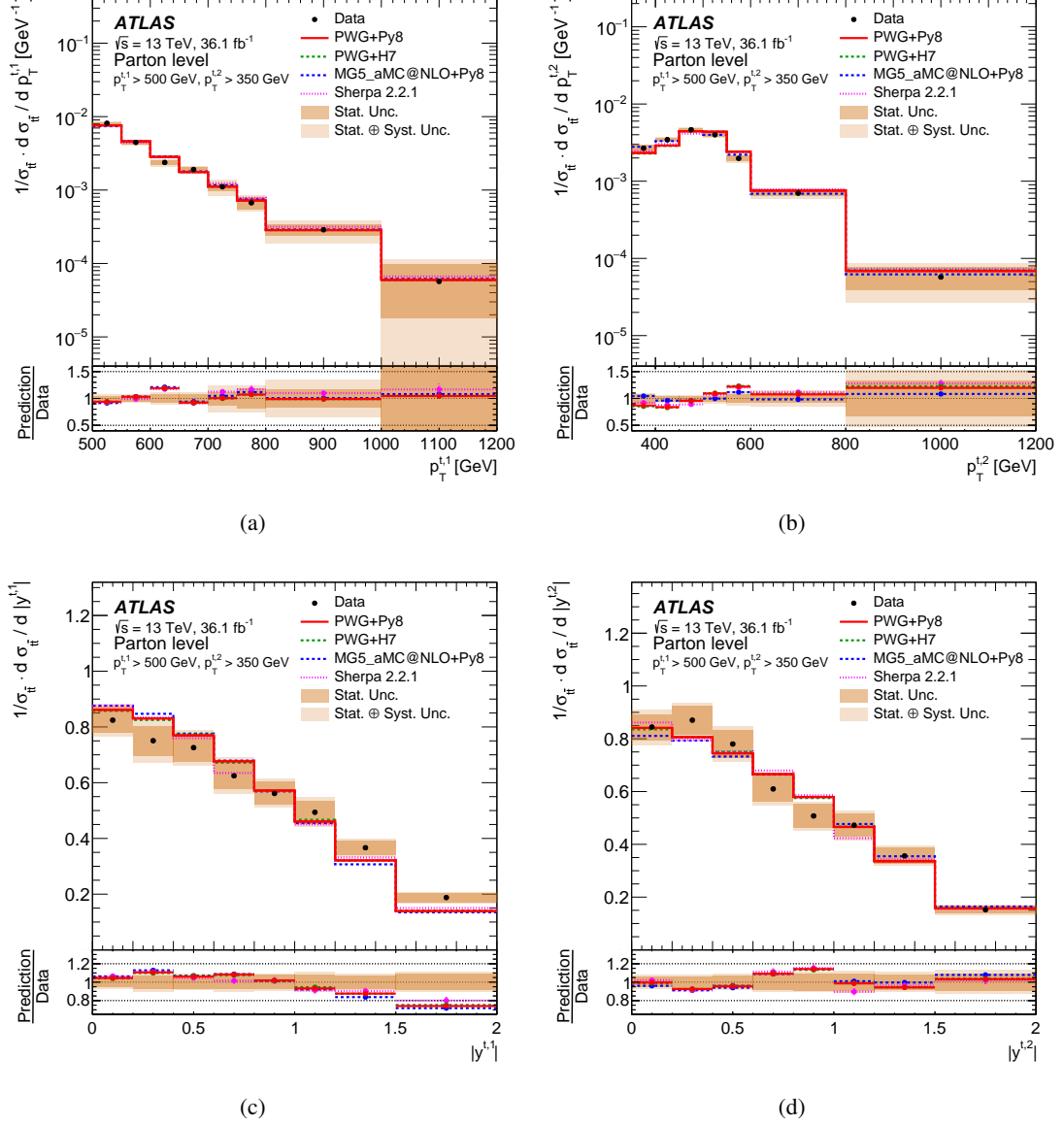


Figure 13: The normalized parton-level differential cross-sections as a function of (a) the transverse momentum of the leading top quark, (b) the transverse momentum of the second-leading top quark, (c) the absolute value of the rapidity of the leading top quark and (d) the absolute value of the rapidity of the second-leading top quark. The orange bands indicate the total uncertainty in the data in each bin. The vertical bars indicate the statistical uncertainties in the theoretical models. The POWHEG+PYTHIA8 event generator is used as the nominal prediction to correct for detector effects, parton showering and hadronization. Data points are placed at the center of each bin. The unfolding has required the leading top-quark $p_T > 500 \text{ GeV}$ and the second-leading top-quark $p_T > 350 \text{ GeV}$.

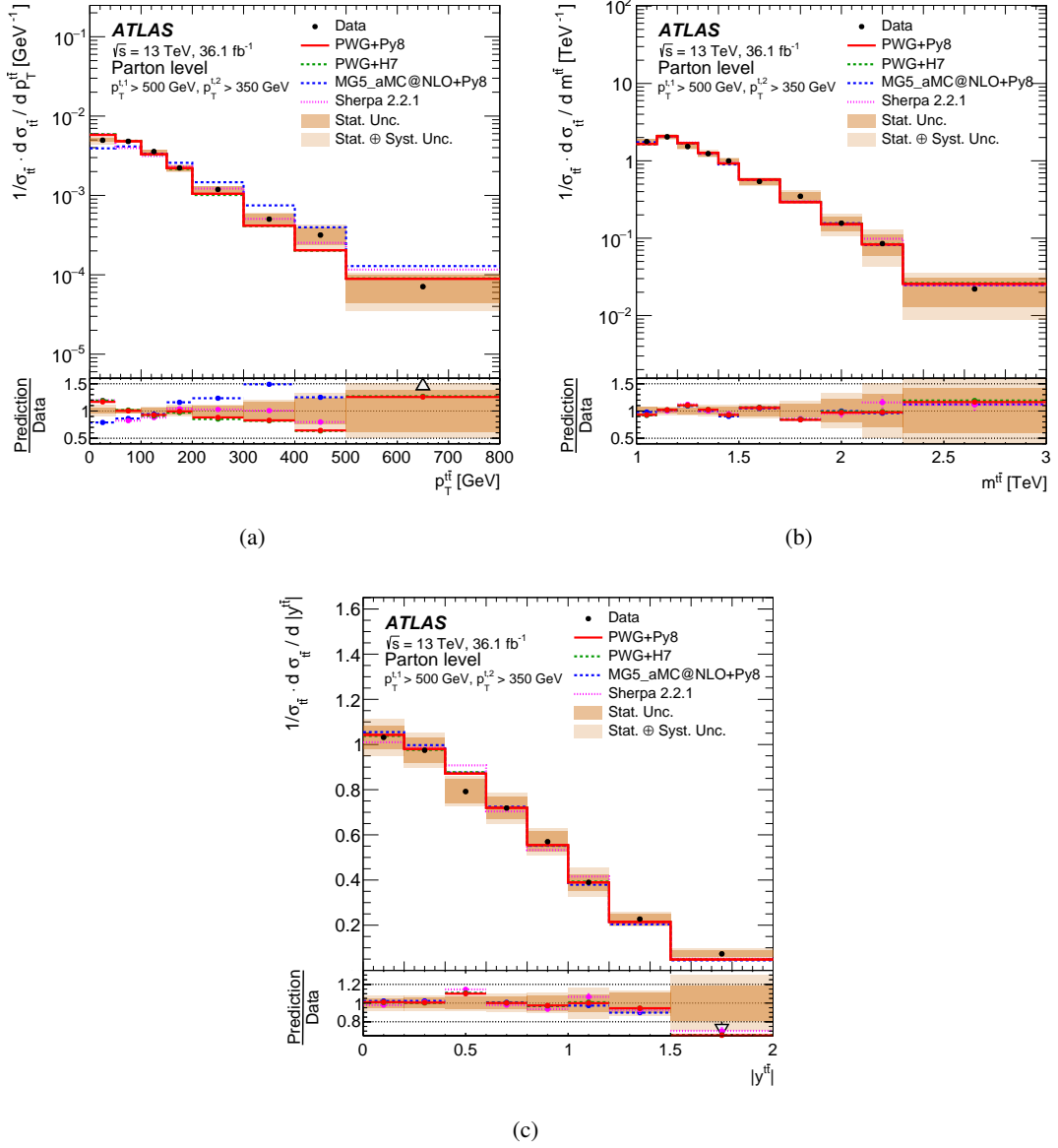


Figure 14: The normalized parton-level differential cross-sections as a function of (a) the $t\bar{t}$ p_T , (b) the $t\bar{t}$ invariant mass and (c) the absolute value of $t\bar{t}$ rapidity. The orange bands indicate the total uncertainty in the data in each bin. The vertical bars indicate the statistical uncertainties in the theoretical models. The POWHEG+PYTHIA8 event generator is used as the nominal prediction to correct for detector effects, parton showering and hadronization. Data points are placed at the center of each bin. The unfolding has required the leading top-quark $p_T > 500 \text{ GeV}$ and the second-leading top-quark $p_T > 350 \text{ GeV}$.

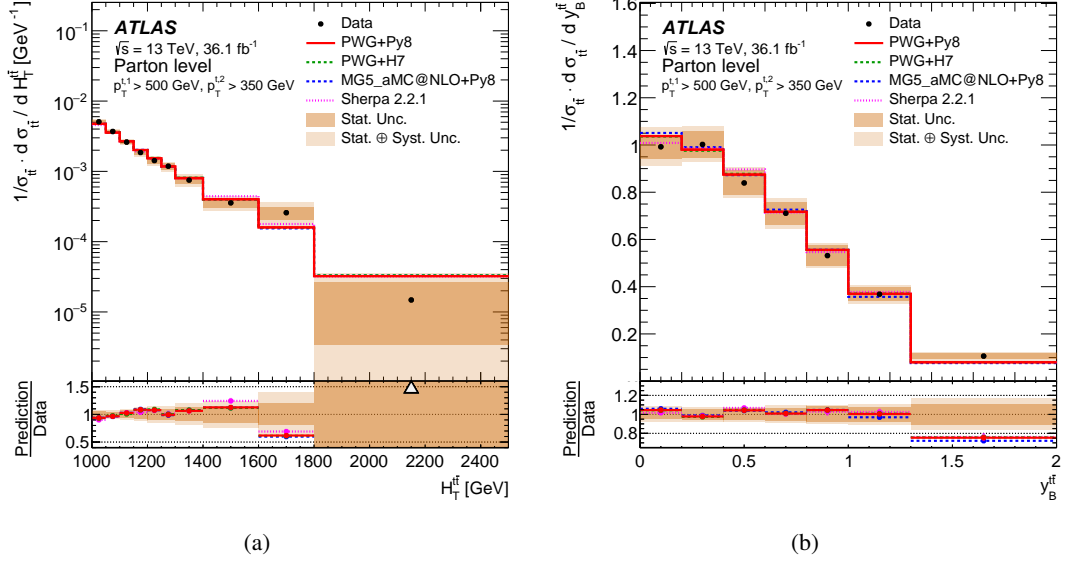


Figure 15: The normalized parton-level differential cross-sections as a function of (a) $H_T^{t\bar{t}}$ and (b) $y_B^{t\bar{t}}$. The orange bands indicate the total uncertainty in the data in each bin. The vertical bars indicate the statistical uncertainties in the theoretical models. The POWHEG+PYTHIA8 event generator is used as the nominal prediction to correct for detector effects, parton showering and hadronization. Data points are placed at the center of each bin. The unfolding has required the leading top-quark $p_T > 500$ GeV and the second-leading top-quark $p_T > 350$ GeV.

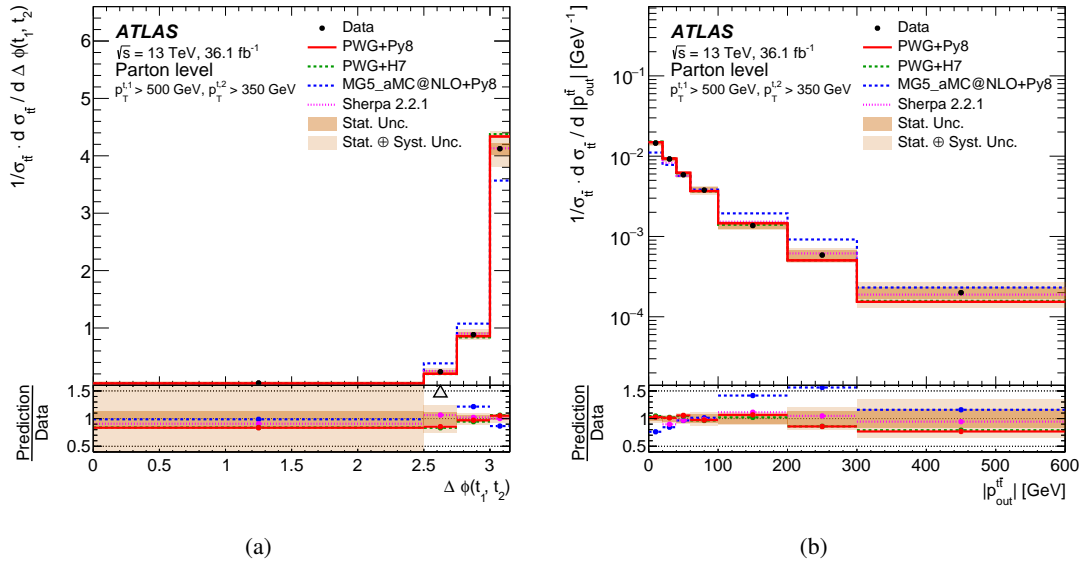


Figure 16: The normalized parton-level differential cross-sections as a function of (a) $\Delta\phi(t_1, t_2)$ and (b) $|p_{out}^{t\bar{t}}|$. The orange bands indicate the total uncertainty in the data in each bin. The vertical bars indicate the statistical uncertainties in the theoretical models. The POWHEG+PYTHIA8 event generator is used as the nominal prediction to correct for detector effects, parton showering and hadronization. Data points are placed at the center of each bin. The unfolding has required the leading top-quark $p_T > 500$ GeV and the second-leading top-quark $p_T > 350$ GeV.

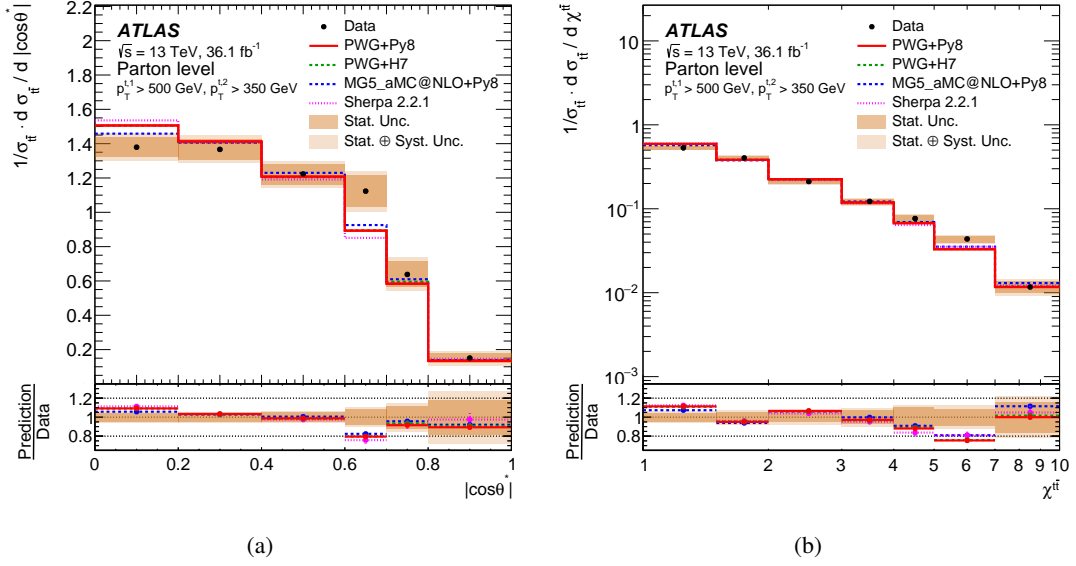


Figure 17: The normalized parton-level differential cross-sections as a function of (a) $\cos \theta^*$ and (b) $\chi^{t\bar{t}}$. The orange bands indicate the total uncertainty in the data in each bin. The vertical bars indicate the statistical uncertainties in the theoretical models. The POWHEG+PYTHIA8 event generator is used as the nominal prediction to correct for detector effects, parton showering and hadronization. Data points are placed at the center of each bin. The unfolding has required the leading top-quark $p_T > 500$ GeV and the second-leading top-quark $p_T > 350$ GeV.

8.3 Fiducial phase-space inclusive cross-section

The cross-section of $t\bar{t}$ production in the fiducial phase space defined in this analysis is determined using the same methodology employed to obtain the unfolded differential cross-sections at particle level, with the exception that all events are grouped into a single bin. The inclusive fiducial cross-section is:

$$\sigma_{\text{fid}} = 292 \pm 7 \text{ (stat)} \pm 76 \text{ (syst) fb.}$$

The systematic uncertainties in this measurement, which are dominated by tagging and modeling uncertainties, are summarized in Table 3.

The resulting inclusive fiducial cross-section measurement is shown in Fig. 18 and compared with various MC predictions. The measured value is below all of the predictions, and in particular is below the POWHEG+PYTHIA8 prediction of 384 ± 36 fb. The uncertainty in this MC prediction is the sum in quadrature of statistical, scale and PDF uncertainties, including the uncertainty in the NNLO+NNLL total cross-section prediction. The scale uncertainty is estimated by determining the envelope of predictions when the factorization μ_F and renormalization μ_R scales are varied by factors of 0.5 and 2.0. The PDF uncertainty is obtained using the PDF4LHC prescription with 30 eigenvectors. All of the predictions are normalized to the NNLO+NNLL total $t\bar{t}$ cross-section.

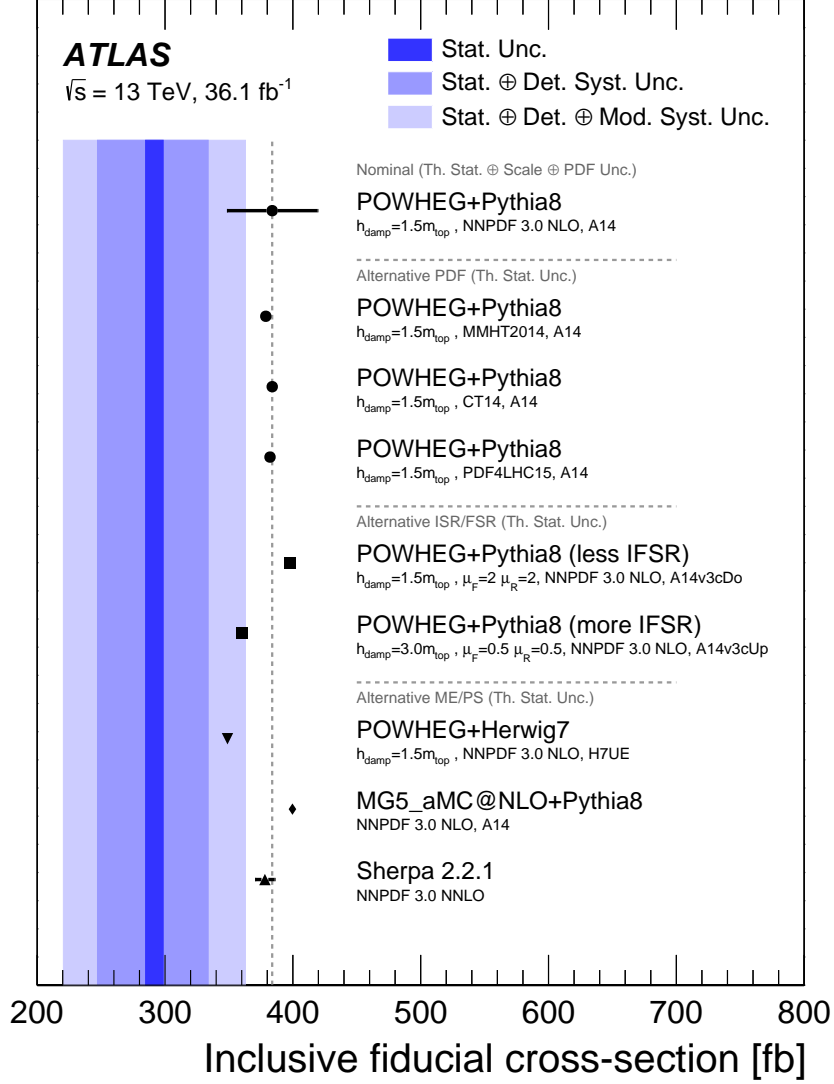


Figure 18: Particle-level fiducial phase-space cross-section. The shaded (blue) bands indicate the statistical, detector and modeling uncertainties in the measurement. The POWHEG+PYTHIA8 event generator is used as the nominal prediction to correct for detector effects. The uncertainty associated with the POWHEG+PYTHIA8 signal model is the sum in quadrature of statistical, scale and PDF uncertainties as well as the uncertainty in the inclusive cross-section prediction. Other predictions show only the statistical uncertainty of the MC sample.

9 Comparisons with Standard Model predictions

The particle-level fiducial phase-space differential cross-sections and the parton-level differential cross-sections are compared with several Standard Model calculations.

The predicted total particle-level cross-section for top-quark pair production in the fiducial phase-space region is larger than the one observed. However, the effect is not statistically significant due to the large systematic uncertainties. A better agreement is found for POWHEG+Herwig7 and to a lesser extent for the predictions of POWHEG+PYTHIA8 with more initial- and final-state radiation.

The information provided by the shapes of the observed differential cross-section measurements is compared to the predictions using the χ^2 test described in Sec. 7.2, which takes into account the correlations between the measured quantities. The largest correlations at the detector-level arise from sources of uncertainty that affect all bins equally, so that the most effective comparison is made using the normalized differential cross-sections where many of the common detector-level uncertainties largely cancel. The χ^2 values and associated p -values that quantify the level of agreement between the measurements and the predictions are shown in Table 4 for the normalized particle-level fiducial phase-space differential cross-sections and in Table 5 for the normalized parton-level differential cross-sections.

The particle-level differential cross-sections are generally well-described by the POWHEG + PYTHIA8, POWHEG + Herwig7, MG5_aMC@NLO+PYTHIA8 and SHERPA event generator predictions. The $t\bar{t}$ differential cross-section as a function of the absolute value of the leading top-quark rapidity (Fig. 7(c)) is broader in the data than the predictions of all Monte Carlo event generators. A similar effect is observed in the $t\bar{t}$ system rapidity differential cross-section (Fig. 8(c)). However, the p -values arising from the χ^2 comparisons are mostly within 0.15 to 0.55, reflecting the overall reasonable agreement of the predictions with the measured differential cross-sections. There are modest differences in the distributions of the production angle $\cos \theta^*$ (Fig. 11(a)) and the variable $\chi^{t\bar{t}}$ (Fig. 11(b)), both showing p -values that are generally below 0.2.

The most significant deviations are in the MG5_aMC@NLO particle-level fiducial phase-space differential cross-sections as a function of $p_T^{t\bar{t}}$ (Fig. 8(a)), $\Delta\phi^{t\bar{t}}$ (Fig. 10(a)) and $|p_{\text{out}}^{t\bar{t}}|$ (Fig. 10(b)) for which the MG5_aMC@NLO+PYTHIA8 MC event generator predicts a harder $p_T^{t\bar{t}}$ spectrum, a broader azimuthal opening angle differential cross-section than what is measured and a slower decline than observed as a function of $|p_{\text{out}}^{t\bar{t}}|$.

There is similar good agreement between the parton-level differential cross-sections and the POWHEG+PYTHIA8, POWHEG+Herwig7, MG5_aMC@NLO + PYTHIA8 and SHERPA predictions, confirming the results of the fiducial phase-space measurements, but with larger uncertainties. As shown in Fig. 14(a), the POWHEG+PYTHIA8 and POWHEG + Herwig7 event generators predict a softer p_T spectrum of the $t\bar{t}$ system, while the MG5_aMC@NLO + PYTHIA8 event generator predicts a harder spectrum. The SHERPA event generator offers a good description of the differential cross-section behavior for $p_T^{t\bar{t}}$ in the range 100 to 500 GeV but predicts a steeper distribution for lower momenta and a higher rate for $p_T^{t\bar{t}} > 500$ GeV than observed.

The modeling uncertainties generally play a dominant role in determining the significance of the difference between the measurements and the nominal POWHEG+PYTHIA8 prediction. It suggests that future work should seek the sources for this potential discrepancy, considering variations in parton shower and hadronization models as well as the matching of higher-order matrix elements with the parton shower model.

Table 4: Comparison between the measured normalized particle-level fiducial phase-space differential cross-sections and the predictions from several SM event generators. For each variable and prediction, a χ^2 and a p -value are calculated using the covariance matrix described in the text, which includes all sources of uncertainty. The number of degrees of freedom (NDF) is equal to $N_b - 1$, where N_b is the number of bins in the distribution.

| Observable | PWG+PY8 | | Δ MC@NLO +PY8 | | PWG+H7 | | PWG+PY8 (more IFSR) | | PWG+PY8 (less IFSR) | | SHERPA 2.2.1 | |
|-------------------------|---------------|------------|----------------------|------------|---------------|------------|------------------------|------------|------------------------|------------|---------------|------------|
| | χ^2 /NDF | p -value | χ^2 /NDF | p -value | χ^2 /NDF | p -value | χ^2 /NDF | p -value | χ^2 /NDF | p -value | χ^2 /NDF | p -value |
| $p_T^{t,1}$ | 7.7/7 | 0.36 | 8.2/7 | 0.32 | 8.0/7 | 0.33 | 9.1/7 | 0.24 | 8.7/7 | 0.27 | 9.3/7 | 0.23 |
| $ y^{t,1} $ | 7.5/5 | 0.18 | 12.2/5 | 0.03 | 6.8/5 | 0.24 | 8.8/5 | 0.12 | 8.1/5 | 0.15 | 4.0/5 | 0.55 |
| $p_T^{t,2}$ | 8.6/6 | 0.20 | 2.6/6 | 0.86 | 9.9/6 | 0.13 | 12.2/6 | 0.06 | 5.0/6 | 0.54 | 5.0/6 | 0.55 |
| $ y^{t,2} $ | 3.7/5 | 0.59 | 4.6/5 | 0.46 | 3.1/5 | 0.68 | 3.5/5 | 0.63 | 3.2/5 | 0.67 | 2.9/5 | 0.72 |
| $m^{t\bar{t}}$ | 4.5/9 | 0.88 | 4.7/9 | 0.86 | 4.0/9 | 0.91 | 5.3/9 | 0.81 | 5.2/9 | 0.82 | 10.0/9 | 0.35 |
| $p_T^{t\bar{t}}$ | 7.8/5 | 0.17 | 20.9/5 | <0.01 | 12.6/5 | 0.03 | 15.0/5 | 0.01 | 1.9/5 | 0.86 | 1.9/5 | 0.87 |
| $ y^{t\bar{t}} $ | 1.1/5 | 0.95 | 2.2/5 | 0.83 | 0.9/5 | 0.97 | 0.8/5 | 0.98 | 1.8/5 | 0.88 | 1.7/5 | 0.89 |
| $\chi^{t\bar{t}}$ | 14.2/6 | 0.03 | 12.7/6 | 0.05 | 13.6/6 | 0.03 | 16.9/6 | <0.01 | 10.1/6 | 0.12 | 18.5/6 | <0.01 |
| $y_B^{t\bar{t}}$ | 2.5/6 | 0.87 | 3.3/6 | 0.77 | 2.2/6 | 0.90 | 2.6/6 | 0.86 | 2.8/6 | 0.84 | 3.0/6 | 0.81 |
| $ p_{out}^{t\bar{t}} $ | 1.9/6 | 0.93 | 53.1/6 | <0.01 | 3.1/6 | 0.80 | 4.2/6 | 0.64 | 4.8/6 | 0.57 | 5.9/6 | 0.44 |
| $\Delta\phi^{t\bar{t}}$ | 0.9/3 | 0.84 | 16.3/3 | <0.01 | 2.0/3 | 0.58 | 3.0/3 | 0.40 | 0.6/3 | 0.89 | 3.4/3 | 0.33 |
| $H_T^{t\bar{t}}$ | 4.8/6 | 0.57 | 5.2/6 | 0.52 | 4.5/6 | 0.61 | 5.0/6 | 0.54 | 5.0/6 | 0.55 | 3.1/6 | 0.80 |
| $\cos\theta^*$ | 9.9/5 | 0.08 | 10.5/5 | 0.06 | 9.3/5 | 0.10 | 12.8/5 | 0.03 | 6.5/5 | 0.26 | 18.7/5 | <0.01 |

Table 5: Comparison between the measured normalized parton-level differential cross-sections and the predictions from several MC event generators. For each variable and prediction, a χ^2 and a p -value are calculated using the covariance matrix described in the text, which includes all sources of uncertainty. The number of degrees of freedom (NDF) is equal to $N_b - 1$, where N_b is the number of bins in the distribution.

| Observable | PWG+PY8 | | Δ MC@NLO +PY8 | | PWG+H7 | | PWG+PY8 (more IFSR) | | PWG+PY8 (less IFSR) | | SHERPA 2.2.1 | |
|-------------------------|---------------|------------|----------------------|------------|---------------|------------|------------------------|------------|------------------------|------------|---------------|------------|
| | χ^2 /NDF | p -value | χ^2 /NDF | p -value | χ^2 /NDF | p -value | χ^2 /NDF | p -value | χ^2 /NDF | p -value | χ^2 /NDF | p -value |
| p_T^t | 3.7/6 | 0.72 | 4.5/6 | 0.61 | 4.0/6 | 0.67 | 3.9/6 | 0.69 | 4.0/6 | 0.68 | 4.3/6 | 0.64 |
| $ y^t $ | 4.3/7 | 0.75 | 4.1/7 | 0.77 | 4.0/7 | 0.78 | 4.4/7 | 0.73 | 4.3/7 | 0.74 | 5.3/7 | 0.62 |
| $p_T^{t,1}$ | 5.9/7 | 0.55 | 7.0/7 | 0.43 | 5.9/7 | 0.55 | 6.4/7 | 0.50 | 6.2/7 | 0.52 | 7.6/7 | 0.37 |
| $ y^{t,1} $ | 5.5/7 | 0.60 | 8.3/7 | 0.31 | 5.1/7 | 0.65 | 5.9/7 | 0.55 | 5.5/7 | 0.60 | 4.7/7 | 0.70 |
| $p_T^{t,2}$ | 5.7/6 | 0.46 | 2.8/6 | 0.83 | 6.1/6 | 0.41 | 4.6/6 | 0.60 | 7.4/6 | 0.29 | 7.0/6 | 0.32 |
| $ y^{t,2} $ | 4.4/7 | 0.73 | 5.1/7 | 0.65 | 4.2/7 | 0.76 | 4.4/7 | 0.73 | 4.3/7 | 0.74 | 5.9/7 | 0.55 |
| $m^{t\bar{t}}$ | 4.0/9 | 0.91 | 3.7/9 | 0.93 | 3.9/9 | 0.92 | 3.9/9 | 0.92 | 4.3/9 | 0.89 | 4.6/9 | 0.86 |
| $p_T^{t\bar{t}}$ | 5.1/7 | 0.65 | 7.0/7 | 0.42 | 6.2/7 | 0.52 | 3.7/7 | 0.81 | 6.8/7 | 0.45 | 30.1/7 | <0.01 |
| $y^{t\bar{t}}$ | 1.8/7 | 0.97 | 2.9/7 | 0.90 | 2.0/7 | 0.96 | 2.0/7 | 0.96 | 1.9/7 | 0.97 | 4.2/7 | 0.76 |
| $\chi^{t\bar{t}}$ | 7.9/6 | 0.24 | 5.0/6 | 0.55 | 7.3/6 | 0.29 | 6.4/6 | 0.38 | 9.0/6 | 0.17 | 7.6/6 | 0.27 |
| $y_B^{t\bar{t}}$ | 1.0/6 | 0.99 | 1.4/6 | 0.96 | 1.0/6 | 0.98 | 1.1/6 | 0.98 | 1.0/6 | 0.99 | 1.0/6 | 0.99 |
| $ p_{out}^{t\bar{t}} $ | 1.7/6 | 0.94 | 16.9/6 | <0.01 | 1.2/6 | 0.98 | 1.9/6 | 0.93 | 2.7/6 | 0.84 | 3.9/6 | 0.69 |
| $\Delta\phi^{t\bar{t}}$ | 0.5/3 | 0.93 | 13.1/3 | <0.01 | 0.7/3 | 0.87 | 0.1/3 | 1.00 | 1.1/3 | 0.78 | 0.2/3 | 0.98 |
| $H_T^{t\bar{t}}$ | 5.2/9 | 0.81 | 5.7/9 | 0.77 | 7.4/9 | 0.60 | 6.9/9 | 0.64 | 5.6/9 | 0.78 | 5.9/9 | 0.75 |
| $\cos\theta^*$ | 5.5/5 | 0.35 | 3.2/5 | 0.66 | 5.3/5 | 0.38 | 5.0/5 | 0.42 | 6.2/5 | 0.29 | 7.8/5 | 0.17 |

These results are in agreement with earlier differential cross-section measurements in the $t\bar{t}$ final states involving at least one lepton [7–14, 16–19]. Those studies observed a “softer” p_T spectrum for the top-quark final states, although the statistical and systematic uncertainties for top quarks with $p_T > 500$ GeV are larger than the measurements reported here. Together, the previous measurements and these results provide a coherent picture that the current NLO Monte Carlo models for $t\bar{t}$ production and decay overestimate the production of highly boosted top quarks.

10 Conclusion

Measurements of differential cross-sections of highly boosted pair-produced top quarks in 13 TeV pp collisions are presented in a data sample of 36.1 fb^{-1} collected by the ATLAS detector at the LHC. The

top-quark pairs are observed in their all-hadronic decay modes. With a combination of top-tagging and b -tagging techniques, an event sample with a $t\bar{t}$ signal-to-background ratio of approximately 3-to-1 is selected. Because most of the decay products of the top quarks are observed in a large- R jet, the kinematics of the top quarks and the $t\bar{t}$ system are well-measured compared with final states involving energetic neutrinos. The measurements are corrected to a fiducial phase space and normalized to the total cross-section for events with leading top quarks with $p_T > 500$ GeV and second-leading top quarks with $p_T > 350$ GeV. Parton-level differential cross-sections are also determined.

The leading and second-leading top-quark p_T differential cross-sections fall by two orders of magnitude over the p_T range from 500 GeV to 1 TeV. The top-quark rapidity distributions show a plateau out to $|y'| \sim 0.6$ and then fall rapidly, reflecting the central production of these top-quark pairs. The measurements show that the $t\bar{t}$ system is produced centrally with limited transverse momentum, though events are observed up to a $p_T^{t\bar{t}}$ of 500 GeV.

The normalized differential cross-sections are compared with several Standard Model predictions for highly boosted pair-produced top quarks, and there is generally good agreement of the predictions with the particle-level and parton-level differential results. In particular, the POWHEG+PYTHIA8, POWHEG+HERWIG7 and SHERPA predictions are consistent with the observed differential cross-sections at particle level and parton level. The most significant discrepancy is in the aMC@NLO+PYTHIA8 predictions for the kinematics of the $t\bar{t}$ system. Qualitatively, both particle- and parton-level rapidity distributions of the leading top quark and of the $t\bar{t}$ system are broader in the data compared with the Monte Carlo generator predictions. Also, there are more modest differences between predicted and observed differential cross-sections as a function of the production angle $\cos \theta^*$ and the variable $\chi^{t\bar{t}}$.

The cross-section for $t\bar{t}$ production in the particle-level fiducial phase space is 292 ± 7 (stat) ± 76 (syst) fb, which can be compared with the POWHEG+PYTHIA8 prediction of 384 ± 36 fb, where the total cross-section has been calculated up to NNLO+NNLL corrections. Improvements in this measurement will come from a better understanding of the models of $t\bar{t}$ production that are the source of the modelling uncertainties.

This analysis shows that studies of boosted top-quark jets can be done with good efficiency and signal-to-background ratios in the all-hadronic channel. This creates opportunities for more detailed studies of high- p_T Standard Model processes, and provides data to test and improve models of $t\bar{t}$ production.

Acknowledgments

We thank CERN for the very successful operation of the LHC, as well as the support staff from our institutions without whom ATLAS could not be operated efficiently.

We acknowledge the support of ANPCyT, Argentina; YerPhI, Armenia; ARC, Australia; BMWFW and FWF, Austria; ANAS, Azerbaijan; SSTC, Belarus; CNPq and FAPESP, Brazil; NSERC, NRC and CFI, Canada; CERN; CONICYT, Chile; CAS, MOST and NSFC, China; COLCIENCIAS, Colombia; MSMT CR, MPO CR and VSC CR, Czech Republic; DNRF and DNSRC, Denmark; IN2P3-CNRS, CEA-DRF/IRFU, France; SRNSF, Georgia; BMBF, HGF, and MPG, Germany; GSRT, Greece; RGC, Hong Kong SAR, China; ISF, I-CORE and Benoziyo Center, Israel; INFN, Italy; MEXT and JSPS, Japan; CNRST, Morocco; NWO, Netherlands; RCN, Norway; MNiSW and NCN, Poland; FCT, Portugal; MNE/IFA, Romania; MES of Russia and NRC KI, Russian Federation; JINR; MESTD, Serbia; MSSR, Slovakia; ARRS and MIZŠ, Slovenia; DST/NRF, South Africa; MINECO, Spain; SRC and Wallenberg Foundation, Sweden; SERI, SNSF and Cantons of Bern and Geneva, Switzerland; MOST, Taiwan;

TAEK, Turkey; STFC, United Kingdom; DOE and NSF, United States of America. In addition, individual groups and members have received support from BCKDF, the Canada Council, CANARIE, CRC, Compute Canada, FQRNT, and the Ontario Innovation Trust, Canada; EPLANET, ERC, ERDF, FP7, Horizon 2020 and Marie Skłodowska-Curie Actions, European Union; Investissements d’Avenir Labex and Idex, ANR, Région Auvergne and Fondation Partager le Savoir, France; DFG and AvH Foundation, Germany; Herakleitos, Thales and Aristeia programmes co-financed by EU-ESF and the Greek NSRF; BSF, GIF and Minerva, Israel; BRF, Norway; CERCA Programme Generalitat de Catalunya, Generalitat Valenciana, Spain; the Royal Society and Leverhulme Trust, United Kingdom.

The crucial computing support from all WLCG partners is acknowledged gratefully, in particular from CERN, the ATLAS Tier-1 facilities at TRIUMF (Canada), NDGF (Denmark, Norway, Sweden), CC-IN2P3 (France), KIT/GridKA (Germany), INFN-CNAF (Italy), NL-T1 (Netherlands), PIC (Spain), ASGC (Taiwan), RAL (UK) and BNL (USA), the Tier-2 facilities worldwide and large non-WLCG resource providers. Major contributors of computing resources are listed in Ref. [\[82\]](#).

References

- [1] M. Czakon et al., *Top-pair production at the LHC through NNLO QCD and NLO EW*, *JHEP* **10** (2017) 186, arXiv: [1705.04105 \[hep-ph\]](#).
- [2] N. Kidonakis, *Next-to-next-to-leading soft-gluon corrections for the top quark cross section and transverse momentum distribution*, *Phys. Rev. D* **82** (2010) 114030, arXiv: [1009.4935 \[hep-ph\]](#).
- [3] V. Ahrens, A. Ferroglia, M. Neubert, B. D. Pecjak, and L. L. Yang, *Renormalization-group improved predictions for top-quark pair production at hadron colliders*, *JHEP* **09** (2010) 097, arXiv: [1003.5827](#).
- [4] C. T. Hill and S. J. Parke, *Top production: Sensitivity to new physics*, *Phys. Rev. D* **49** (1994) 4454, arXiv: [hep-ph/9312324](#).
- [5] R. Frederix and F. Maltoni, *Top pair invariant mass distribution: a window on new physics*, *JHEP* **01** (2009) 047, arXiv: [0712.2355 \[hep-ph\]](#).
- [6] B. Hespel, F. Maltoni and E. Vryonidou, *Signal background interference effects in heavy scalar production and decay to a top-anti-top pair*, *JHEP* **10** (2016) 016, arXiv: [1606.04149 \[hep-ph\]](#).
- [7] ATLAS Collaboration, *Measurements of top quark pair relative differential cross-sections with ATLAS in pp collisions at $\sqrt{s} = 7$ TeV*, *Eur. Phys. J. C* **73** (2013) 2261, arXiv: [1207.5644 \[hep-ex\]](#).
- [8] ATLAS Collaboration, *Measurements of normalized differential cross-sections for $t\bar{t}$ production in pp collisions at $\sqrt{s} = 7$ TeV using the ATLAS detector*, *Phys. Rev. D* **90** (2014) 072004, arXiv: [1407.0371 \[hep-ex\]](#).
- [9] ATLAS Collaboration, *Differential top-antitop cross-section measurements as a function of observables constructed from final-state particles using pp collisions at $\sqrt{s} = 7$ TeV in the ATLAS detector*, *JHEP* **06** (2015) 100, arXiv: [1502.05923 \[hep-ex\]](#).
- [10] ATLAS Collaboration, *Measurement of the differential cross-section of highly boosted top quarks as a function of their transverse momentum in $\sqrt{s} = 8$ TeV proton-proton collisions using the ATLAS detector*, *Phys. Rev. D* **93** (2016) 032009, arXiv: [1510.03818 \[hep-ex\]](#).
- [11] ATLAS Collaboration, *Measurements of top-quark pair differential cross-sections in the lepton+jets channel in pp collisions at $\sqrt{s} = 8$ TeV using the ATLAS detector*, *Eur. Phys. J. C* **76** (2016) 538, arXiv: [1511.04716 \[hep-ex\]](#).
- [12] ATLAS Collaboration, *Measurement of top quark pair differential cross-sections in the dilepton channel in pp collisions at $\sqrt{s} = 7$ and 8 TeV with ATLAS*, *Phys. Rev. D* **94** (2016) 092003, arXiv: [1607.07281 \[hep-ex\]](#).
- [13] ATLAS Collaboration, *Measurements of top-quark pair differential cross-sections in the $e\mu$ channel in pp collisions at $\sqrt{s} = 13$ TeV using the ATLAS detector*, *Eur. Phys. J. C* **77** (2017) 292, arXiv: [1612.05220 \[hep-ex\]](#).
- [14] ATLAS Collaboration, *Measurements of top-quark pair differential cross-sections in the lepton+jets channel in pp collisions at $\sqrt{s}=13$ TeV using the ATLAS detector*, (2017), arXiv: [1708.00727 \[hep-ex\]](#).
- [15] CMS Collaboration, *Measurement of differential top-quark-pair production cross sections in pp collisions at $\sqrt{s} = 7$ TeV*, *Eur. Phys. J. C* **73** (2013) 2339, arXiv: [1211.2220 \[hep-ex\]](#).

- [16] CMS Collaboration, *Measurement of the differential cross section for top quark pair production in pp collisions at $\sqrt{s} = 8$ TeV*, *Eur. Phys. J. C* **75** (2015) 542, arXiv: [1505.04480 \[hep-ex\]](#).
- [17] CMS Collaboration, *Measurement of the integrated and differential $t\bar{t}$ production cross sections for high- p_t top quarks in pp collisions at $\sqrt{s} = 8$ TeV*, *Phys. Rev. D* **94** (2016) 072002, arXiv: [1605.00116 \[hep-ex\]](#).
- [18] CMS Collaboration, *Measurement of differential cross sections for top quark pair production using the lepton+jets final state in proton-proton collisions at 13 TeV*, *Phys. Rev. D* **95** (2017) 092001, arXiv: [1610.04191 \[hep-ex\]](#).
- [19] CMS Collaboration, *Measurement of double-differential cross sections for top quark pair production in pp collisions at $\sqrt{s} = 8$ TeV and impact on parton distribution functions*, *Eur. Phys. J. C* **77** (2017) 459, arXiv: [1703.01630 \[hep-ex\]](#).
- [20] ATLAS Collaboration, *Search for resonances decaying into top-quark pairs using fully hadronic decays in pp collisions with ATLAS at $\sqrt{s} = 7$ TeV*, *JHEP* **01** (2013) 116, arXiv: [1211.2202 \[hep-ex\]](#).
- [21] ATLAS Collaboration, *Search for New Phenomena in Dijet Angular Distributions in Proton-Proton Collisions at $\sqrt{s} = 8$ TeV Measured with the ATLAS Detector*, *Phys. Rev. Lett.* **114** (2015) 221802, arXiv: [1504.00357 \[hep-ex\]](#).
- [22] L. Apanasevich et al., *Evidence for Parton k_T Effects in High- p_T Particle Production*, *Phys. Rev. Lett.* **81** (1998) 2642.
- [23] ATLAS Collaboration, *Search for new phenomena in dijet events using 37 fb^{-1} of pp collision data collected at $\sqrt{s} = 13$ TeV with the ATLAS detector*, *Phys. Rev. D* **96** (2017) 052004, arXiv: [1703.09127 \[hep-ex\]](#).
- [24] A. Denner, S. Dittmaier, S. Kallweit, and S. Pozzorini, *NLO QCD corrections to $WWbb$ production at hadron colliders*, *Phys. Rev. Lett.* **106** (2011) 052001, arXiv: [1012.3975 \[hep-ph\]](#).
- [25] G. Bevilacqua, M. Czakon, A. van Hameren, C. G. Papadopoulos, and M. Worek, *Complete off-shell effects in top quark pair hadroproduction with leptonic decay at next-to-leading order*, *JHEP* **02** (2011) 083, arXiv: [1012.4230 \[hep-ph\]](#).
- [26] ATLAS Collaboration, *The ATLAS Experiment at the CERN Large Hadron Collider*, *JINST* **3** (2008) S08003.
- [27] ATLAS Collaboration, *ATLAS Insertable B-Layer Technical Design Report*, ATLAS-TDR-19 (2010), URL: <https://cds.cern.ch/record/1291633>, *ATLAS Insertable B-Layer Technical Design Report Addendum*, ATLAS-TDR-19-ADD-1 (2012), URL: <http://cds.cern.ch/record/1451888>.
- [28] ATLAS Collaboration, *Performance of the ATLAS Trigger System in 2015*, *Eur. Phys. J. C* **77** (2017) 317, arXiv: [1611.09661 \[hep-ex\]](#).
- [29] T. Sjöstrand, S. Mrenna, and P. Z. Skands, *A brief introduction to PYTHIA 8.1*, *Comput. Phys. Commun.* **178** (2008) 852, arXiv: [0710.3820 \[hep-ph\]](#).
- [30] ATLAS Collaboration, *Further ATLAS tunes of PYTHIA 6 and Pythia 8*, ATL-PHYS-PUB-2011-014, 2011, URL: <https://cds.cern.ch/record/1400677>.
- [31] A. Martin, W. Stirling, R. Thorne, and G. Watt, *Parton distributions for the LHC*, *Eur. Phys. J. C* **63** (2009) 189, arXiv: [0901.0002 \[hep-ph\]](#).
- [32] S. Agostinelli et al., *GEANT4: a simulation toolkit*, *Nucl. Instrum. Methods Phys. A* **506** (2003) 250.

- [33] ATLAS Collaboration, *The ATLAS Simulation Infrastructure*, *Eur. Phys. J. C* **70** (2010) 823, arXiv: [1005.4568 \[hep-ex\]](#).
- [34] S. Frixione, P. Nason, and G. Ridolfi, *A positive-weight next-to-leading-order Monte Carlo for heavy flavour hadroproduction*, *JHEP* **09** (2007) 126, arXiv: [0707.3088 \[hep-ph\]](#).
- [35] J. Alwall, R. Frederix, S. Frixione, V. Hirschi, F. Maltoni, et al., *The automated computation of tree-level and next-to-leading order differential cross sections, and their matching to parton shower simulations*, *JHEP* **07** (2014) 079, arXiv: [1405.0301 \[hep-ph\]](#).
- [36] T. Gleisberg, S. Höche, F. Krauss, M. Schönherr, S. Schumann, et al., *Event generation with SHERPA 1.1*, *JHEP* **02** (2009) 007, arXiv: [0811.4622 \[hep-ph\]](#).
- [37] S. Hoeche, F. Krauss, M. Schonherr, and F. Siegert, *A critical appraisal of NLO+PS matching methods*, *JHEP* **09** (2012) 049, arXiv: [1111.1220 \[hep-ph\]](#).
- [38] ATLAS Collaboration, *Studies on top-quark Monte Carlo modelling for Top2016*, ATL-PHYS-PUB-2016-020, 2016, URL: <https://cds.cern.ch/record/2216168>.
- [39] S. Alioli, K. Hamilton, P. Nason, C. Oleari, and E. Re, *Jet pair production in POWHEG*, *JHEP* **04** (2011) 081, arXiv: [1012.3380 \[hep-ph\]](#).
- [40] ATLAS Collaboration, *ATLAS Pythia 8 tunes to 7 TeV data*, ATL-PHYS-PUB-2014-021, 2014, URL: <https://cds.cern.ch/record/1966419>.
- [41] R. D. Ball et al., *Parton distributions with LHC data*, *Nucl. Phys. B* **867** (2013) 244, arXiv: [1207.1303 \[hep-ph\]](#).
- [42] J. Bellm et al., *Herwig 7.0/Herwig++ 3.0 release note*, *Eur. Phys. J. C* **76** (2016) 196, arXiv: [1512.01178 \[hep-ph\]](#).
- [43] S. Höche, F. Krauss, M. Schonherr, and F. Siegert, *QCD matrix elements + parton showers: The NLO case*, *JHEP* **04** (2013) 027, arXiv: [1207.5030 \[hep-ph\]](#).
- [44] H.-L. Lai, M. Guzzi, J. Huston, Z. Li, P. M. Nadolsky, et al., *New parton distributions for collider physics*, *Phys. Rev. D* **82** (2010) 074024, arXiv: [1007.2241 \[hep-ph\]](#).
- [45] P. Artoisenet, R. Frederix, O. Mattelaer, and R. Rietkerk, *Automatic spin-entangled decays of heavy resonances in Monte Carlo simulations*, *JHEP* **03** (2013) 015, arXiv: [1212.3460 \[hep-ph\]](#).
- [46] T. Sjöstrand, S. Mrenna, and P. Z. Skands, *PYTHIA 6.4 Physics and Manual*, *JHEP* **05** (2006) 026, arXiv: [hep-ph/0603175](#).
- [47] P. Z. Skands, *Tuning Monte Carlo generators: The Perugia tunes*, *Phys. Rev. D* **82** (2010) 074018, arXiv: [1005.3457 \[hep-ph\]](#).
- [48] D. J. Lange, *The EvtGen particle decay simulation package*, *Nucl. Instrum. Meth. A* **462** (2001) 152.
- [49] M. Czakon, P. Fiedler, and A. Mitov, *Total Top-Quark Pair-Production Cross Section at Hadron Colliders Through $O(\alpha_s^4)$* , *Phys. Rev. Lett.* **110** (2013) 252004, arXiv: [1303.6254 \[hep-ph\]](#).
- [50] N. Kidonakis, *Top quark production*, 2013, arXiv: [1311.0283 \[hep-ph\]](#).
- [51] ATLAS Collaboration, *Electron efficiency measurements with the ATLAS detector using 2012 LHC proton-proton collision data*, *Eur. Phys. J. C* **77** (2017) 195, arXiv: [1612.01456 \[hep-ex\]](#).
- [52] ATLAS Collaboration, *Electron efficiency measurements with the ATLAS detector using the 2015 LHC proton-proton collision data*, ATL-CONF-2016-024 (2016), URL: <https://cds.cern.ch/record/2157687>.

- [53] ATLAS Collaboration, *Muon reconstruction performance of the ATLAS detector in proton–proton collision data at $\sqrt{s} = 13$ TeV*, [Eur. Phys. J. C **76** \(2016\) 292](#), arXiv: [1603.05598 \[hep-ex\]](#).
- [54] M. Cacciari, G. P. Salam, and G. Soyez, *The anti- k_t jet clustering algorithm*, [JHEP **04** \(2008\) 063](#), arXiv: [0802.1189 \[hep-ph\]](#).
- [55] M. Cacciari, G. P. Salam, and G. Soyez, *FastJet User Manual*, [Eur. Phys. J. C **72** \(2012\) 1896](#), arXiv: [1111.6097 \[hep-ph\]](#).
- [56] ATLAS Collaboration, *Jet energy measurement with the ATLAS detector in proton–proton collisions at $\sqrt{s} = 7$ TeV*, [Eur. Phys. J. C **73** \(2013\) 2304](#), arXiv: [1112.6426 \[hep-ex\]](#).
- [57] ATLAS Collaboration, *Jet energy measurement with the ATLAS detector in proton–proton collisions at $\sqrt{s} = 7$ TeV*, [Eur. Phys. J. C **73** \(2013\) 2304](#), arXiv: [1112.6426 \[hep-ex\]](#).
- [58] ATLAS Collaboration, *Jet energy measurement and its systematic uncertainty in proton–proton collisions at $\sqrt{s} = 7$ TeV with the ATLAS detector*, [Eur. Phys. J. C **75** \(2015\) 17](#), arXiv: [1406.0076 \[hep-ex\]](#).
- [59] ATLAS Collaboration, *Single hadron response measurement and calorimeter jet energy scale uncertainty with the ATLAS detector at the LHC*, [Eur. Phys. J. C **73** \(2013\) 2305](#), arXiv: [1203.1302 \[hep-ex\]](#).
- [60] ATLAS Collaboration, *Jet energy scale measurements and their systematic uncertainties in proton–proton collisions at $\sqrt{s} = 13$ TeV with the ATLAS detector*, [Phys. Rev. D **96** \(2017\) 072002](#), arXiv: [1703.09665 \[hep-ex\]](#).
- [61] ATLAS Collaboration, *Performance of pile-up mitigation techniques for jets in pp collisions at $\sqrt{s} = 8$ TeV using the ATLAS detector*, [Eur. Phys. J. C **76** \(2016\) 581](#), arXiv: [1510.03823 \[hep-ex\]](#).
- [62] ATLAS Collaboration, *Performance of b-jet identification in the ATLAS experiment*, [JINST **11** \(2016\) P04008](#), arXiv: [1512.01094 \[hep-ex\]](#).
- [63] ATLAS Collaboration, *Optimisation of the ATLAS b-tagging performance for the 2016 LHC Run*, ATL-PHYS-PUB-2016-012, 2016, URL: <https://cds.cern.ch/record/2160731>.
- [64] ATLAS Collaboration, *Performance of jet substructure techniques for large- R jets in proton–proton collisions at $\sqrt{s} = 7$ TeV using the ATLAS detector*, [JHEP **09** \(2013\) 076](#), arXiv: [1306.4945 \[hep-ex\]](#).
- [65] D. Krohn, J. Thaler, and L.-T. Wang, *Jet trimming*, [JHEP **02** \(2010\) 084](#), arXiv: [0912.1342 \[hep-ph\]](#).
- [66] ATLAS Collaboration, *Boosted hadronic top identification at ATLAS for early 13 TeV data*, ATL-PHYS-PUB-2015-053, 2015, URL: <https://cds.cern.ch/record/2116351>.
- [67] J. Thaler and K. V. Tilburg, *Identifying boosted objects with N -subjettiness*, [JHEP **03** \(2011\) 015](#), arXiv: [1011.2268 \[hep-ph\]](#).
- [68] J. Thaler and K. V. Tilburg, *Maximizing boosted top identification by minimizing N -subjettiness*, [JHEP **02** \(2012\) 093](#), arXiv: [1108.2701 \[hep-ph\]](#).
- [69] ATLAS Collaboration, *Measurement of the inclusive jet cross-section in proton–proton collisions at $\sqrt{s} = 7$ TeV using 4.5 fb^{-1} of data with the ATLAS detector*, [JHEP **02** \(2015\) 153](#), arXiv: [1410.8857 \[hep-ex\]](#), Erratum: [JHEP **09** \(2015\) 141](#).
- [70] ATLAS Collaboration, *ATLAS measurements of the properties of jets for boosted particle searches*, [Phys. Rev. D **86** \(2012\) 072006](#), arXiv: [1206.5369 \[hep-ex\]](#).

- [71] ATLAS Collaboration, *Jet mass reconstruction with the ATLAS Detector in early Run 2 data*, ATLAS-CONF-2016-035, 2016, URL: <https://cds.cern.ch/record/2200211>.
- [72] M. Cacciari, G. P. Salam, and G. Soyez, *The catchment area of jets*, JHEP 04 (2008) 005, arXiv: [0802.1188 \[hep-ph\]](#).
- [73] G. D’Agostini, *A Multidimensional unfolding method based on Bayes’ theorem*, Nucl. Instrum. Meth. A **362** (1995) 487.
- [74] T. Adye, *Unfolding algorithms and tests using RooUnfold*, 2011, arXiv: [1105.1160 \[physics.data-an\]](#).
- [75] Particle Data Group, C. Patrignani, et al., *Chin. Phys. C* **40** (2016) 100001, URL: <https://pdg.lbl.gov/>.
- [76] ATLAS Collaboration, *Measurement of large radius jet mass reconstruction performance at $\sqrt{s} = 8$ TeV using the ATLAS detector*, ATLAS-CONF-2016-008, 2016, URL: <https://cds.cern.ch/record/2139642>.
- [77] ATLAS Collaboration, *Jet Calibration and Systematic Uncertainties for Jets Reconstructed in the ATLAS Detector at $\sqrt{s} = 13$ TeV*, ATL-PHYS-PUB-2015-015, 2015, URL: <https://cds.cern.ch/record/2037613>.
- [78] ATLAS Collaboration, *Jet energy resolution in proton-proton collisions at $\sqrt{s} = 7$ TeV recorded in 2010 with the ATLAS detector*, Eur. Phys. J. C **73** (2013) 2306, arXiv: [1210.6210 \[hep-ex\]](#).
- [79] ATLAS Collaboration, *Electron performance measurements with the ATLAS detector using the 2010 LHC proton-proton collision data*, Eur. Phys. J. C **72** (2012) 1909, arXiv: [1110.3174 \[hep-ex\]](#).
- [80] J. Butterworth et al., *PDF4LHC recommendations for LHC Run II*, J. Phys. G **43** (2016) 023001, arXiv: [1510.03865 \[hep-ph\]](#).
- [81] ATLAS Collaboration, *Luminosity determination in pp collisions at $\sqrt{s} = 8$ TeV using the ATLAS detector at the LHC*, Eur. Phys. J. C **76** (2016) 653, arXiv: [1608.03953 \[hep-ex\]](#).
- [82] ATLAS Collaboration, *ATLAS Computing Acknowledgements 2016–2017*, ATL-GEN-PUB-2016-002, URL: <https://cds.cern.ch/record/2202407>.

The ATLAS Collaboration

M. Aaboud^{137d}, G. Aad⁸⁸, B. Abbott¹¹⁵, O. Abidinov^{12,*}, B. Abeloos¹¹⁹, S.H. Abidi¹⁶¹, O.S. AbouZeid¹³⁹, N.L. Abraham¹⁵¹, H. Abramowicz¹⁵⁵, H. Abreu¹⁵⁴, Y. Abulaiti^{148a,148b}, B.S. Acharya^{167a,167b,a}, S. Adachi¹⁵⁷, L. Adamczyk^{41a}, J. Adelman¹¹⁰, M. Adersberger¹⁰², T. Adye¹³³, A.A. Affolder¹³⁹, Y. Afik¹⁵⁴, C. Agheorghiesei^{28c}, J.A. Aguilar-Saavedra^{128a,128f}, S.P. Ahlen²⁴, F. Ahmadov^{68,b}, G. Aielli^{135a,135b}, S. Akatsuka⁷¹, H. Akerstedt^{148a,148b}, T.P.A. Åkesson⁸⁴, E. Akilli⁵², A.V. Akimov⁹⁸, G.L. Alberghi^{22a,22b}, J. Albert¹⁷², P. Albicocco⁵⁰, M.J. Alconada Verzini⁷⁴, S. Alderweireldt¹⁰⁸, M. Aleksa³², I.N. Aleksandrov⁶⁸, C. Alexa^{28b}, G. Alexander¹⁵⁵, T. Alexopoulos¹⁰, M. Alhroob¹¹⁵, B. Ali¹³⁰, M. Aliev^{76a,76b}, G. Alimonti^{94a}, J. Alison³³, S.P. Alkire³⁸, B.M.M. Allbrooke¹⁵¹, B.W. Allen¹¹⁸, P.P. Allport¹⁹, A. Aloisio^{106a,106b}, A. Alonso³⁹, F. Alonso⁷⁴, C. Alpigiani¹⁴⁰, A.A. Alshehri⁵⁶, M.I. Alstady⁸⁸, B. Alvarez Gonzalez³², D. Álvarez Piqueras¹⁷⁰, M.G. Alvigi^{106a,106b}, B.T. Amadio¹⁶, Y. Amaral Coutinho^{26a}, C. Amelung²⁵, D. Amidei⁹², S.P. Amor Dos Santos^{128a,128c}, S. Amoroso³², C. Anastopoulos¹⁴¹, L.S. Ancu⁵², N. Andari¹⁹, T. Andeen¹¹, C.F. Anders^{60b}, J.K. Anders⁷⁷, K.J. Anderson³³, A. Andreazza^{94a,94b}, V. Andrei^{60a}, S. Angelidakis³⁷, I. Angelozzi¹⁰⁹, A. Angerami³⁸, A.V. Anisenkov^{111,c}, N. Anjos¹³, A. Annovi^{126a}, C. Antel^{60a}, M. Antonelli⁵⁰, A. Antonov^{100,*}, D.J. Antrim¹⁶⁶, F. Anulli^{134a}, M. Aoki⁶⁹, L. Aperio Bella³², G. Arabidze⁹³, Y. Arai⁶⁹, J.P. Araque^{128a}, V. Araujo Ferraz^{26a}, A.T.H. Arce⁴⁸, R.E. Ardell⁸⁰, F.A. Arduh⁷⁴, J-F. Arguin⁹⁷, S. Argyropoulos⁶⁶, M. Arik^{20a}, A.J. Armbruster³², L.J. Armitage⁷⁹, O. Arnaez¹⁶¹, H. Arnold⁵¹, M. Arratia³⁰, O. Arslan²³, A. Artamonov^{99,*}, G. Artoni¹²², S. Artz⁸⁶, S. Asai¹⁵⁷, N. Asbah⁴⁵, A. Ashkenazi¹⁵⁵, L. Asquith¹⁵¹, K. Assamagan²⁷, R. Astalos^{146a}, M. Atkinson¹⁶⁹, N.B. Atlay¹⁴³, K. Augsten¹³⁰, G. Avolio³², B. Axen¹⁶, M.K. Ayoub^{35a}, G. Azuelos^{97,d}, A.E. Baas^{60a}, M.J. Baca¹⁹, H. Bachacou¹³⁸, K. Bachas^{76a,76b}, M. Backes¹²², P. Bagnaia^{134a,134b}, M. Bahmani⁴², H. Bahrasemani¹⁴⁴, J.T. Baines¹³³, M. Bajic³⁹, O.K. Baker¹⁷⁹, P.J. Bakker¹⁰⁹, E.M. Baldin^{111,c}, P. Balek¹⁷⁵, F. Balli¹³⁸, W.K. Balunas¹²⁴, E. Banas⁴², A. Bandyopadhyay²³, Sw. Banerjee^{176,e}, A.A.E. Bannoura¹⁷⁷, L. Barak¹⁵⁵, E.L. Barberio⁹¹, D. Barberis^{53a,53b}, M. Barbero⁸⁸, T. Barillari¹⁰³, M-S Barisits⁶⁵, J.T. Barkeloo¹¹⁸, T. Barklow¹⁴⁵, N. Barlow³⁰, S.L. Barnes^{36b}, B.M. Barnett¹³³, R.M. Barnett¹⁶, Z. Barnovska-Blenessy^{36c}, A. Baroncelli^{136a}, G. Barone²⁵, A.J. Barr¹²², L. Barranco Navarro¹⁷⁰, F. Barreiro⁸⁵, J. Barreiro Guimarães da Costa^{35a}, R. Bartoldus¹⁴⁵, A.E. Barton⁷⁵, P. Bartos^{146a}, A. Basalaev¹²⁵, A. Bassalat^{119,f}, R.L. Bates⁵⁶, S.J. Batista¹⁶¹, J.R. Batley³⁰, M. Battaglia¹³⁹, M. Bauce^{134a,134b}, F. Bauer¹³⁸, K.T. Bauer¹⁶⁶, H.S. Bawa^{145,g}, J.B. Beacham¹¹³, M.D. Beattie⁷⁵, T. Beau⁸³, P.H. Beauchemin¹⁶⁵, P. Bechtel²³, H.P. Beck^{18,h}, H.C. Beck⁵⁸, K. Becker¹²², M. Becker⁸⁶, C. Becot¹¹², A.J. Beddall^{20e}, A. Beddall^{20b}, V.A. Bednyakov⁶⁸, M. Bedognetti¹⁰⁹, C.P. Bee¹⁵⁰, T.A. Beermann³², M. Begalli^{26a}, M. Biegel²⁷, J.K. Behr⁴⁵, A.S. Bell⁸¹, G. Bella¹⁵⁵, L. Bellagamba^{22a}, A. Bellerive³¹, M. Bellomo¹⁵⁴, K. Belotskiy¹⁰⁰, O. Beltramello³², N.L. Belyaev¹⁰⁰, O. Benary^{155,*}, D. Benckekroun^{137a}, M. Bender¹⁰², N. Benekos¹⁰, Y. Benhammou¹⁵⁵, E. Benhar Noccioli¹⁷⁹, J. Benitez⁶⁶, D.P. Benjamin⁴⁸, M. Benoit⁵², J.R. Bensinger²⁵, S. Bentvelsen¹⁰⁹, L. Beresford¹²², M. Beretta⁵⁰, D. Berge¹⁰⁹, E. Bergeaas Kuutmann¹⁶⁸, N. Berger⁵, L.J. Bergsten²⁵, J. Beringer¹⁶, S. Berlendis⁵⁷, N.R. Bernard⁸⁹, G. Bernardi⁸³, C. Bernius¹⁴⁵, F.U. Bernlochner²³, T. Berry⁸⁰, P. Berta⁸⁶, C. Bertella^{35a}, G. Bertoli^{148a,148b}, I.A. Bertram⁷⁵, C. Bertsche⁴⁵, G.J. Besjes³⁹, O. Bessidskaia Bylund^{148a,148b}, M. Bessner⁴⁵, N. Besson¹³⁸, A. Bethani⁸⁷, S. Bethke¹⁰³, A. Betti²³, A.J. Bevan⁷⁹, J. Beyer¹⁰³, R.M. Bianchi¹²⁷, O. Biebel¹⁰², D. Biedermann¹⁷, R. Bielski⁸⁷, K. Bierwagen⁸⁶, N.V. Biesuz^{126a,126b}, M. Biglietti^{136a}, T.R.V. Billoud⁹⁷, H. Bilokon⁵⁰, M. Bindi⁵⁸, A. Bingul^{20b}, C. Bini^{134a,134b}, S. Biondi^{22a,22b}, T. Bisanz⁵⁸, C. Bittrich⁴⁷, D.M. Bjergaard⁴⁸, J.E. Black¹⁴⁵, K.M. Black²⁴, R.E. Blair⁶, T. Blazek^{146a}, I. Bloch⁴⁵, C. Blocker²⁵, A. Blue⁵⁶, U. Blumenschein⁷⁹, Dr. Blunier^{34a}, G.J. Bobbink¹⁰⁹, V.S. Bobrovnikov^{111,c}, S.S. Bocchetta⁸⁴,

A. Bocci⁴⁸, C. Bock¹⁰², M. Boehler⁵¹, D. Boerner¹⁷⁷, D. Bogavac¹⁰², A.G. Bogdanchikov¹¹¹,
 C. Bohm^{148a}, V. Boisvert⁸⁰, P. Bokan^{168,i}, T. Bold^{41a}, A.S. Boldyrev¹⁰¹, A.E. Bolz^{60b}, M. Bomben⁸³,
 M. Bona⁷⁹, J.S. Bonilla¹¹⁸, M. Boonekamp¹³⁸, A. Borisov¹³², G. Borissov⁷⁵, J. Bortfeldt³²,
 D. Bortoletto¹²², V. Bortolotto^{62a}, D. Boscherini^{22a}, M. Bosman¹³, J.D. Bossio Sola²⁹, J. Boudreau¹²⁷,
 E.V. Bouhova-Thacker⁷⁵, D. Boumediene³⁷, C. Bourdarios¹¹⁹, S.K. Boutle⁵⁶, A. Boveia¹¹³, J. Boyd³²,
 I.R. Boyko⁶⁸, A.J. Bozson⁸⁰, J. Bracinik¹⁹, A. Brandt⁸, G. Brandt¹⁷⁷, O. Brandt^{60a}, F. Braren⁴⁵,
 U. Bratzler¹⁵⁸, B. Brau⁸⁹, J.E. Brau¹¹⁸, W.D. Breaden Madden⁵⁶, K. Brendlinger⁴⁵, A.J. Brennan⁹¹,
 L. Brenner¹⁰⁹, R. Brenner¹⁶⁸, S. Bressler¹⁷⁵, D.L. Briglin¹⁹, T.M. Bristow⁴⁹, D. Britton⁵⁶,
 D. Britzger^{60b}, I. Brock²³, R. Brock⁹³, G. Brooijmans³⁸, T. Brooks⁸⁰, W.K. Brooks^{34b}, E. Brost¹¹⁰,
 J.H. Broughton¹⁹, P.A. Bruckman de Renstrom⁴², D. Bruncko^{146b}, A. Bruni^{22a}, G. Bruni^{22a},
 L.S. Bruni¹⁰⁹, S. Bruno^{135a,135b}, B.H. Brunt³⁰, M. Bruschi^{22a}, N. Bruscino¹²⁷, P. Bryant³³,
 L. Bryngemark⁴⁵, T. Buanes¹⁵, Q. Buat¹⁴⁴, P. Buchholz¹⁴³, A.G. Buckley⁵⁶, I.A. Budagov⁶⁸,
 F. Buehrer⁵¹, M.K. Bugge¹²¹, O. Bulekov¹⁰⁰, D. Bullock⁸, T.J. Burch¹¹⁰, S. Burdin⁷⁷, C.D. Burgard¹⁰⁹,
 A.M. Burger⁵, B. Burghgrave¹¹⁰, K. Burka⁴², S. Burke¹³³, I. Burmeister⁴⁶, J.T.P. Burr¹²², D. Büscher⁵¹,
 V. Büscher⁸⁶, E. Buschmann⁵⁸, P. Bussey⁵⁶, J.M. Butler²⁴, C.M. Buttar⁵⁶, J.M. Butterworth⁸¹, P. Butti³²,
 W. Buttinger²⁷, A. Buzatu¹⁵³, A.R. Buzykaev^{111,c}, S. Cabrera Urbán¹⁷⁰, D. Caforio¹³⁰, H. Cai¹⁶⁹,
 V.M.M. Cairo², O. Cakir^{4a}, N. Calace⁵², P. Calafiura¹⁶, A. Calandri⁸⁸, G. Calderini⁸³, P. Calfayan⁶⁴,
 G. Callea^{40a,40b}, L.P. Caloba^{26a}, S. Calvente Lopez⁸⁵, D. Calvet³⁷, S. Calvet³⁷, T.P. Calvet⁸⁸,
 R. Camacho Toro³³, S. Camarda³², P. Camarri^{135a,135b}, D. Cameron¹²¹, R. Caminal Armadans¹⁶⁹,
 C. Camincher⁵⁷, S. Campana³², M. Campanelli⁸¹, A. Camplani^{94a,94b}, A. Campoverde¹⁴³,
 V. Canale^{106a,106b}, M. Cano Bret^{36b}, J. Cantero¹¹⁶, T. Cao¹⁵⁵, M.D.M. Capeans Garrido³², I. Caprini^{28b},
 M. Caprini^{28b}, M. Capua^{40a,40b}, R.M. Carbone³⁸, R. Cardarelli^{135a}, F. Cardillo⁵¹, I. Carli¹³¹, T. Carli³²,
 G. Carlino^{106a}, B.T. Carlson¹²⁷, L. Carminati^{94a,94b}, R.M.D. Carney^{148a,148b}, S. Caron¹⁰⁸, E. Carquin^{34b},
 S. Carrá^{94a,94b}, G.D. Carrillo-Montoya³², D. Casadei¹⁹, M.P. Casado^{13,j}, A.F. Casha¹⁶¹, M. Casolino¹³,
 D.W. Casper¹⁶⁶, R. Castelijns¹⁰⁹, V. Castillo Gimenez¹⁷⁰, N.F. Castro^{128a}, A. Catinaccio³²,
 J.R. Catmore¹²¹, A. Cattai³², J. Caudron²³, V. Cavaliere¹⁶⁹, E. Cavallaro¹³, D. Cavalli^{94a},
 M. Cavalli-Sforza¹³, V. Cavasinni^{126a,126b}, E. Celebi^{20d}, F. Ceradini^{136a,136b}, L. Cerda Alberich¹⁷⁰,
 A.S. Cerqueira^{26b}, A. Cerri¹⁵¹, L. Cerrito^{135a,135b}, F. Cerutti¹⁶, A. Cervelli^{22a,22b}, S.A. Cetin^{20d},
 A. Chafaq^{137a}, D. Chakraborty¹¹⁰, S.K. Chan⁵⁹, W.S. Chan¹⁰⁹, Y.L. Chan^{62a}, P. Chang¹⁶⁹,
 J.D. Chapman³⁰, D.G. Charlton¹⁹, C.C. Chau³¹, C.A. Chavez Barajas¹⁵¹, S. Che¹¹³,
 S. Cheatham^{167a,167c}, A. Chegwidan⁹³, S. Chekanov⁶, S.V. Chekulaev^{163a}, G.A. Chelkov^{68,k},
 M.A. Chelstowska³², C. Chen^{36c}, C. Chen⁶⁷, H. Chen²⁷, J. Chen^{36c}, J. Chen³⁸, S. Chen^{35b}, S. Chen¹⁵⁷,
 X. Chen^{35c,l}, Y. Chen⁷⁰, H.C. Cheng⁹², H.J. Cheng^{35a,35d}, A. Cheplakov⁶⁸, E. Cheremushkina¹³²,
 R. Cherkaoui El Moursli^{137e}, E. Cheu⁷, K. Cheung⁶³, L. Chevalier¹³⁸, V. Chiarella⁵⁰, G. Chiarelli^{126a},
 G. Chiodini^{76a}, A.S. Chisholm³², A. Chitan^{28b}, Y.H. Chiu¹⁷², M.V. Chizhov⁶⁸, K. Choi⁶⁴,
 A.R. Chomont³⁷, S. Chouridou¹⁵⁶, Y.S. Chow^{62a}, V. Christodoulou⁸¹, M.C. Chu^{62a}, J. Chudoba¹²⁹,
 A.J. Chuinard⁹⁰, J.J. Chwastowski⁴², L. Chytka¹¹⁷, A.K. Ciftci^{4a}, D. Cinca⁴⁶, V. Cindro⁷⁸, I.A. Cioară²³,
 A. Ciocio¹⁶, F. Ciotto^{106a,106b}, Z.H. Citron¹⁷⁵, M. Citterio^{94a}, M. Ciubancan^{28b}, A. Clark⁵²,
 M.R. Clark³⁸, P.J. Clark⁴⁹, R.N. Clarke¹⁶, C. Clement^{148a,148b}, Y. Coadou⁸⁸, M. Cokal^{167a,167c},
 A. Coccaro⁵², J. Cochran⁶⁷, L. Colasurdo¹⁰⁸, B. Cole³⁸, A.P. Colijn¹⁰⁹, J. Collot⁵⁷, T. Colombo¹⁶⁶,
 P. Conde Muiño^{128a,128b}, E. Coniavitis⁵¹, S.H. Connell^{147b}, I.A. Connelly⁸⁷, S. Constantinescu^{28b},
 G. Conti³², F. Conventi^{106a,m}, A.M. Cooper-Sarkar¹²², F. Cormier¹⁷¹, K.J.R. Cormier¹⁶¹,
 M. Corradi^{134a,134b}, E.E. Corrigan⁸⁴, F. Corriveau^{90,n}, A. Cortes-Gonzalez³², G. Costa^{94a}, M.J. Costa¹⁷⁰,
 D. Costanzo¹⁴¹, G. Cottin³⁰, G. Cowan⁸⁰, B.E. Cox⁸⁷, K. Cranmer¹¹², S.J. Crawley⁵⁶, R.A. Creager¹²⁴,
 G. Cree³¹, S. Crépe-Renaudin⁵⁷, F. Crescioli⁸³, W.A. Cribbs^{148a,148b}, M. Cristinziani²³, V. Croft¹¹²,
 G. Crosetti^{40a,40b}, A. Cueto⁸⁵, T. Cuhadar Donszelmann¹⁴¹, A.R. Cukierman¹⁴⁵, J. Cummings¹⁷⁹,
 M. Curatolo⁵⁰, J. Cúth⁸⁶, S. Czekierda⁴², P. Czodrowski³², G. D'amen^{22a,22b}, S. D'Auria⁵⁶,

L. D'era⁸³, M. D'Onofrio⁷⁷, M.J. Da Cunha Sargedas De Sousa^{128a,128b}, C. Da Via⁸⁷,
 W. Dabrowski^{41a}, T. Dado^{146a}, T. Dai⁹², O. Dale¹⁵, F. Dallaire⁹⁷, C. Dallapiccola⁸⁹, M. Dam³⁹,
 J.R. Dandoy¹²⁴, M.F. Daneri²⁹, N.P. Dang^{176,e}, N.S. Dann⁸⁷, M. Danninger¹⁷¹, M. Dano Hoffmann¹³⁸,
 V. Dao¹⁵⁰, G. Darbo^{53a}, S. Darmora⁸, J. Dassoulas³, A. Dattagupta¹¹⁸, T. Daubney⁴⁵, W. Davey²³,
 C. David⁴⁵, T. Davidek¹³¹, D.R. Davis⁴⁸, P. Davison⁸¹, E. Dawe⁹¹, I. Dawson¹⁴¹, K. De⁸,
 R. de Asmundis^{106a}, A. De Benedetti¹¹⁵, S. De Castro^{22a,22b}, S. De Cecco⁸³, N. De Groot¹⁰⁸,
 P. de Jong¹⁰⁹, H. De la Torre⁹³, F. De Lorenzi⁶⁷, A. De Maria⁵⁸, D. De Pedis^{134a}, A. De Salvo^{134a},
 U. De Sanctis^{135a,135b}, A. De Santo¹⁵¹, K. De Vasconcelos Corga⁸⁸, J.B. De Vivie De Regie¹¹⁹,
 R. Debbe²⁷, C. Debenedetti¹³⁹, D.V. Dedovich⁶⁸, N. Dehghanian³, I. Deigaard¹⁰⁹, M. Del Gaudio^{40a,40b},
 J. Del Peso⁸⁵, D. Delgove¹¹⁹, F. Deliot¹³⁸, C.M. Delitzsch⁷, A. Dell'Acqua³², L. Dell'Asta²⁴,
 M. Della Pietra^{106a,106b}, D. della Volpe⁵², M. Delmastro⁵, C. Delporte¹¹⁹, P.A. Delsart⁵⁷,
 D.A. DeMarco¹⁶¹, S. Demers¹⁷⁹, M. Demichev⁶⁸, A. Demilly⁸³, S.P. Denisov¹³², D. Denysiuk¹³⁸,
 D. Derendarz⁴², J.E. Derkaoui^{137d}, F. Derue⁸³, P. Dervan⁷⁷, K. Desch²³, C. Deterre⁴⁵, K. Dette¹⁶¹,
 M.R. Devesa²⁹, P.O. Deviveiros³², A. Dewhurst¹³³, S. Dhaliwal²⁵, F.A. Di Bello⁵²,
 A. Di Ciaccio^{135a,135b}, L. Di Ciaccio⁵, W.K. Di Clemente¹²⁴, C. Di Donato^{106a,106b}, A. Di Girolamo³²,
 B. Di Girolamo³², B. Di Micco^{136a,136b}, R. Di Nardo³², K.F. Di Petrillo⁵⁹, A. Di Simone⁵¹,
 R. Di Sipio¹⁶¹, D. Di Valentino³¹, C. Diaconu⁸⁸, M. Diamond¹⁶¹, F.A. Dias³⁹, M.A. Diaz^{34a},
 J. Dickinson¹⁶, E.B. Diehl⁹², J. Dietrich¹⁷, S. Díez Cornell⁴⁵, A. Dimitrievska¹⁶, J. Dingfelder²³,
 P. Dita^{28b}, S. Dita^{28b}, F. Dittus³², F. Djama⁸⁸, T. Djobava^{54b}, J.I. Djuvsland^{60a}, M.A.B. do Vale^{26c},
 M. Dobre^{28b}, D. Dodsworth²⁵, C. Doglioni⁸⁴, J. Dolejsi¹³¹, Z. Dolezal¹³¹, M. Donadelli^{26d},
 S. Donati^{126a,126b}, J. Donini³⁷, J. Dopke¹³³, A. Doria^{106a}, M.T. Dova⁷⁴, A.T. Doyle⁵⁶, E. Drechsler⁵⁸,
 M. Dris¹⁰, Y. Du^{36a}, J. Duarte-Camperderros¹⁵⁵, F. Dubinin⁹⁸, A. Dubreuil⁵², E. Duchovni¹⁷⁵,
 G. Duckeck¹⁰², A. Ducourthial⁸³, O.A. Ducu^{97,o}, D. Duda¹⁰⁹, A. Dudarev³², A.Ch. Dudder⁸⁶,
 E.M. Duffield¹⁶, L. Duflot¹¹⁹, M. Dührssen³², C. Dulsen¹⁷⁷, M. Dumancic¹⁷⁵, A.E. Dumitriu^{28b,p},
 A.K. Duncan⁵⁶, M. Dunford^{60a}, A. Duperrin⁸⁸, H. Duran Yildiz^{4a}, M. Düren⁵⁵, A. Durglishvili^{54b},
 D. Duschinger⁴⁷, B. Dutta⁴⁵, D. Duvnjak¹, M. Dyndal⁴⁵, B.S. Dziedzic⁴², C. Eckardt⁴⁵, K.M. Ecker¹⁰³,
 R.C. Edgar⁹², T. Eifert³², G. Eigen¹⁵, K. Einsweiler¹⁶, T. Ekelof¹⁶⁸, M. El Kacimi^{137c}, R. El Kosseifi⁸⁸,
 V. Ellajosyula⁸⁸, M. Ellert¹⁶⁸, S. Elles⁵, F. Ellinghaus¹⁷⁷, A.A. Elliot¹⁷², N. Ellis³², J. Elmsheuser²⁷,
 M. Elsing³², D. Emelianov¹³³, Y. Enari¹⁵⁷, J.S. Ennis¹⁷³, M.B. Epland⁴⁸, J. Erdmann⁴⁶, A. Ereditato¹⁸,
 M. Ernst²⁷, S. Errede¹⁶⁹, M. Escalier¹¹⁹, C. Escobar¹⁷⁰, B. Esposito⁵⁰, O. Estrada Pastor¹⁷⁰,
 A.I. Etienne¹³⁸, E. Etzion¹⁵⁵, H. Evans⁶⁴, A. Ezhilov¹²⁵, M. Ezzi^{137e}, F. Fabbri^{22a,22b}, L. Fabbri^{22a,22b},
 V. Fabiani¹⁰⁸, G. Facini⁸¹, R.M. Fakhruddinov¹³², S. Falciano^{134a}, R.J. Falla⁸¹, J. Faltova³², Y. Fang^{35a},
 M. Fanti^{94a,94b}, A. Farbin⁸, A. Farilla^{136a}, E.M. Farina^{123a,123b}, T. Farooque⁹³, S. Farrell¹⁶,
 S.M. Farrington¹⁷³, P. Farthouat³², F. Fassi^{137e}, P. Fassnacht³², D. Fassouliotis⁹, M. Fauci Giannelli⁴⁹,
 A. Favareto^{53a,53b}, W.J. Fawcett¹²², L. Fayard¹¹⁹, O.L. Fedin^{125,q}, W. Fedorko¹⁷¹, S. Feigl¹²¹,
 L. Feligioni⁸⁸, C. Feng^{36a}, E.J. Feng³², M. Feng⁴⁸, M.J. Fenton⁵⁶, A.B. Fenyuk¹³², L. Feremenga⁸,
 P. Fernandez Martinez¹⁷⁰, J. Ferrando⁴⁵, A. Ferrari¹⁶⁸, P. Ferrari¹⁰⁹, R. Ferrari^{123a},
 D.E. Ferreira de Lima^{60b}, A. Ferrer¹⁷⁰, D. Ferrere⁵², C. Ferretti⁹², F. Fiedler⁸⁶, A. Filipčič⁷⁸,
 M. Filipuzzi⁴⁵, F. Filthaut¹⁰⁸, M. Fincke-Keeler¹⁷², K.D. Finelli²⁴, M.C.N. Fiolhais^{128a,128c,r},
 L. Fiorini¹⁷⁰, C. Fischer¹³, J. Fischer¹⁷⁷, W.C. Fisher⁹³, N. Flaschel⁴⁵, I. Fleck¹⁴³, P. Fleischmann⁹²,
 R.R.M. Fletcher¹²⁴, T. Flick¹⁷⁷, B.M. Flierl¹⁰², L.R. Flores Castillo^{62a}, N. Fomin¹⁵, G.T. Forcolin⁸⁷,
 A. Formica¹³⁸, F.A. Förster¹³, A. Forti⁸⁷, A.G. Foster¹⁹, D. Fournier¹¹⁹, H. Fox⁷⁵, S. Fracchia¹⁴¹,
 P. Francavilla^{126a,126b}, M. Franchini^{22a,22b}, S. Franchino^{60a}, D. Francis³², L. Franconi¹²¹, M. Franklin⁵⁹,
 M. Frate¹⁶⁶, M. Fraternali^{123a,123b}, D. Freeborn⁸¹, S.M. Fressard-Batraneanu³², B. Freund⁹⁷,
 W.S. Freund^{26a}, D. Froidevaux³², J.A. Frost¹²², C. Fukunaga¹⁵⁸, T. Fusayasu¹⁰⁴, J. Fuster¹⁷⁰,
 O. Gabizon¹⁵⁴, A. Gabrielli^{22a,22b}, A. Gabrielli¹⁶, G.P. Gach^{41a}, S. Gadatsch³², S. Gadomski⁸⁰,
 G. Gagliardi^{53a,53b}, L.G. Gagnon⁹⁷, C. Galea¹⁰⁸, B. Galhardo^{128a,128c}, E.J. Gallas¹²², B.J. Gallop¹³³,

P. Gallus¹³⁰, G. Galster³⁹, K.K. Gan¹¹³, S. Ganguly¹⁷⁵, Y. Gao⁷⁷, Y.S. Gao^{145,g}, F.M. Garay Walls^{34a}, C. García¹⁷⁰, J.E. García Navarro¹⁷⁰, J.A. García Pascual^{35a}, M. Garcia-Sciveres¹⁶, R.W. Gardner³³, N. Garelli¹⁴⁵, V. Garonne¹²¹, A. Gascon Bravo⁴⁵, K. Gasnikova⁴⁵, C. Gatti⁵⁰, A. Gaudiello^{53a,53b}, G. Gaudio^{123a}, I.L. Gavrilenko⁹⁸, C. Gay¹⁷¹, G. Gaycken²³, E.N. Gazis¹⁰, C.N.P. Gee¹³³, J. Geisen⁵⁸, M. Geisen⁸⁶, M.P. Geisler^{60a}, K. Gellerstedt^{148a,148b}, C. Gemme^{53a}, M.H. Genest⁵⁷, C. Geng⁹², S. Gentile^{134a,134b}, C. Gentsos¹⁵⁶, S. George⁸⁰, D. Gerbaudo¹³, G. Geßner⁴⁶, S. Ghasemi¹⁴³, M. Ghneimat²³, B. Giacobbe^{22a}, S. Giagu^{134a,134b}, N. Giangiacomi^{22a,22b}, P. Giannetti^{126a}, S.M. Gibson⁸⁰, M. Gignac¹⁷¹, M. Gilchriese¹⁶, D. Gillberg³¹, G. Gilles¹⁷⁷, D.M. Gingrich^{3,d}, M.P. Giordani^{167a,167c}, F.M. Giorgi^{22a}, P.F. Giraud¹³⁸, P. Giromini⁵⁹, G. Giugliarelli^{167a,167c}, D. Giugni^{94a}, F. Giuli¹²², M. Giulini^{60b}, B.K. Gjølsten¹²¹, S. Gkaitatzis¹⁵⁶, I. Gkialas^{9,s}, E.L. Gkougkousis¹³, P. Gkoutoumis¹⁰, L.K. Gladilin¹⁰¹, C. Glasman⁸⁵, J. Glatzer¹³, P.C.F. Glaysheer⁴⁵, A. Glazov⁴⁵, M. Goblirsch-Kolb²⁵, J. Godlewski⁴², S. Goldfarb⁹¹, T. Golling⁵², D. Golubkov¹³², A. Gomes^{128a,128b,128d}, R. Gonçalves^{128a}, R. Goncalves Gama^{26a}, J. Goncalves Pinto Firmino Da Costa¹³⁸, G. Gonella⁵¹, L. Gonella¹⁹, A. Gongadze⁶⁸, F. Gonnella¹⁹, J.L. Gonski⁵⁹, S. González de la Hoz¹⁷⁰, S. Gonzalez-Sevilla⁵², L. Goossens³², P.A. Gorbounov⁹⁹, H.A. Gordon²⁷, B. Gorini³², E. Gorini^{76a,76b}, A. Gorišek⁷⁸, A.T. Goshaw⁴⁸, C. Gössling⁴⁶, M.I. Gostkin⁶⁸, C.A. Gottardo²³, C.R. Goudet¹¹⁹, D. Goujdami^{137c}, A.G. Goussiou¹⁴⁰, N. Govender^{147b,t}, C. Goy⁵, E. Gozani¹⁵⁴, I. Grabowska-Bold^{41a}, P.O.J. Gradin¹⁶⁸, E.C. Graham⁷⁷, J. Gramling¹⁶⁶, E. Gramstad¹²¹, S. Grancagnolo¹⁷, V. Gratchev¹²⁵, P.M. Gravila^{28f}, C. Gray⁵⁶, H.M. Gray¹⁶, Z.D. Greenwood^{82,u}, C. Grefe²³, K. Gregersen⁸¹, I.M. Gregor⁴⁵, P. Grenier¹⁴⁵, K. Grevtsov⁵, J. Griffiths⁸, A.A. Grillo¹³⁹, K. Grimm⁷⁵, S. Grinstein^{13,v}, Ph. Gris³⁷, J.-F. Grivaz¹¹⁹, S. Groh⁸⁶, E. Gross¹⁷⁵, J. Grosse-Knetter⁵⁸, G.C. Grossi⁸², Z.J. Grout⁸¹, A. Grummer¹⁰⁷, L. Guan⁹², W. Guan¹⁷⁶, J. Guenther³², F. Guescini^{163a}, D. Guest¹⁶⁶, O. Gueta¹⁵⁵, B. Gui¹¹³, E. Guido^{53a,53b}, T. Guillemin⁵, S. Guindon³², U. Gul⁵⁶, C. Gumpert³², J. Guo^{36b}, W. Guo⁹², Y. Guo^{36c,w}, R. Gupta⁴³, S. Gurbuz^{20a}, G. Gustavino¹¹⁵, B.J. Gutelman¹⁵⁴, P. Gutierrez¹¹⁵, N.G. Gutierrez Ortiz⁸¹, C. Gutsche⁸¹, C. Guyot¹³⁸, M.P. Guzik^{41a}, C. Gwenlan¹²², C.B. Gwilliam⁷⁷, A. Haas¹¹², C. Haber¹⁶, H.K. Hadavand⁸, N. Haddad^{137e}, A. Hadeef⁸⁸, S. Hageböck²³, M. Hagihara¹⁶⁴, H. Hakobyan^{180,*}, M. Haleem⁴⁵, J. Haley¹¹⁶, G. Halladjian⁹³, G.D. Hallewell⁸⁸, K. Hamacher¹⁷⁷, P. Hamal¹¹⁷, K. Hamano¹⁷², A. Hamilton^{147a}, G.N. Hamity¹⁴¹, P.G. Hamnett⁴⁵, K. Han^{36c,x}, L. Han^{36c}, S. Han^{35a,35d}, K. Hanagaki^{69,y}, K. Hanawa¹⁵⁷, M. Hance¹³⁹, D.M. Handl¹⁰², B. Haney¹²⁴, R. Hankache⁸³, P. Hanke^{60a}, J.B. Hansen³⁹, J.D. Hansen³⁹, M.C. Hansen²³, P.H. Hansen³⁹, K. Hara¹⁶⁴, A.S. Hard¹⁷⁶, T. Harenberg¹⁷⁷, F. Hariri¹¹⁹, S. Harkusha⁹⁵, P.F. Harrison¹⁷³, N.M. Hartmann¹⁰², Y. Hasegawa¹⁴², A. Hasib⁴⁹, S. Hassani¹³⁸, S. Haug¹⁸, R. Hauser⁹³, L. Hauswald⁴⁷, L.B. Havener³⁸, M. Havranek¹³⁰, C.M. Hawkes¹⁹, R.J. Hawkins³², D. Hayden⁹³, C.P. Hays¹²², J.M. Hays⁷⁹, H.S. Hayward⁷⁷, S.J. Haywood¹³³, T. Heck⁸⁶, V. Hedberg⁸⁴, L. Heelan⁸, S. Heer²³, K.K. Heidegger⁵¹, S. Heim⁴⁵, T. Heim¹⁶, B. Heinemann^{45,z}, J.J. Heinrich¹⁰², L. Heinrich¹¹², C. Heinz⁵⁵, J. Hejbal¹²⁹, L. Helary³², A. Held¹⁷¹, S. Hellman^{148a,148b}, C. Helsen³², R.C.W. Henderson⁷⁵, Y. Heng¹⁷⁶, S. Henkelmann¹⁷¹, A.M. Henriques Correia³², S. Henrot-Versille¹¹⁹, G.H. Herbert¹⁷, H. Herde²⁵, V. Herget¹⁷⁸, Y. Hernández Jiménez^{147c}, H. Herr⁸⁶, G. Herten⁵¹, R. Hertenberger¹⁰², L. Hervas³², T.C. Herwig¹²⁴, G.G. Hesketh⁸¹, N.P. Hessey^{163a}, J.W. Hetherly⁴³, S. Higashino⁶⁹, E. Higón-Rodríguez¹⁷⁰, K. Hildebrand³³, E. Hill¹⁷², J.C. Hill³⁰, K.H. Hiller⁴⁵, S.J. Hillier¹⁹, M. Hils⁴⁷, I. Hinchliffe¹⁶, M. Hirose⁵¹, D. Hirschbuehl¹⁷⁷, B. Hiti⁷⁸, O. Hladik¹²⁹, D.R. Hlaluku^{147c}, X. Hoad⁴⁹, J. Hobbs¹⁵⁰, N. Hod^{163a}, M.C. Hodgkinson¹⁴¹, P. Hodgson¹⁴¹, A. Hoecker³², M.R. Hoferkamp¹⁰⁷, F. Hoenig¹⁰², D. Hohn²³, T.R. Holmes³³, M. Holzbock¹⁰², M. Homann⁴⁶, S. Honda¹⁶⁴, T. Honda⁶⁹, T.M. Hong¹²⁷, B.H. Hooberman¹⁶⁹, W.H. Hopkins¹¹⁸, Y. Horii¹⁰⁵, A.J. Horton¹⁴⁴, J.-Y. Hostachy⁵⁷, A. Hostiuc¹⁴⁰, S. Hou¹⁵³, A. Hoummada^{137a}, J. Howarth⁸⁷, J. Hoya⁷⁴, M. Hrabovsky¹¹⁷, J. Hrdinka³², I. Hristova¹⁷, J. Hrivnac¹¹⁹, T. Hryn'ova⁵, A. Hrynevich⁹⁶, P.J. Hsu⁶³, S.-C. Hsu¹⁴⁰, Q. Hu²⁷, S. Hu^{36b}, Y. Huang^{35a}, Z. Hubacek¹³⁰, F. Hubaut⁸⁸, F. Huegging²³, T.B. Huffman¹²², E.W. Hughes³⁸,

M. Huhtinen³², R.F.H. Hunter³¹, P. Huo¹⁵⁰, N. Huseynov^{68,b}, J. Huston⁹³, J. Huth⁵⁹, R. Hyneman⁹², G. Iacobucci⁵², G. Iakovidis²⁷, I. Ibragimov¹⁴³, L. Iconomidou-Fayard¹¹⁹, Z. Idrissi^{137e}, P. Iengo³², O. Igonkina^{109,aa}, T. Iizawa¹⁷⁴, Y. Ikegami⁶⁹, M. Ikeno⁶⁹, Y. Ilchenko^{11,ab}, D. Iliadis¹⁵⁶, N. Ilic¹⁴⁵, F. Iltzsche⁴⁷, G. Introzzi^{123a,123b}, P. Ioannou^{9,*}, M. Iodice^{136a}, K. Iordanidou³⁸, V. Ippolito⁵⁹, M.F. Isacson¹⁶⁸, N. Ishijima¹²⁰, M. Ishino¹⁵⁷, M. Ishitsuka¹⁵⁹, C. Issever¹²², S. Istin^{20a}, F. Ito¹⁶⁴, J.M. Iturbe Ponce^{62a}, R. Iuppa^{162a,162b}, H. Iwasaki⁶⁹, J.M. Izen⁴⁴, V. Izzo^{106a}, S. Jabbar³, P. Jacka¹²⁹, P. Jackson¹, R.M. Jacobs²³, V. Jain², G. Jakel¹⁷⁷, K.B. Jakobi⁸⁶, K. Jakobs⁵¹, S. Jakobsen⁶⁵, T. Jakoubek¹²⁹, D.O. Jamin¹¹⁶, D.K. Jana⁸², R. Jansky⁵², J. Janssen²³, M. Janus⁵⁸, P.A. Janus^{41a}, G. Jarlskog⁸⁴, N. Javadov^{68,b}, T. Javůrek⁵¹, M. Javurkova⁵¹, F. Jeanneau¹³⁸, L. Jeanty¹⁶, J. Jejelava^{54a,ac}, A. Jelinskas¹⁷³, P. Jenni^{51,ad}, C. Jeske¹⁷³, S. Jézéquel⁵, H. Ji¹⁷⁶, J. Jia¹⁵⁰, H. Jiang⁶⁷, Y. Jiang^{36c}, Z. Jiang¹⁴⁵, S. Jiggins⁸¹, J. Jimenez Pena¹⁷⁰, S. Jin^{35b}, A. Jinaru^{28b}, O. Jinnouchi¹⁵⁹, H. Jivan^{147c}, P. Johansson¹⁴¹, K.A. Johns⁷, C.A. Johnson⁶⁴, W.J. Johnson¹⁴⁰, K. Jon-And^{148a,148b}, R.W.L. Jones⁷⁵, S.D. Jones¹⁵¹, S. Jones⁷, T.J. Jones⁷⁷, J. Jongmanns^{60a}, P.M. Jorge^{128a,128b}, J. Jovicevic^{163a}, X. Ju¹⁷⁶, A. Juste Rozas^{13,v}, M.K. Köhler¹⁷⁵, A. Kaczmarek⁴², M. Kado¹¹⁹, H. Kagan¹¹³, M. Kagan¹⁴⁵, S.J. Kahn⁸⁸, T. Kaji¹⁷⁴, E. Kajomovitz¹⁵⁴, C.W. Kalderon⁸⁴, A. Kaluza⁸⁶, S. Kama⁴³, A. Kamenshchikov¹³², N. Kanaya¹⁵⁷, L. Kanjir⁷⁸, Y. Kano¹⁵⁷, V.A. Kantserov¹⁰⁰, J. Kanzaki⁶⁹, B. Kaplan¹¹², L.S. Kaplan¹⁷⁶, D. Kar^{147c}, K. Karakostas¹⁰, N. Karastathis¹⁰, M.J. Kareem^{163b}, E. Karentzos¹⁰, S.N. Karpov⁶⁸, Z.M. Karpova⁶⁸, V. Kartvelishvili⁷⁵, A.N. Karyukhin¹³², K. Kasahara¹⁶⁴, L. Kashif¹⁷⁶, R.D. Kass¹¹³, A. Kastanas¹⁴⁹, Y. Kataoka¹⁵⁷, C. Kato¹⁵⁷, A. Katre⁵², J. Katzy⁴⁵, K. Kawade⁷⁰, K. Kawagoe⁷³, T. Kawamoto¹⁵⁷, G. Kawamura⁵⁸, E.F. Kay⁷⁷, V.F. Kazanin^{111,c}, R. Keeler¹⁷², R. Kehoe⁴³, J.S. Keller³¹, E. Kellermann⁸⁴, J.J. Kempster⁸⁰, J. Kendrick¹⁹, H. Keoshkerian¹⁶¹, O. Kepka¹²⁹, B.P. Kerševan⁷⁸, S. Kersten¹⁷⁷, R.A. Keyes⁹⁰, M. Khader¹⁶⁹, F. Khalil-zada¹², A. Khanov¹¹⁶, A.G. Kharlamov^{111,c}, T. Kharlamova^{111,c}, A. Khodinov¹⁶⁰, T.J. Khoo⁵², V. Khovanskiy^{99,*}, E. Khramov⁶⁸, J. Khubua^{54b,ae}, S. Kido⁷⁰, M. Kiehn⁵², C.R. Kilby⁸⁰, H.Y. Kim⁸, S.H. Kim¹⁶⁴, Y.K. Kim³³, N. Kimura^{167a,167c}, O.M. Kind¹⁷, B.T. King⁷⁷, D. Kirchmeier⁴⁷, J. Kirk¹³³, A.E. Kiryunin¹⁰³, T. Kishimoto¹⁵⁷, D. Kisielewska^{41a}, V. Kitali⁴⁵, O. Kivernyk⁵, E. Kladiva^{146b}, T. Klapdor-Kleingrothaus⁵¹, M.H. Klein⁹², M. Klein⁷⁷, U. Klein⁷⁷, K. Kleinknecht⁸⁶, P. Klimek¹¹⁰, A. Klimentov²⁷, R. Klingenberg^{46,*}, T. Klingl²³, T. Klioutchnikova³², F.F. Klitzner¹⁰², E.-E. Kluge^{60a}, P. Kluit¹⁰⁹, S. Kluth¹⁰³, E. Kneringer⁶⁵, E.B.F.G. Knoops⁸⁸, A. Knue⁵¹, A. Kobayashi¹⁵⁷, D. Kobayashi⁷³, T. Kobayashi¹⁵⁷, M. Kobel⁴⁷, M. Kocian¹⁴⁵, P. Kodys¹³¹, T. Koffas³¹, E. Koffeman¹⁰⁹, N.M. Köhler¹⁰³, T. Koi¹⁴⁵, M. Kolb^{60b}, I. Koletsou⁵, T. Kondo⁶⁹, N. Kondrashova^{36b}, K. Köneke⁵¹, A.C. König¹⁰⁸, T. Kono^{69,af}, R. Konoplich^{112,ag}, N. Konstantinidis⁸¹, B. Konya⁸⁴, R. Kopeliansky⁶⁴, S. Koperny^{41a}, K. Korcyl⁴², K. Kordas¹⁵⁶, A. Korn⁸¹, I. Korolkov¹³, E.V. Korolkova¹⁴¹, O. Kortner¹⁰³, S. Kortner¹⁰³, T. Kosek¹³¹, V.V. Kostyukhin²³, A. Kotwal⁴⁸, A. Koulouris¹⁰, A. Kourkoumeli-Charalampidi^{123a,123b}, C. Kourkoumelis⁹, E. Kourlitis¹⁴¹, V. Kouskoura²⁷, A.B. Kowalewska⁴², R. Kowalewski¹⁷², T.Z. Kowalski^{41a}, C. Kozakai¹⁵⁷, W. Kozanecki¹³⁸, A.S. Kozhin¹³², V.A. Kramarenko¹⁰¹, G. Kramberger⁷⁸, D. Krasnopevtsev¹⁰⁰, M.W. Krasny⁸³, A. Krasznahorkay³², D. Krauss¹⁰³, J.A. Kremer^{41a}, J. Kretzschmar⁷⁷, K. Kreutzfeldt⁵⁵, P. Krieger¹⁶¹, K. Krizka¹⁶, K. Kroeninger⁴⁶, H. Kroha¹⁰³, J. Kroll¹²⁹, J. Kroll¹²⁴, J. Kroseberg²³, J. Krstic¹⁴, U. Kruchonak⁶⁸, H. Krüger²³, N. Krumnack⁶⁷, M.C. Kruse⁴⁸, T. Kubota⁹¹, H. Kucuk⁸¹, S. Kудay^{4b}, J.T. Kuechler¹⁷⁷, S. Kuehn³², A. Kugel^{60a}, F. Kuger¹⁷⁸, T. Kuhl⁴⁵, V. Kukhtin⁶⁸, R. Kukla⁸⁸, Y. Kulchitsky⁹⁵, S. Kuleshov^{34b}, Y.P. Kulinich¹⁶⁹, M. Kuna¹¹, T. Kunigo⁷¹, A. Kupco¹²⁹, T. Kupfer⁴⁶, O. Kuprash¹⁵⁵, H. Kurashige⁷⁰, L.L. Kurchaninov^{163a}, Y.A. Kurochkin⁹⁵, M.G. Kurth^{35a,35d}, E.S. Kuwertz¹⁷², M. Kuze¹⁵⁹, J. Kvita¹¹⁷, T. Kwan¹⁷², D. Kyriazopoulos¹⁴¹, A. La Rosa¹⁰³, J.L. La Rosa Navarro^{26d}, L. La Rotonda^{40a,40b}, F. La Ruffa^{40a,40b}, C. Lacasta¹⁷⁰, F. Lacava^{134a,134b}, J. Lacey⁴⁵, D.P.J. Lack⁸⁷, H. Lacker¹⁷, D. Lacour⁸³, E. Ladygin⁶⁸, R. Lafaye⁵, B. Laforge⁸³, S. Lai⁵⁸, S. Lammers⁶⁴, W. Lampl⁷, E. Lançon²⁷, U. Landgraf⁵¹, M.P.J. Landon⁷⁹, M.C. Lanfermann⁵²,

V.S. Lang⁴⁵, J.C. Lange¹³, R.J. Langenberg³², A.J. Lankford¹⁶⁶, F. Lanni²⁷, K. Lantzsch²³, A. Lanza^{123a}, A. Lapertosa^{53a,53b}, S. Laplace⁸³, J.F. Laporte¹³⁸, T. Lari^{94a}, F. Lasagni Manghi^{22a,22b}, M. Lassnig³², T.S. Lau^{62a}, P. Laurelli⁵⁰, W. Lavrijsen¹⁶, A.T. Law¹³⁹, P. Laycock⁷⁷, T. Lazovich⁵⁹, M. Lazzaroni^{94a,94b}, B. Le⁹¹, O. Le Dortz⁸³, E. Le Guirriec⁸⁸, E.P. Le Quilleuc¹³⁸, M. LeBlanc⁷, T. LeCompte⁶, F. Ledroit-Guillon⁵⁷, C.A. Lee²⁷, G.R. Lee^{34a}, S.C. Lee¹⁵³, L. Lee⁵⁹, B. Lefebvre⁹⁰, G. Lefebvre⁸³, M. Lefebvre¹⁷², F. Legger¹⁰², C. Leggett¹⁶, G. Lehmann Miotto³², X. Lei⁷, W.A. Leight⁴⁵, M.A.L. Leite^{26d}, R. Leitner¹³¹, D. Lellouch¹⁷⁵, B. Lemmer⁵⁸, K.J.C. Leney⁸¹, T. Lenz²³, B. Lenzi³², R. Leone⁷, S. Leone^{126a}, C. Leonidopoulos⁴⁹, G. Lerner¹⁵¹, C. Leroy⁹⁷, R. Les¹⁶¹, A.A.J. Lesage¹³⁸, C.G. Lester³⁰, M. Levchenko¹²⁵, J. Levêque⁵, D. Levin⁹², L.J. Levinson¹⁷⁵, M. Levy¹⁹, D. Lewis⁷⁹, B. Li^{36c,w}, C.-Q. Li^{36c}, H. Li¹⁵⁰, L. Li^{36b}, Q. Li^{35a,35d}, Q. Li^{36c}, S. Li⁴⁸, X. Li^{36b}, Y. Li¹⁴³, Z. Liang^{35a}, B. Liberti^{135a}, A. Liblong¹⁶¹, K. Lie^{62c}, A. Limosani¹⁵², C.Y. Lin³⁰, K. Lin⁹³, S.C. Lin¹⁸², T.H. Lin⁸⁶, R.A. Linck⁶⁴, B.E. Lindquist¹⁵⁰, A.E. Lioni⁵², E. Lipeles¹²⁴, A. Lipniacka¹⁵, M. Lisovsky^{60b}, T.M. Liss^{169,ah}, A. Lister¹⁷¹, A.M. Litke¹³⁹, B. Liu⁶⁷, H. Liu⁹², H. Liu²⁷, J.K.K. Liu¹²², J. Liu^{36a}, J.B. Liu^{36c}, K. Liu⁸⁸, L. Liu¹⁶⁹, M. Liu^{36c}, Y.L. Liu^{36c}, Y. Liu^{36c}, M. Livan^{123a,123b}, A. Lleres⁵⁷, J. Llorente Merino^{35a}, S.L. Lloyd⁷⁹, C.Y. Lo^{62b}, F. Lo Sterzo⁴³, E.M. Lobodzinska⁴⁵, P. Loch⁷, F.K. Loebinger⁸⁷, A. Loesle⁵¹, K.M. Loew²⁵, T. Lohse¹⁷, K. Lohwasser¹⁴¹, M. Lokajicek¹²⁹, B.A. Long²⁴, J.D. Long¹⁶⁹, R.E. Long⁷⁵, L. Longo^{76a,76b}, K.A. Looper¹¹³, J.A. Lopez^{34b}, I. Lopez Paz¹³, A. Lopez Solis⁸³, J. Lorenz¹⁰², N. Lorenzo Martinez⁵, M. Losada²¹, P.J. Lösel¹⁰², X. Lou^{35a}, A. Lounis¹¹⁹, J. Love⁶, P.A. Love⁷⁵, H. Lu^{62a}, N. Lu⁹², Y.J. Lu⁶³, H.J. Lubatti¹⁴⁰, C. Luci^{134a,134b}, A. Lucotte⁵⁷, C. Luedtke⁵¹, F. Luehring⁶⁴, W. Lukas⁶⁵, L. Luminari^{134a}, B. Lund-Jensen¹⁴⁹, M.S. Lutz⁸⁹, P.M. Luzi⁸³, D. Lynn²⁷, R. Lysak¹²⁹, E. Lytken⁸⁴, F. Lyu^{35a}, V. Lyubushkin⁶⁸, H. Ma²⁷, L.L. Ma^{36a}, Y. Ma^{36a}, G. Maccarrone⁵⁰, A. Macchiolo¹⁰³, C.M. Macdonald¹⁴¹, B. Maček⁷⁸, J. Machado Miguens^{124,128b}, D. Madaffari¹⁷⁰, R. Madar³⁷, W.F. Mader⁴⁷, A. Madsen⁴⁵, N. Madysa⁴⁷, J. Maeda⁷⁰, S. Maeland¹⁵, T. Maeno²⁷, A.S. Maevskiy¹⁰¹, V. Magerl⁵¹, C. Maiani¹¹⁹, C. Maidantchik^{26a}, T. Maier¹⁰², A. Maio^{128a,128b,128d}, O. Majersky^{146a}, S. Majewski¹¹⁸, Y. Makida⁶⁹, N. Makovec¹¹⁹, B. Malaescu⁸³, Pa. Malecki⁴², V.P. Maleev¹²⁵, F. Malek⁵⁷, U. Mallik⁶⁶, D. Malon⁶, C. Malone³⁰, S. Maltezos¹⁰, S. Malyukov³², J. Mamuzic¹⁷⁰, G. Mancini⁵⁰, I. Mandić⁷⁸, J. Maneira^{128a,128b}, L. Manhaes de Andrade Filho^{26b}, J. Manjarres Ramos⁴⁷, K.H. Mankinen⁸⁴, A. Mann¹⁰², A. Manousos³², B. Mansoulie¹³⁸, J.D. Mansour^{35a}, R. Mantifel⁹⁰, M. Mantoani⁵⁸, S. Manzoni^{94a,94b}, L. Mapelli³², G. Marceca²⁹, L. March⁵², L. Marchese¹²², G. Marchiori⁸³, M. Marcisovsky¹²⁹, C.A. Marin Tobon³², M. Marjanovic³⁷, D.E. Marley⁹², F. Marroquim^{26a}, S.P. Marsden⁸⁷, Z. Marshall¹⁶, M.U.F. Martensson¹⁶⁸, S. Marti-Garcia¹⁷⁰, C.B. Martin¹¹³, T.A. Martin¹⁷³, V.J. Martin⁴⁹, B. Martin dit Latour¹⁵, M. Martinez^{13,v}, V.I. Martinez Outschoorn¹⁶⁹, S. Martin-Haugh¹³³, V.S. Martoiu^{28b}, A.C. Martyniuk⁸¹, A. Marzin³², L. Masetti⁸⁶, T. Mashimo¹⁵⁷, R. Mashinistov⁹⁸, J. Masik⁸⁷, A.L. Maslennikov^{111,c}, L.H. Mason⁹¹, L. Massa^{135a,135b}, P. Mastrandrea⁵, A. Mastroberardino^{40a,40b}, T. Masubuchi¹⁵⁷, P. Mättig¹⁷⁷, J. Maurer^{28b}, S.J. Maxfield⁷⁷, D.A. Maximov^{111,c}, R. Mazini¹⁵³, I. Maznas¹⁵⁶, S.M. Mazza^{94a,94b}, N.C. Mc Fadden¹⁰⁷, G. Mc Goldrick¹⁶¹, S.P. Mc Kee⁹², A. McCarn⁹², R.L. McCarthy¹⁵⁰, T.G. McCarthy¹⁰³, L.I. McClymont⁸¹, E.F. McDonald⁹¹, J.A. Mcfayden³², G. Mchedlidze⁵⁸, S.J. McMahon¹³³, P.C. McNamara⁹¹, C.J. McNicol¹⁷³, R.A. McPherson^{172,n}, S. Meehan¹⁴⁰, T.J. Megy⁵¹, S. Mehlhase¹⁰², A. Mehta⁷⁷, T. Meideck⁵⁷, K. Meier^{60a}, B. Meirose⁴⁴, D. Melini^{170,ai}, B.R. Mellado Garcia^{147c}, J.D. Mellenthin⁵⁸, M. Melo^{146a}, F. Meloni¹⁸, A. Melzer²³, S.B. Menary⁸⁷, L. Meng⁷⁷, X.T. Meng⁹², A. Mengarelli^{22a,22b}, S. Menke¹⁰³, E. Meoni^{40a,40b}, S. Mergelmeyer¹⁷, C. Merlassino¹⁸, P. Mermod⁵², L. Merola^{106a,106b}, C. Meroni^{94a}, F.S. Merritt³³, A. Messina^{134a,134b}, J. Metcalfe⁶, A.S. Mete¹⁶⁶, C. Meyer¹²⁴, J.-P. Meyer¹³⁸, J. Meyer¹⁰⁹, H. Meyer Zu Theenhausen^{60a}, F. Miano¹⁵¹, R.P. Middleton¹³³, S. Miglioranzì^{53a,53b}, L. Mijović⁴⁹, G. Mikenberg¹⁷⁵, M. Mikestikova¹²⁹, M. Mikuž⁷⁸, M. Milesi⁹¹, A. Milic¹⁶¹, D.A. Millar⁷⁹, D.W. Miller³³, C. Mills⁴⁹, A. Milov¹⁷⁵, D.A. Milstead^{148a,148b},

A.A. Minaenko¹³², Y. Minami¹⁵⁷, I.A. Minashvili^{54b}, A.I. Mincer¹¹², B. Mindur^{41a}, M. Mineev⁶⁸,
 Y. Minegishi¹⁵⁷, Y. Ming¹⁷⁶, L.M. Mir¹³, A. Mirto^{76a,76b}, K.P. Mistry¹²⁴, T. Mitani¹⁷⁴, J. Mitrevski¹⁰²,
 V.A. Mitsou¹⁷⁰, A. Miucci¹⁸, P.S. Miyagawa¹⁴¹, A. Mizukami⁶⁹, J.U. Mjörnmark⁸⁴, T. Mkrtchyan¹⁸⁰,
 M. Mlynarikova¹³¹, T. Moa^{148a,148b}, K. Mochizuki⁹⁷, P. Mogg⁵¹, S. Mohapatra³⁸, S. Molander^{148a,148b},
 R. Moles-Valls²³, M.C. Mondragon⁹³, K. Mönig⁴⁵, J. Monk³⁹, E. Monnier⁸⁸, A. Montalbano¹⁵⁰,
 J. Montejó Berlingen³², F. Monticelli⁷⁴, S. Monzani^{94a}, R.W. Moore³, N. Morange¹¹⁹, D. Moreno²¹,
 M. Moreno Llácer³², P. Moretini^{53a}, M. Morgenstern¹⁰⁹, S. Morgenstern³², D. Mori¹⁴⁴, T. Mori¹⁵⁷,
 M. Morii⁵⁹, M. Morinaga¹⁷⁴, V. Morisbak¹²¹, A.K. Morley³², G. Mornacchi³², J.D. Morris⁷⁹,
 L. Morvaj¹⁵⁰, P. Moschovakos¹⁰, M. Mosidze^{54b}, H.J. Moss¹⁴¹, J. Moss^{145,aj}, K. Motohashi¹⁵⁹,
 R. Mount¹⁴⁵, E. Mountricha²⁷, E.J.W. Moyse⁸⁹, S. Muanza⁸⁸, F. Mueller¹⁰³, J. Mueller¹²⁷,
 R.S.P. Mueller¹⁰², D. Muenstermann⁷⁵, P. Mullen⁵⁶, G.A. Mullier¹⁸, F.J. Munoz Sanchez⁸⁷,
 W.J. Murray^{173,133}, H. Musheghyan³², M. Muškinja⁷⁸, C. Mwewa^{147a}, A.G. Myagkov^{132,ak}, J. Myers¹¹⁸,
 M. Myska¹³⁰, B.P. Nachman¹⁶, O. Nackenhorst⁴⁶, K. Nagai¹²², R. Nagai^{69,af}, K. Nagano⁶⁹,
 Y. Nagasaka⁶¹, K. Nagata¹⁶⁴, M. Nagel⁵¹, E. Nagy⁸⁸, A.M. Nairz³², Y. Nakahama¹⁰⁵, K. Nakamura⁶⁹,
 T. Nakamura¹⁵⁷, I. Nakano¹¹⁴, R.F. Naranjo Garcia⁴⁵, R. Narayan¹¹, D.I. Narrias Villar^{60a},
 I. Naryshkin¹²⁵, T. Naumann⁴⁵, G. Navarro²¹, R. Nayyar⁷, H.A. Neal⁹², P.Yu. Nechaeva⁹⁸, T.J. Neep¹³⁸,
 A. Negri^{123a,123b}, M. Negrini^{22a}, S. Nektarijevic¹⁰⁸, C. Nellist⁵⁸, A. Nelson¹⁶⁶, M.E. Nelson¹²²,
 S. Nemecek¹²⁹, P. Nemethy¹¹², M. Nessi^{32,al}, M.S. Neubauer¹⁶⁹, M. Neumann¹⁷⁷, P.R. Newman¹⁹,
 T.Y. Ng^{62c}, Y.S. Ng¹⁷, T. Nguyen Manh⁹⁷, R.B. Nickerson¹²², R. Nicolaidou¹³⁸, J. Nielsen¹³⁹,
 N. Nikiforou¹¹, V. Nikolaenko^{132,ak}, I. Nikolic-Audit⁸³, K. Nikolopoulos¹⁹, P. Nilsson²⁷, Y. Ninomiya⁶⁹,
 A. Nisati^{134a}, N. Nishu^{36b}, R. Nisius¹⁰³, I. Nitsche⁴⁶, T. Nitta¹⁷⁴, T. Nobe¹⁵⁷, Y. Noguchi⁷¹,
 M. Nomachi¹²⁰, I. Nomidis³¹, M.A. Nomura²⁷, T. Nooney⁷⁹, M. Nordberg³², N. Norjoharuddeen¹²²,
 O. Novgorodova⁴⁷, M. Nozaki⁶⁹, L. Nozka¹¹⁷, K. Ntekas¹⁶⁶, E. Nurse⁸¹, F. Nuti⁹¹, K. O'Connor²⁵,
 D.C. O'Neil¹⁴⁴, A.A. O'Rourke⁴⁵, V. O'Shea⁵⁶, F.G. Oakham^{31,d}, H. Oberlack¹⁰³, T. Obermann²³,
 J. Ocariz⁸³, A. Ochi⁷⁰, I. Ochoa³⁸, J.P. Ochoa-Ricoux^{34a}, S. Oda⁷³, S. Odaka⁶⁹, A. Oh⁸⁷, S.H. Oh⁴⁸,
 C.C. Ohm¹⁴⁹, H. Ohman¹⁶⁸, H. Oide^{53a,53b}, H. Okawa¹⁶⁴, Y. Okumura¹⁵⁷, T. Okuyama⁶⁹, A. Olariu^{28b},
 L.F. Oleiro Seabra^{128a}, S.A. Olivares Pino^{34a}, D. Oliveira Damazio²⁷, J.L. Oliver¹, M.J.R. Olsson³³,
 A. Olszewski⁴², J. Olszowska⁴², A. Onofre^{128a,128e}, K. Onogi¹⁰⁵, P.U.E. Onyisi^{11,ab}, H. Oppen¹²¹,
 M.J. Oreglia³³, Y. Oren¹⁵⁵, D. Orestano^{136a,136b}, E.C. Orgill⁸⁷, N. Orlando^{62b}, R.S. Orr¹⁶¹,
 B. Osculati^{53a,53b,*}, R. Ospanov^{36c}, G. Otero y Garzon²⁹, H. Otono⁷³, M. Ouchrif^{137d}, F. Ould-Saada¹²¹,
 A. Ouraou¹³⁸, K.P. Oussoren¹⁰⁹, Q. Ouyang^{35a}, M. Owen⁵⁶, R.E. Owen¹⁹, V.E. Ozcan^{20a}, N. Ozturk⁸,
 K. Pachal¹⁴⁴, A. Pacheco Pages¹³, L. Pacheco Rodriguez¹³⁸, C. Padilla Aranda¹³, S. Pagan Griso¹⁶,
 M. Paganini¹⁷⁹, F. Paige²⁷, G. Palacino⁶⁴, S. Palazzo^{40a,40b}, S. Palestini³², M. Palka^{41b}, D. Pallin³⁷,
 E.St. Panagiotopoulou¹⁰, I. Panagoulas¹⁰, C.E. Pandini⁵², J.G. Panduro Vazquez⁸⁰, P. Pani³²,
 S. Panitkin²⁷, D. Pantea^{28b}, L. Paolozzi⁵², Th.D. Papadopoulou¹⁰, K. Papageorgiou^{9,s}, A. Paramonov⁶,
 D. Paredes Hernandez¹⁷⁹, A.J. Parker⁷⁵, M.A. Parker³⁰, K.A. Parker⁴⁵, F. Parodi^{53a,53b}, J.A. Parsons³⁸,
 U. Parzefall⁵¹, V.R. Pascuzzi¹⁶¹, J.M. Pasner¹³⁹, E. Pasqualucci^{134a}, S. Passaggio^{53a}, Fr. Pastore⁸⁰,
 S. Pataia⁸⁶, J.R. Pater⁸⁷, T. Pauly³², B. Pearson¹⁰³, S. Pedraza Lopez¹⁷⁰, R. Pedro^{128a,128b},
 S.V. Peleganchuk^{111,c}, O. Penc¹²⁹, C. Peng^{35a,35d}, H. Peng^{36c}, J. Penwell⁶⁴, B.S. Peralva^{26b},
 M.M. Perego¹³⁸, D.V. Perepelitsa²⁷, F. Peri¹⁷, L. Perini^{94a,94b}, H. Pernegger³², S. Perrella^{106a,106b},
 R. Peschke⁴⁵, V.D. Peshekhonov^{68,*}, K. Peters⁴⁵, R.F.Y. Peters⁸⁷, B.A. Petersen³², T.C. Petersen³⁹,
 E. Petit⁵⁷, A. Petridis¹, C. Petridou¹⁵⁶, P. Petroff¹¹⁹, E. Petrolo^{134a}, M. Petrov¹²², F. Petrucci^{136a,136b},
 N.E. Pettersson⁸⁹, A. Peyaud¹³⁸, R. Pezoa^{34b}, T. Pham⁹¹, F.H. Phillips⁹³, P.W. Phillips¹³³,
 G. Piacquadio¹⁵⁰, E. Pianori¹⁷³, A. Picazio⁸⁹, M.A. Pickering¹²², R. Piegaia²⁹, J.E. Pilcher³³,
 A.D. Pilkington⁸⁷, M. Pinamonti^{135a,135b}, J.L. Pinfold³, H. Pirumov⁴⁵, M. Pitt¹⁷⁵, L. Plazak^{146a},
 M.-A. Pleier²⁷, V. Pleskot⁸⁶, E. Plotnikova⁶⁸, D. Pluth⁶⁷, P. Podberezko¹¹¹, R. Poettgen⁸⁴,
 R. Poggi^{123a,123b}, L. Poggioli¹¹⁹, I. Pogrebnyak⁹³, D. Pohl²³, I. Pokharel⁵⁸, G. Polesello^{123a}, A. Poley⁴⁵,

A. Policicchio^{40a,40b}, R. Polifka³², A. Polini^{22a}, C.S. Pollard⁴⁵, V. Polychronakos²⁷, K. Pommès³², D. Ponomarenko¹⁰⁰, L. Pontecorvo^{134a}, G.A. Popeneciu^{28d}, D.M. Portillo Quintero⁸³, S. Pospisil¹³⁰, K. Potamianos⁴⁵, I.N. Potrap⁶⁸, C.J. Potter³⁰, H. Potti¹¹, T. Poulsen⁸⁴, J. Poveda³², M.E. Pozo Astigarraga³², P. Pralavorio⁸⁸, A. Pranko¹⁶, S. Prell⁶⁷, D. Price⁸⁷, M. Primavera^{76a}, S. Prince⁹⁰, N. Proklova¹⁰⁰, K. Prokofiev^{62c}, F. Prokoshin^{34b}, S. Protopopescu²⁷, J. Proudfoot⁶, M. Przybycien^{41a}, A. Puri¹⁶⁹, P. Puzo¹¹⁹, J. Qian⁹², Y. Qin⁸⁷, A. Quadt⁵⁸, M. Queitsch-Maitland⁴⁵, D. Quilty⁵⁶, S. Raddum¹²¹, V. Radeka²⁷, V. Radescu¹²², S.K. Radhakrishnan¹⁵⁰, P. Radloff¹¹⁸, P. Rados⁹¹, F. Ragusa^{94a,94b}, G. Rahal¹⁸¹, J.A. Raine⁸⁷, S. Rajagopalan²⁷, T. Rashid¹¹⁹, S. Raspopov⁵, M.G. Ratti^{94a,94b}, D.M. Rauch⁴⁵, F. Rauscher¹⁰², S. Rave⁸⁶, I. Ravinovich¹⁷⁵, J.H. Rawling⁸⁷, M. Raymond³², A.L. Read¹²¹, N.P. Readioff⁵⁷, M. Reale^{76a,76b}, D.M. Rebuzzi^{123a,123b}, A. Redelbach¹⁷⁸, G. Redlinger²⁷, R. Reece¹³⁹, R.G. Reed^{147c}, K. Reeves⁴⁴, L. Rehnisch¹⁷, J. Reichert¹²⁴, A. Reiss⁸⁶, C. Rembser³², H. Ren^{35a,35d}, M. Rescigno^{134a}, S. Resconi^{94a}, E.D. Resseguie¹²⁴, S. Rettie¹⁷¹, E. Reynolds¹⁹, O.L. Rezanova^{111,c}, P. Reznicek¹³¹, R. Rezvani⁹⁷, R. Richter¹⁰³, S. Richter⁸¹, E. Richter-Was^{41b}, O. Ricken²³, M. Ridel⁸³, P. Rieck¹⁰³, C.J. Riegel¹⁷⁷, J. Rieger⁵⁸, O. Rifki¹¹⁵, M. Rijssenbeek¹⁵⁰, A. Rimoldi^{123a,123b}, M. Rimoldi¹⁸, L. Rinaldi^{22a}, G. Ripellino¹⁴⁹, B. Ristić³², E. Ritsch³², I. Riu¹³, J.C. Rivera Vergara^{34a}, F. Rizatdinova¹¹⁶, E. Rizvi⁷⁹, C. Rizzi¹³, R.T. Roberts⁸⁷, S.H. Robertson^{90,n}, A. Robichaud-Veronneau⁹⁰, D. Robinson³⁰, J.E.M. Robinson⁴⁵, A. Robson⁵⁶, E. Rocco⁸⁶, C. Roda^{126a,126b}, Y. Rodina^{88,am}, S. Rodriguez Bosca¹⁷⁰, A. Rodriguez Perez¹³, D. Rodriguez Rodriguez¹⁷⁰, S. Roe³², C.S. Rogan⁵⁹, O. Røhne¹²¹, J. Roloff⁵⁹, A. Romaniouk¹⁰⁰, M. Romano^{22a,22b}, S.M. Romano Saez³⁷, E. Romero Adam¹⁷⁰, N. Rompotis⁷⁷, M. Ronzani⁵¹, L. Roos⁸³, S. Rosati^{134a}, K. Rosbach⁵¹, P. Rose¹³⁹, N.-A. Rosien⁵⁸, E. Rossi^{106a,106b}, L.P. Rossi^{53a}, J.H.N. Rosten³⁰, R. Rosten¹⁴⁰, M. Rotaru^{28b}, J. Rothberg¹⁴⁰, D. Rousseau¹¹⁹, D. Roy^{147c}, A. Rozanov⁸⁸, Y. Rozen¹⁵⁴, X. Ruan^{147c}, F. Rubbo¹⁴⁵, F. Rühr⁵¹, A. Ruiz-Martinez³¹, Z. Rurikova⁵¹, N.A. Rusakovich⁶⁸, H.L. Russell⁹⁰, J.P. Rutherford⁷, N. Ruthmann³², E.M. Rüttinger⁴⁵, Y.F. Ryabov¹²⁵, M. Rybar¹⁶⁹, G. Rybkin¹¹⁹, S. Ryu⁶, A. Ryzhov¹³², G.F. Rzehorz⁵⁸, A.F. Saavedra¹⁵², G. Sabato¹⁰⁹, S. Sacerdoti²⁹, H.F.-W. Sadrozinski¹³⁹, R. Sadykov⁶⁸, F. Safai Tehrani^{134a}, P. Saha¹¹⁰, M. Sahinsoy^{60a}, M. Saimpert⁴⁵, M. Saito¹⁵⁷, T. Saito¹⁵⁷, H. Sakamoto¹⁵⁷, Y. Sakurai¹⁷⁴, G. Salamanna^{136a,136b}, J.E. Salazar Loyola^{34b}, D. Salek¹⁰⁹, P.H. Sales De Bruin¹⁶⁸, D. Salihagic¹⁰³, A. Salnikov¹⁴⁵, J. Salt¹⁷⁰, D. Salvatore^{40a,40b}, F. Salvatore¹⁵¹, A. Salvucci^{62a,62b,62c}, A. Salzburger³², D. Sammel⁵¹, D. Sampsonidis¹⁵⁶, D. Sampsonidou¹⁵⁶, J. Sánchez¹⁷⁰, A. Sanchez Pineda^{167a,167c}, H. Sandaker¹²¹, R.L. Sandbach⁷⁹, C.O. Sander⁴⁵, M. Sandhoff¹⁷⁷, C. Sandoval²¹, D.P.C. Sankey¹³³, M. Sannino^{53a,53b}, Y. Sano¹⁰⁵, A. Sansoni⁵⁰, C. Santoni³⁷, H. Santos^{128a}, I. Santoyo Castillo¹⁵¹, A. Saprnov⁶⁸, J.G. Saraiva^{128a,128d}, O. Sasaki⁶⁹, K. Sato¹⁶⁴, E. Sauvan⁵, G. Savage⁸⁰, P. Savard^{161,d}, N. Savic¹⁰³, C. Sawyer¹³³, L. Sawyer^{82,u}, C. Sbarra^{22a}, A. Sbrizzi^{22a,22b}, T. Scanlon⁸¹, D.A. Scannicchio¹⁶⁶, J. Schaarschmidt¹⁴⁰, P. Schacht¹⁰³, B.M. Schachtner¹⁰², D. Schaefer³³, L. Schaefer¹²⁴, J. Schaeffer⁸⁶, S. Schaepe³², U. Schäfer⁸⁶, A.C. Schaffer¹¹⁹, D. Schaile¹⁰², R.D. Schamberger¹⁵⁰, V.A. Schegelsky¹²⁵, D. Scheirich¹³¹, F. Schenck¹⁷, M. Schernau¹⁶⁶, C. Schiavi^{53a,53b}, S. Schier¹³⁹, L.K. Schildgen²³, C. Schillo⁵¹, M. Schioppa^{40a,40b}, S. Schlenker³², K.R. Schmidt-Sommerfeld¹⁰³, K. Schmieden³², C. Schmitt⁸⁶, S. Schmitt⁴⁵, S. Schmitz⁸⁶, U. Schnoor⁵¹, L. Schoeffel¹³⁸, A. Schoening^{60b}, B.D. Schoenrock⁹³, E. Schopf²³, M. Schott⁸⁶, J.F.P. Schouwenberg¹⁰⁸, J. Schovancova³², S. Schramm⁵², N. Schuh⁸⁶, A. Schulte⁸⁶, M.J. Schultens²³, H.-C. Schultz-Coulon^{60a}, M. Schumacher⁵¹, B.A. Schumm¹³⁹, Ph. Schune¹³⁸, A. Schwartzman¹⁴⁵, T.A. Schwarz⁹², H. Schweiger⁸⁷, Ph. Schwemling¹³⁸, R. Schwienhorst⁹³, J. Schwindling¹³⁸, A. Sciandra²³, G. Sciolla²⁵, M. Scornajenghi^{40a,40b}, F. Scuri^{126a}, F. Scutti⁹¹, J. Searcy⁹², P. Seema²³, S.C. Seidel¹⁰⁷, A. Seiden¹³⁹, J.M. Seixas^{26a}, G. Sekhniaidze^{106a}, K. Sekhon⁹², S.J. Sekula⁴³, N. Semprini-Cesari^{22a,22b}, S. Senkin³⁷, C. Serfon¹²¹, L. Serin¹¹⁹, L. Serkin^{167a,167b}, M. Sessa^{136a,136b}, R. Seuster¹⁷², H. Severini¹¹⁵, T. Šfiligoj⁷⁸, F. Sforza¹⁶⁵, A. Sfyrla⁵², E. Shabalina⁵⁸, N.W. Shaikh^{148a,148b}, L.Y. Shan^{35a}, R. Shang¹⁶⁹, J.T. Shank²⁴,

M. Shapiro¹⁶, P.B. Shatalov⁹⁹, K. Shaw^{167a,167b}, S.M. Shaw⁸⁷, A. Shcherbakova^{148a,148b}, C.Y. Shehu¹⁵¹,
Y. Shen¹¹⁵, N. Sherafati³¹, A.D. Sherman²⁴, P. Sherwood⁸¹, L. Shi^{153,an}, S. Shimizu⁷⁰,
C.O. Shimmin¹⁷⁹, M. Shimojima¹⁰⁴, I.P.J. Shipsey¹²², S. Shirabe⁷³, M. Shiyakova^{68,ao}, J. Shlomi¹⁷⁵,
A. Shmeleva⁹⁸, D. Shoaleh Saadi⁹⁷, M.J. Shochet³³, S. Shojaii⁹¹, D.R. Shope¹¹⁵, S. Shrestha¹¹³,
E. Shulga¹⁰⁰, M.A. Shupe⁷, P. Sicho¹²⁹, A.M. Sickles¹⁶⁹, P.E. Sidebo¹⁴⁹, E. Sideras Haddad^{147c},
O. Sidiropoulou¹⁷⁸, A. Sidoti^{22a,22b}, F. Siegert⁴⁷, Dj. Sijacki¹⁴, J. Silva^{128a,128d}, M. Silva Jr.¹⁷⁶,
S.B. Silverstein^{148a}, V. Simak¹³⁰, L. Simic⁶⁸, S. Simion¹¹⁹, E. Simioni⁸⁶, B. Simmons⁸¹, M. Simon⁸⁶,
P. Sinervo¹⁶¹, N.B. Sinev¹¹⁸, M. Sioli^{22a,22b}, G. Siragusa¹⁷⁸, I. Siral⁹², S.Yu. Sivoklov¹⁰¹,
J. Sjölin^{148a,148b}, M.B. Skinner⁷⁵, P. Skubic¹¹⁵, M. Slater¹⁹, T. Slavicek¹³⁰, M. Slawinska⁴², K. Sliwa¹⁶⁵,
R. Slovak¹³¹, V. Smakhtin¹⁷⁵, B.H. Smart⁵, J. Smiesko^{146a}, N. Smirnov¹⁰⁰, S.Yu. Smirnov¹⁰⁰,
Y. Smirnov¹⁰⁰, L.N. Smirnova^{101,ap}, O. Smirnova⁸⁴, J.W. Smith⁵⁸, M.N.K. Smith³⁸, R.W. Smith³⁸,
M. Smizanska⁷⁵, K. Smolek¹³⁰, A.A. Snesarev⁹⁸, I.M. Snyder¹¹⁸, S. Snyder²⁷, R. Sobie^{172,n},
F. Socher⁴⁷, A. Soffer¹⁵⁵, A. Søggaard⁴⁹, D.A. Soh¹⁵³, G. Sokhrannyi⁷⁸, C.A. Solans Sanchez³²,
M. Solar¹³⁰, E.Yu. Soldatov¹⁰⁰, U. Soldevila¹⁷⁰, A.A. Solodkov¹³², A. Soloshenko⁶⁸,
O.V. Solovyanov¹³², V. Solovyeve¹²⁵, P. Sommer¹⁴¹, H. Son¹⁶⁵, A. Sopczak¹³⁰, D. Sosa^{60b},
C.L. Sotiropoulou^{126a,126b}, S. Sottocornola^{123a,123b}, R. Soualah^{167a,167c}, A.M. Soukharev^{111,c},
D. South⁴⁵, B.C. Sowden⁸⁰, S. Spagnolo^{76a,76b}, M. Spalla^{126a,126b}, M. Spangenberg¹⁷³, F. Spanò⁸⁰,
D. Sperlich¹⁷, F. Spettel¹⁰³, T.M. Spieker^{60a}, R. Spighi^{22a}, G. Spigo³², L.A. Spiller⁹¹, M. Spousta¹³¹,
R.D. St. Denis^{56,*}, A. Stabile^{94a,94b}, R. Stamen^{60a}, S. Stamm¹⁷, E. Stanecka⁴², R.W. Stanek⁶,
C. Stanescu^{136a}, M.M. Stanitzki⁴⁵, B.S. Stapf¹⁰⁹, S. Stapnes¹²¹, E.A. Starchenko¹³², G.H. Stark³³,
J. Stark⁵⁷, S.H. Stark³⁹, P. Staroba¹²⁹, P. Starovoitov^{60a}, S. Stärz³², R. Staszewski⁴², M. Stegler⁴⁵,
P. Steinberg²⁷, B. Stelzer¹⁴⁴, H.J. Stelzer³², O. Stelzer-Chilton^{163a}, H. Stenzel⁵⁵, T.J. Stevenson⁷⁹,
G.A. Stewart⁵⁶, M.C. Stockton¹¹⁸, M. Stoebe⁹⁰, G. Stoica^{28b}, P. Stolte⁵⁸, S. Stonjek¹⁰³, A.R. Stradling⁸,
A. Straessner⁴⁷, M.E. Stramaglia¹⁸, J. Strandberg¹⁴⁹, S. Strandberg^{148a,148b}, M. Strauss¹¹⁵,
P. Strizenecek^{146b}, R. Ströhmer¹⁷⁸, D.M. Strom¹¹⁸, R. Stroynowski⁴³, A. Strubig⁴⁹, S.A. Stucci²⁷,
B. Stugu¹⁵, N.A. Styles⁴⁵, D. Su¹⁴⁵, J. Su¹²⁷, S. Suchek^{60a}, Y. Sugaya¹²⁰, M. Suk¹³⁰, V.V. Sulin⁹⁸,
DMS Sultan⁵², S. Sultansoy^{4c}, T. Sumida⁷¹, S. Sun⁵⁹, X. Sun³, K. Suruliz¹⁵¹, C.J.E. Suster¹⁵²,
M.R. Sutton¹⁵¹, S. Suzuki⁶⁹, M. Svatos¹²⁹, M. Swiatlowski³³, S.P. Swift², A. Sydorenko⁸⁶, I. Sykora^{146a},
T. Sykora¹³¹, D. Ta⁵¹, K. Tackmann⁴⁵, J. Taenzer¹⁵⁵, A. Taffard¹⁶⁶, R. Tafirout^{163a}, E. Tahirovic⁷⁹,
N. Taiblum¹⁵⁵, H. Takai²⁷, R. Takashima⁷², E.H. Takasugi¹⁰³, K. Takeda⁷⁰, T. Takeshita¹⁴², Y. Takubo⁶⁹,
M. Talby⁸⁸, A.A. Talyshev^{111,c}, J. Tanaka¹⁵⁷, M. Tanaka¹⁵⁹, R. Tanaka¹¹⁹, R. Tanioka⁷⁰,
B.B. Tannenwald¹¹³, S. Tapia Araya^{34b}, S. Tapprogge⁸⁶, S. Tarem¹⁵⁴, G.F. Tartarelli^{94a}, P. Tas¹³¹,
M. Tasevsky¹²⁹, T. Tashiro⁷¹, E. Tassi^{40a,40b}, A. Tavares Delgado^{128a,128b}, Y. Tayalati^{137e}, A.C. Taylor¹⁰⁷,
A.J. Taylor⁴⁹, G.N. Taylor⁹¹, P.T.E. Taylor⁹¹, W. Taylor^{163b}, P. Teixeira-Dias⁸⁰, D. Temple¹⁴⁴,
H. Ten Kate³², P.K. Teng¹⁵³, J.J. Teoh¹²⁰, F. Tepel¹⁷⁷, S. Terada⁶⁹, K. Terashi¹⁵⁷, J. Terron⁸⁵, S. Terzo¹³,
M. Testa⁵⁰, R.J. Teuscher^{161,n}, S.J. Thais¹⁷⁹, T. Theveneaux-Pelzer⁸⁸, F. Thiele³⁹, J.P. Thomas¹⁹,
J. Thomas-Wilsker⁸⁰, P.D. Thompson¹⁹, A.S. Thompson⁵⁶, L.A. Thomsen¹⁷⁹, E. Thomson¹²⁴, Y. Tian³⁸,
M.J. Tibbets¹⁶, R.E. Ticse Torres⁵⁸, V.O. Tikhomirov^{98,aq}, Yu.A. Tikhonov^{111,c}, S. Timoshenko¹⁰⁰,
P. Tipton¹⁷⁹, S. Tisserant⁸⁸, K. Todome¹⁵⁹, S. Todorova-Nova⁵, S. Todt⁴⁷, J. Tojo⁷³, S. Tokár^{146a},
K. Tokushuku⁶⁹, E. Tolley¹¹³, L. Tomlinson⁸⁷, M. Tomoto¹⁰⁵, L. Tompkins^{145,ar}, K. Toms¹⁰⁷, B. Tong⁵⁹,
P. Tornambe⁵¹, E. Torrence¹¹⁸, H. Torres⁴⁷, E. Torró Pastor¹⁴⁰, J. Toth^{88,as}, F. Touchard⁸⁸, D.R. Tovey¹⁴¹,
C.J. Treado¹¹², T. Trefzger¹⁷⁸, F. Tresoldi¹⁵¹, A. Tricoli²⁷, I.M. Trigger^{163a}, S. Trincas-Duvold⁸³,
M.F. Tripiana¹³, W. Trischuk¹⁶¹, B. Trocme⁵⁷, A. Trofymov⁴⁵, C. Troncon^{94a}, M. Trovatelli¹⁷²,
L. Truong^{147b}, M. Trzebinski⁴², A. Trzupek⁴², K.W. Tsang^{62a}, J.C-L. Tseng¹²², P.V. Tsiareshka⁹⁵,
N. Tsirintanis⁹, S. Tsiskaridze¹³, V. Tsiskaridze⁵¹, E.G. Tskhadadze^{54a}, I.I. Tsukerman⁹⁹, V. Tsulaia¹⁶,
S. Tsuno⁶⁹, D. Tsybychev¹⁵⁰, Y. Tu^{62b}, A. Tudorache^{28b}, V. Tudorache^{28b}, T.T. Tulbure^{28a}, A.N. Tuna⁵⁹,
S. Turchikhin⁶⁸, D. Turgeman¹⁷⁵, I. Turk Cakir^{4b,at}, R. Turra^{94a}, P.M. Tuts³⁸, G. Uccielli^{22a,22b},

I. Ueda⁶⁹, M. Ughetto^{148a,148b}, F. Ukegawa¹⁶⁴, G. Unal³², A. Undrus²⁷, G. Unel¹⁶⁶, F.C. Ungaro⁹¹, Y. Unno⁶⁹, K. Uno¹⁵⁷, J. Urban^{146b}, P. Urquijo⁹¹, P. Urrejola⁸⁶, G. Usai⁸, J. Usui⁶⁹, L. Vacavant⁸⁸, V. Vacek¹³⁰, B. Vachon⁹⁰, K.O.H. Vadla¹²¹, A. Vaidya⁸¹, C. Valderanis¹⁰², E. Valdes Santurio^{148a,148b}, M. Valente⁵², S. Valentinetti^{22a,22b}, A. Valero¹⁷⁰, L. Valéry¹³, A. Vallier⁵, J.A. Valls Ferrer¹⁷⁰, W. Van Den Wollenberg¹⁰⁹, H. van der Graaf¹⁰⁹, P. van Gemmeren⁶, J. Van Nieuwkoop¹⁴⁴, I. van Vulpen¹⁰⁹, M.C. van Woerden¹⁰⁹, M. Vanadia^{135a,135b}, W. Vandelli³², A. Vaniachine¹⁶⁰, P. Vankov¹⁰⁹, G. Vardanyan¹⁸⁰, R. Vari^{134a}, E.W. Varnes⁷, C. Varni^{53a,53b}, T. Varol⁴³, D. Varouchas¹¹⁹, A. Vartapetian⁸, K.E. Varvell¹⁵², J.G. Vasquez¹⁷⁹, G.A. Vasquez^{34b}, F. Vazeille³⁷, D. Vazquez Furelos¹³, T. Vazquez Schroeder⁹⁰, J. Veatch⁵⁸, V. Veeraraghavan⁷, L.M. Veloce¹⁶¹, F. Veloso^{128a,128c}, S. Veneziano^{134a}, A. Ventura^{76a,76b}, M. Venturi¹⁷², N. Venturi³², V. Vercesi^{123a}, M. Verducci^{136a,136b}, W. Verkerke¹⁰⁹, A.T. Vermeulen¹⁰⁹, J.C. Vermeulen¹⁰⁹, M.C. Vetterli^{144,d}, N. Viaux Maira^{34b}, O. Viazlo⁸⁴, I. Vichou^{169,*}, T. Vickey¹⁴¹, O.E. Vickey Boeriu¹⁴¹, G.H.A. Viehhauser¹²², S. Viel¹⁶, L. Vignani¹²², M. Villa^{22a,22b}, M. Villaplana Perez^{94a,94b}, E. Vilucchi⁵⁰, M.G. Vinciter³¹, V.B. Vinogradov⁶⁸, A. Vishwakarma⁴⁵, C. Vittori^{22a,22b}, I. Vivarelli¹⁵¹, S. Vlachos¹⁰, M. Vogel¹⁷⁷, P. Vokac¹³⁰, G. Volpi¹³, S.E. von Buddenbrock^{147c}, H. von der Schmitt¹⁰³, E. von Toerne²³, V. Vorobel¹³¹, K. Vorobev¹⁰⁰, M. Vos¹⁷⁰, R. Voss³², J.H. Vossebeld⁷⁷, N. Vranjes¹⁴, M. Vranjes Milosavljevic¹⁴, V. Vrba¹³⁰, M. Vreeswijk¹⁰⁹, R. Vuillermet³², I. Vukotic³³, P. Wagner²³, W. Wagner¹⁷⁷, J. Wagner-Kuhr¹⁰², H. Wahlberg⁷⁴, S. Wahrmund⁴⁷, K. Wakamiya⁷⁰, J. Walder⁷⁵, R. Walker¹⁰², W. Walkowiak¹⁴³, V. Wallangen^{148a,148b}, A.M. Wang⁵⁹, C. Wang^{36a,p}, F. Wang¹⁷⁶, H. Wang¹⁶, H. Wang³, J. Wang⁴⁵, J. Wang¹⁵², Q. Wang¹¹⁵, R.-J. Wang⁸³, R. Wang⁶, S.M. Wang¹⁵³, T. Wang³⁸, W. Wang^{153,au}, W. Wang^{36c,av}, Z. Wang^{36b}, C. Wanotayaroj⁴⁵, A. Warburton⁹⁰, C.P. Ward³⁰, D.R. Wardrope⁸¹, A. Washbrook⁴⁹, P.M. Watkins¹⁹, A.T. Watson¹⁹, M.F. Watson¹⁹, G. Watts¹⁴⁰, S. Watts⁸⁷, B.M. Waugh⁸¹, A.F. Webb¹¹, S. Webb⁸⁶, M.S. Weber¹⁸, S.M. Weber^{60a}, S.A. Weber³¹, J.S. Webster⁶, A.R. Weidberg¹²², B. Weinert⁶⁴, J. Weingarten⁵⁸, M. Weirich⁸⁶, C. Weiser⁵¹, P.S. Wells³², T. Wenaus²⁷, T. Wengler³², S. Wenig³², N. Wermes²³, M.D. Werner⁶⁷, P. Werner³², M. Wessels^{60a}, T.D. Weston¹⁸, K. Whalen¹¹⁸, N.L. Whallon¹⁴⁰, A.M. Wharton⁷⁵, A.S. White⁹², A. White⁸, M.J. White¹, R. White^{34b}, D. Whiteson¹⁶⁶, B.W. Whitmore⁷⁵, F.J. Wickens¹³³, W. Wiedenmann¹⁷⁶, M. WIELERS¹³³, C. Wiglesworth³⁹, L.A.M. Wiik-Fuchs⁵¹, A. Wildauer¹⁰³, F. Wilk⁸⁷, H.G. Wilkens³², H.H. Williams¹²⁴, S. Williams³⁰, C. Willis⁹³, S. Willocq⁸⁹, J.A. Wilson¹⁹, I. Wingerter-Seetz⁵, E. Winkels¹⁵¹, F. Winklmeier¹¹⁸, O.J. Winston¹⁵¹, B.T. Winter²³, M. Wittgen¹⁴⁵, M. Wobisch^{82,u}, A. Wolf⁸⁶, T.M.H. Wolf¹⁰⁹, R. Wolff⁸⁸, M.W. Wolter⁴², H. Wolters^{128a,128c}, V.W.S. Wong¹⁷¹, N.L. Woods¹³⁹, S.D. Worm¹⁹, B.K. Wosiek⁴², J. Wotschack³², K.W. Wozniak⁴², M. Wu³³, S.L. Wu¹⁷⁶, X. Wu⁵², Y. Wu⁹², T.R. Wyatt⁸⁷, B.M. Wynne⁴⁹, S. Xella³⁹, Z. Xi⁹², L. Xia^{35c}, D. Xu^{35a}, L. Xu²⁷, T. Xu¹³⁸, W. Xu⁹², B. Yabsley¹⁵², S. Yacoob^{147a}, K. Yajima¹²⁰, D.P. Yallup⁸¹, D. Yamaguchi¹⁵⁹, Y. Yamaguchi¹⁵⁹, A. Yamamoto⁶⁹, S. Yamamoto¹⁵⁷, T. Yamanaka¹⁵⁷, F. Yamane⁷⁰, M. Yamatani¹⁵⁷, T. Yamazaki¹⁵⁷, Y. Yamazaki⁷⁰, Z. Yan²⁴, H. Yang^{36b}, H. Yang¹⁶, S. Yang⁶⁶, Y. Yang¹⁵³, Z. Yang¹⁵, W.-M. Yao¹⁶, Y.C. Yap⁴⁵, Y. Yasu⁶⁹, E. Yatsenko⁵, K.H. Yau Wong²³, J. Ye⁴³, S. Ye²⁷, I. Yeletsikh⁶⁸, E. Yigitbasi²⁴, E. Yildirim⁸⁶, K. Yorita¹⁷⁴, K. Yoshihara¹²⁴, C. Young¹⁴⁵, C.J.S. Young³², J. Yu⁸, J. Yu⁶⁷, S.P.Y. Yuen²³, I. Yusuff^{30,aw}, B. Zabinski⁴², G. Zacharis¹⁰, R. Zaidan¹³, A.M. Zaitsev^{132,ak}, N. Zakharchuk⁴⁵, J. Zalieckas¹⁵, A. Zaman¹⁵⁰, S. Zambito⁵⁹, D. Zanzi³², C. Zeitnitz¹⁷⁷, G. Zemaityte¹²², J.C. Zeng¹⁶⁹, Q. Zeng¹⁴⁵, O. Zenin¹³², T. Ženiš^{146a}, D. Zerwas¹¹⁹, D. Zhang^{36a}, D. Zhang⁹², F. Zhang¹⁷⁶, G. Zhang^{36c,av}, H. Zhang¹¹⁹, J. Zhang⁶, L. Zhang⁵¹, L. Zhang^{36c}, M. Zhang¹⁶⁹, P. Zhang^{35b}, R. Zhang²³, R. Zhang^{36c,p}, X. Zhang^{36a}, Y. Zhang^{35a,35d}, Z. Zhang¹¹⁹, X. Zhao⁴³, Y. Zhao^{36a,x}, Z. Zhao^{36c}, A. Zhemchugov⁶⁸, B. Zhou⁹², C. Zhou¹⁷⁶, L. Zhou⁴³, M. Zhou^{35a,35d}, M. Zhou¹⁵⁰, N. Zhou^{36b}, Y. Zhou⁷, C.G. Zhu^{36a}, H. Zhu^{35a}, J. Zhu⁹², Y. Zhu^{36c}, X. Zhuang^{35a}, K. Zhukov⁹⁸, A. Zibell¹⁷⁸, D. Zieminska⁶⁴, N.I. Zimine⁶⁸, S. Zimmermann⁵¹, Z. Zinonos¹⁰³, M. Zinser⁸⁶, M. Ziolkowski¹⁴³, L. Živković¹⁴, G. Zobernig¹⁷⁶, A. Zoccoli^{22a,22b}, R. Zou³³, M. zur Nedden¹⁷, L. Zwalinski³².

- ¹ Department of Physics, University of Adelaide, Adelaide, Australia
- ² Physics Department, SUNY Albany, Albany NY, United States of America
- ³ Department of Physics, University of Alberta, Edmonton AB, Canada
- ⁴ ^(a) Department of Physics, Ankara University, Ankara; ^(b) Istanbul Aydin University, Istanbul; ^(c) Division of Physics, TOBB University of Economics and Technology, Ankara, Turkey
- ⁵ LAPP, CNRS/IN2P3 and Université Savoie Mont Blanc, Annecy-le-Vieux, France
- ⁶ High Energy Physics Division, Argonne National Laboratory, Argonne IL, United States of America
- ⁷ Department of Physics, University of Arizona, Tucson AZ, United States of America
- ⁸ Department of Physics, The University of Texas at Arlington, Arlington TX, United States of America
- ⁹ Physics Department, National and Kapodistrian University of Athens, Athens, Greece
- ¹⁰ Physics Department, National Technical University of Athens, Zografou, Greece
- ¹¹ Department of Physics, The University of Texas at Austin, Austin TX, United States of America
- ¹² Institute of Physics, Azerbaijan Academy of Sciences, Baku, Azerbaijan
- ¹³ Institut de Física d'Altes Energies (IFAE), The Barcelona Institute of Science and Technology, Barcelona, Spain
- ¹⁴ Institute of Physics, University of Belgrade, Belgrade, Serbia
- ¹⁵ Department for Physics and Technology, University of Bergen, Bergen, Norway
- ¹⁶ Physics Division, Lawrence Berkeley National Laboratory and University of California, Berkeley CA, United States of America
- ¹⁷ Department of Physics, Humboldt University, Berlin, Germany
- ¹⁸ Albert Einstein Center for Fundamental Physics and Laboratory for High Energy Physics, University of Bern, Bern, Switzerland
- ¹⁹ School of Physics and Astronomy, University of Birmingham, Birmingham, United Kingdom
- ²⁰ ^(a) Department of Physics, Bogazici University, Istanbul; ^(b) Department of Physics Engineering, Gaziantep University, Gaziantep; ^(d) Istanbul Bilgi University, Faculty of Engineering and Natural Sciences, Istanbul; ^(e) Bahcesehir University, Faculty of Engineering and Natural Sciences, Istanbul, Turkey
- ²¹ Centro de Investigaciones, Universidad Antonio Narino, Bogota, Colombia
- ²² ^(a) INFN Sezione di Bologna; ^(b) Dipartimento di Fisica e Astronomia, Università di Bologna, Bologna, Italy
- ²³ Physikalisches Institut, University of Bonn, Bonn, Germany
- ²⁴ Department of Physics, Boston University, Boston MA, United States of America
- ²⁵ Department of Physics, Brandeis University, Waltham MA, United States of America
- ²⁶ ^(a) Universidade Federal do Rio De Janeiro COPPE/EE/IF, Rio de Janeiro; ^(b) Electrical Circuits Department, Federal University of Juiz de Fora (UFJF), Juiz de Fora; ^(c) Federal University of Sao Joao del Rei (UFSJ), Sao Joao del Rei; ^(d) Instituto de Fisica, Universidade de Sao Paulo, Sao Paulo, Brazil
- ²⁷ Physics Department, Brookhaven National Laboratory, Upton NY, United States of America
- ²⁸ ^(a) Transilvania University of Brasov, Brasov; ^(b) Horia Hulubei National Institute of Physics and Nuclear Engineering, Bucharest; ^(c) Department of Physics, Alexandru Ioan Cuza University of Iasi, Iasi; ^(d) National Institute for Research and Development of Isotopic and Molecular Technologies, Physics Department, Cluj Napoca; ^(e) University Politehnica Bucharest, Bucharest; ^(f) West University in Timisoara, Timisoara, Romania
- ²⁹ Departamento de Física, Universidad de Buenos Aires, Buenos Aires, Argentina
- ³⁰ Cavendish Laboratory, University of Cambridge, Cambridge, United Kingdom
- ³¹ Department of Physics, Carleton University, Ottawa ON, Canada
- ³² CERN, Geneva, Switzerland
- ³³ Enrico Fermi Institute, University of Chicago, Chicago IL, United States of America

- ³⁴ (a) Departamento de Física, Pontificia Universidad Católica de Chile, Santiago; (b) Departamento de Física, Universidad Técnica Federico Santa María, Valparaíso, Chile
- ³⁵ (a) Institute of High Energy Physics, Chinese Academy of Sciences, Beijing; (b) Department of Physics, Nanjing University, Jiangsu; (c) Physics Department, Tsinghua University, Beijing 100084; (d) University of Chinese Academy of Science (UCAS), Beijing, China
- ³⁶ (a) School of Physics, Shandong University, Shandong; (b) School of Physics and Astronomy, Key Laboratory for Particle Physics, Astrophysics and Cosmology, Ministry of Education; Shanghai Key Laboratory for Particle Physics and Cosmology, Shanghai Jiao Tong University; (c) Department of Modern Physics and State Key Laboratory of Particle Detection and Electronics, University of Science and Technology of China, Anhui, China
- ³⁷ Université Clermont Auvergne, CNRS/IN2P3, LPC, Clermont-Ferrand, France
- ³⁸ Nevis Laboratory, Columbia University, Irvington NY, United States of America
- ³⁹ Niels Bohr Institute, University of Copenhagen, Kobenhavn, Denmark
- ⁴⁰ (a) INFN Gruppo Collegato di Cosenza, Laboratori Nazionali di Frascati; (b) Dipartimento di Fisica, Università della Calabria, Rende, Italy
- ⁴¹ (a) AGH University of Science and Technology, Faculty of Physics and Applied Computer Science, Krakow; (b) Marian Smoluchowski Institute of Physics, Jagiellonian University, Krakow, Poland
- ⁴² Institute of Nuclear Physics Polish Academy of Sciences, Krakow, Poland
- ⁴³ Physics Department, Southern Methodist University, Dallas TX, United States of America
- ⁴⁴ Physics Department, University of Texas at Dallas, Richardson TX, United States of America
- ⁴⁵ DESY, Hamburg and Zeuthen, Germany
- ⁴⁶ Lehrstuhl für Experimentelle Physik IV, Technische Universität Dortmund, Dortmund, Germany
- ⁴⁷ Institut für Kern- und Teilchenphysik, Technische Universität Dresden, Dresden, Germany
- ⁴⁸ Department of Physics, Duke University, Durham NC, United States of America
- ⁴⁹ SUPA - School of Physics and Astronomy, University of Edinburgh, Edinburgh, United Kingdom
- ⁵⁰ INFN e Laboratori Nazionali di Frascati, Frascati, Italy
- ⁵¹ Fakultät für Mathematik und Physik, Albert-Ludwigs-Universität, Freiburg, Germany
- ⁵² Departement de Physique Nucleaire et Corpusculaire, Université de Genève, Geneva, Switzerland
- ⁵³ (a) INFN Sezione di Genova; (b) Dipartimento di Fisica, Università di Genova, Genova, Italy
- ⁵⁴ (a) E. Andronikashvili Institute of Physics, Iv. Javakhishvili Tbilisi State University, Tbilisi; (b) High Energy Physics Institute, Tbilisi State University, Tbilisi, Georgia
- ⁵⁵ II Physikalisches Institut, Justus-Liebig-Universität Giessen, Giessen, Germany
- ⁵⁶ SUPA - School of Physics and Astronomy, University of Glasgow, Glasgow, United Kingdom
- ⁵⁷ Laboratoire de Physique Subatomique et de Cosmologie, Université Grenoble-Alpes, CNRS/IN2P3, Grenoble, France
- ⁵⁸ II Physikalisches Institut, Georg-August-Universität, Göttingen, Germany
- ⁵⁹ Laboratory for Particle Physics and Cosmology, Harvard University, Cambridge MA, United States of America
- ⁶⁰ (a) Kirchhoff-Institut für Physik, Ruprecht-Karls-Universität Heidelberg, Heidelberg; (b) Physikalisches Institut, Ruprecht-Karls-Universität Heidelberg, Heidelberg, Germany
- ⁶¹ Faculty of Applied Information Science, Hiroshima Institute of Technology, Hiroshima, Japan
- ⁶² (a) Department of Physics, The Chinese University of Hong Kong, Shatin, N.T., Hong Kong; (b) Department of Physics, The University of Hong Kong, Hong Kong; (c) Department of Physics and Institute for Advanced Study, The Hong Kong University of Science and Technology, Clear Water Bay, Kowloon, Hong Kong, China
- ⁶³ Department of Physics, National Tsing Hua University, Hsinchu, Taiwan
- ⁶⁴ Department of Physics, Indiana University, Bloomington IN, United States of America

- 65 Institut für Astro- und Teilchenphysik, Leopold-Franzens-Universität, Innsbruck, Austria
- 66 University of Iowa, Iowa City IA, United States of America
- 67 Department of Physics and Astronomy, Iowa State University, Ames IA, United States of America
- 68 Joint Institute for Nuclear Research, JINR Dubna, Dubna, Russia
- 69 KEK, High Energy Accelerator Research Organization, Tsukuba, Japan
- 70 Graduate School of Science, Kobe University, Kobe, Japan
- 71 Faculty of Science, Kyoto University, Kyoto, Japan
- 72 Kyoto University of Education, Kyoto, Japan
- 73 Research Center for Advanced Particle Physics and Department of Physics, Kyushu University, Fukuoka, Japan
- 74 Instituto de Física La Plata, Universidad Nacional de La Plata and CONICET, La Plata, Argentina
- 75 Physics Department, Lancaster University, Lancaster, United Kingdom
- 76 ^(a) INFN Sezione di Lecce; ^(b) Dipartimento di Matematica e Fisica, Università del Salento, Lecce, Italy
- 77 Oliver Lodge Laboratory, University of Liverpool, Liverpool, United Kingdom
- 78 Department of Experimental Particle Physics, Jožef Stefan Institute and Department of Physics, University of Ljubljana, Ljubljana, Slovenia
- 79 School of Physics and Astronomy, Queen Mary University of London, London, United Kingdom
- 80 Department of Physics, Royal Holloway University of London, Surrey, United Kingdom
- 81 Department of Physics and Astronomy, University College London, London, United Kingdom
- 82 Louisiana Tech University, Ruston LA, United States of America
- 83 Laboratoire de Physique Nucléaire et de Hautes Energies, UPMC and Université Paris-Diderot and CNRS/IN2P3, Paris, France
- 84 Fysiska institutionen, Lunds universitet, Lund, Sweden
- 85 Departamento de Física Teórica C-15, Universidad Autónoma de Madrid, Madrid, Spain
- 86 Institut für Physik, Universität Mainz, Mainz, Germany
- 87 School of Physics and Astronomy, University of Manchester, Manchester, United Kingdom
- 88 CPPM, Aix-Marseille Université and CNRS/IN2P3, Marseille, France
- 89 Department of Physics, University of Massachusetts, Amherst MA, United States of America
- 90 Department of Physics, McGill University, Montreal QC, Canada
- 91 School of Physics, University of Melbourne, Victoria, Australia
- 92 Department of Physics, The University of Michigan, Ann Arbor MI, United States of America
- 93 Department of Physics and Astronomy, Michigan State University, East Lansing MI, United States of America
- 94 ^(a) INFN Sezione di Milano; ^(b) Dipartimento di Fisica, Università di Milano, Milano, Italy
- 95 B.I. Stepanov Institute of Physics, National Academy of Sciences of Belarus, Minsk, Republic of Belarus
- 96 Research Institute for Nuclear Problems of Byelorussian State University, Minsk, Republic of Belarus
- 97 Group of Particle Physics, University of Montreal, Montreal QC, Canada
- 98 P.N. Lebedev Physical Institute of the Russian Academy of Sciences, Moscow, Russia
- 99 Institute for Theoretical and Experimental Physics (ITEP), Moscow, Russia
- 100 National Research Nuclear University MEPhI, Moscow, Russia
- 101 D.V. Skobel'syn Institute of Nuclear Physics, M.V. Lomonosov Moscow State University, Moscow, Russia
- 102 Fakultät für Physik, Ludwig-Maximilians-Universität München, München, Germany
- 103 Max-Planck-Institut für Physik (Werner-Heisenberg-Institut), München, Germany
- 104 Nagasaki Institute of Applied Science, Nagasaki, Japan

- ¹⁰⁵ Graduate School of Science and Kobayashi-Maskawa Institute, Nagoya University, Nagoya, Japan
- ¹⁰⁶ ^(a) INFN Sezione di Napoli; ^(b) Dipartimento di Fisica, Università di Napoli, Napoli, Italy
- ¹⁰⁷ Department of Physics and Astronomy, University of New Mexico, Albuquerque NM, United States of America
- ¹⁰⁸ Institute for Mathematics, Astrophysics and Particle Physics, Radboud University Nijmegen/Nikhef, Nijmegen, Netherlands
- ¹⁰⁹ Nikhef National Institute for Subatomic Physics and University of Amsterdam, Amsterdam, Netherlands
- ¹¹⁰ Department of Physics, Northern Illinois University, DeKalb IL, United States of America
- ¹¹¹ Budker Institute of Nuclear Physics, SB RAS, Novosibirsk, Russia
- ¹¹² Department of Physics, New York University, New York NY, United States of America
- ¹¹³ Ohio State University, Columbus OH, United States of America
- ¹¹⁴ Faculty of Science, Okayama University, Okayama, Japan
- ¹¹⁵ Homer L. Dodge Department of Physics and Astronomy, University of Oklahoma, Norman OK, United States of America
- ¹¹⁶ Department of Physics, Oklahoma State University, Stillwater OK, United States of America
- ¹¹⁷ Palacký University, RCPTM, Olomouc, Czech Republic
- ¹¹⁸ Center for High Energy Physics, University of Oregon, Eugene OR, United States of America
- ¹¹⁹ LAL, Univ. Paris-Sud, CNRS/IN2P3, Université Paris-Saclay, Orsay, France
- ¹²⁰ Graduate School of Science, Osaka University, Osaka, Japan
- ¹²¹ Department of Physics, University of Oslo, Oslo, Norway
- ¹²² Department of Physics, Oxford University, Oxford, United Kingdom
- ¹²³ ^(a) INFN Sezione di Pavia; ^(b) Dipartimento di Fisica, Università di Pavia, Pavia, Italy
- ¹²⁴ Department of Physics, University of Pennsylvania, Philadelphia PA, United States of America
- ¹²⁵ National Research Centre "Kurchatov Institute" B.P.Konstantinov Petersburg Nuclear Physics Institute, St. Petersburg, Russia
- ¹²⁶ ^(a) INFN Sezione di Pisa; ^(b) Dipartimento di Fisica E. Fermi, Università di Pisa, Pisa, Italy
- ¹²⁷ Department of Physics and Astronomy, University of Pittsburgh, Pittsburgh PA, United States of America
- ¹²⁸ ^(a) Laboratório de Instrumentação e Física Experimental de Partículas - LIP, Lisboa; ^(b) Faculdade de Ciências, Universidade de Lisboa, Lisboa; ^(c) Department of Physics, University of Coimbra, Coimbra; ^(d) Centro de Física Nuclear da Universidade de Lisboa, Lisboa; ^(e) Departamento de Física, Universidade do Minho, Braga; ^(f) Departamento de Física Teórica y del Cosmos, Universidad de Granada, Granada; ^(g) Dep Física and CEFITEC of Faculdade de Ciências e Tecnologia, Universidade Nova de Lisboa, Caparica, Portugal
- ¹²⁹ Institute of Physics, Academy of Sciences of the Czech Republic, Praha, Czech Republic
- ¹³⁰ Czech Technical University in Prague, Praha, Czech Republic
- ¹³¹ Charles University, Faculty of Mathematics and Physics, Prague, Czech Republic
- ¹³² State Research Center Institute for High Energy Physics (Protvino), NRC KI, Russia
- ¹³³ Particle Physics Department, Rutherford Appleton Laboratory, Didcot, United Kingdom
- ¹³⁴ ^(a) INFN Sezione di Roma; ^(b) Dipartimento di Fisica, Sapienza Università di Roma, Roma, Italy
- ¹³⁵ ^(a) INFN Sezione di Roma Tor Vergata; ^(b) Dipartimento di Fisica, Università di Roma Tor Vergata, Roma, Italy
- ¹³⁶ ^(a) INFN Sezione di Roma Tre; ^(b) Dipartimento di Matematica e Fisica, Università Roma Tre, Roma, Italy
- ¹³⁷ ^(a) Faculté des Sciences Ain Chock, Réseau Universitaire de Physique des Hautes Energies - Université Hassan II, Casablanca; ^(b) Centre National de l'Energie des Sciences Techniques Nucleaires,

Rabat; ^(c) Faculté des Sciences Semlalia, Université Cadi Ayyad, LPHEA-Marrakech; ^(d) Faculté des Sciences, Université Mohamed Premier and LTPM, Oujda; ^(e) Faculté des sciences, Université Mohammed V, Rabat, Morocco

¹³⁸ DSM/IRFU (Institut de Recherches sur les Lois Fondamentales de l'Univers), CEA Saclay (Commissariat à l'Energie Atomique et aux Energies Alternatives), Gif-sur-Yvette, France

¹³⁹ Santa Cruz Institute for Particle Physics, University of California Santa Cruz, Santa Cruz CA, United States of America

¹⁴⁰ Department of Physics, University of Washington, Seattle WA, United States of America

¹⁴¹ Department of Physics and Astronomy, University of Sheffield, Sheffield, United Kingdom

¹⁴² Department of Physics, Shinshu University, Nagano, Japan

¹⁴³ Department Physik, Universität Siegen, Siegen, Germany

¹⁴⁴ Department of Physics, Simon Fraser University, Burnaby BC, Canada

¹⁴⁵ SLAC National Accelerator Laboratory, Stanford CA, United States of America

¹⁴⁶ ^(a) Faculty of Mathematics, Physics & Informatics, Comenius University, Bratislava; ^(b) Department of Subnuclear Physics, Institute of Experimental Physics of the Slovak Academy of Sciences, Kosice, Slovak Republic

¹⁴⁷ ^(a) Department of Physics, University of Cape Town, Cape Town; ^(b) Department of Physics, University of Johannesburg, Johannesburg; ^(c) School of Physics, University of the Witwatersrand, Johannesburg, South Africa

¹⁴⁸ ^(a) Department of Physics, Stockholm University; ^(b) The Oskar Klein Centre, Stockholm, Sweden

¹⁴⁹ Physics Department, Royal Institute of Technology, Stockholm, Sweden

¹⁵⁰ Departments of Physics & Astronomy and Chemistry, Stony Brook University, Stony Brook NY, United States of America

¹⁵¹ Department of Physics and Astronomy, University of Sussex, Brighton, United Kingdom

¹⁵² School of Physics, University of Sydney, Sydney, Australia

¹⁵³ Institute of Physics, Academia Sinica, Taipei, Taiwan

¹⁵⁴ Department of Physics, Technion: Israel Institute of Technology, Haifa, Israel

¹⁵⁵ Raymond and Beverly Sackler School of Physics and Astronomy, Tel Aviv University, Tel Aviv, Israel

¹⁵⁶ Department of Physics, Aristotle University of Thessaloniki, Thessaloniki, Greece

¹⁵⁷ International Center for Elementary Particle Physics and Department of Physics, The University of Tokyo, Tokyo, Japan

¹⁵⁸ Graduate School of Science and Technology, Tokyo Metropolitan University, Tokyo, Japan

¹⁵⁹ Department of Physics, Tokyo Institute of Technology, Tokyo, Japan

¹⁶⁰ Tomsk State University, Tomsk, Russia

¹⁶¹ Department of Physics, University of Toronto, Toronto ON, Canada

¹⁶² ^(a) INFN-TIFPA; ^(b) University of Trento, Trento, Italy

¹⁶³ ^(a) TRIUMF, Vancouver BC; ^(b) Department of Physics and Astronomy, York University, Toronto ON, Canada

¹⁶⁴ Faculty of Pure and Applied Sciences, and Center for Integrated Research in Fundamental Science and Engineering, University of Tsukuba, Tsukuba, Japan

¹⁶⁵ Department of Physics and Astronomy, Tufts University, Medford MA, United States of America

¹⁶⁶ Department of Physics and Astronomy, University of California Irvine, Irvine CA, United States of America

¹⁶⁷ ^(a) INFN Gruppo Collegato di Udine, Sezione di Trieste, Udine; ^(b) ICTP, Trieste; ^(c) Dipartimento di Chimica, Fisica e Ambiente, Università di Udine, Udine, Italy

¹⁶⁸ Department of Physics and Astronomy, University of Uppsala, Uppsala, Sweden

- ¹⁶⁹ Department of Physics, University of Illinois, Urbana IL, United States of America
- ¹⁷⁰ Instituto de Fisica Corpuscular (IFIC), Centro Mixto Universidad de Valencia - CSIC, Spain
- ¹⁷¹ Department of Physics, University of British Columbia, Vancouver BC, Canada
- ¹⁷² Department of Physics and Astronomy, University of Victoria, Victoria BC, Canada
- ¹⁷³ Department of Physics, University of Warwick, Coventry, United Kingdom
- ¹⁷⁴ Waseda University, Tokyo, Japan
- ¹⁷⁵ Department of Particle Physics, The Weizmann Institute of Science, Rehovot, Israel
- ¹⁷⁶ Department of Physics, University of Wisconsin, Madison WI, United States of America
- ¹⁷⁷ Fakultät für Mathematik und Naturwissenschaften, Fachgruppe Physik, Bergische Universität Wuppertal, Wuppertal, Germany
- ¹⁷⁸ Fakultät für Physik und Astronomie, Julius-Maximilians-Universität, Würzburg, Germany
- ¹⁷⁹ Department of Physics, Yale University, New Haven CT, United States of America
- ¹⁸⁰ Yerevan Physics Institute, Yerevan, Armenia
- ¹⁸¹ Centre de Calcul de l'Institut National de Physique Nucléaire et de Physique des Particules (IN2P3), Villeurbanne, France
- ¹⁸² Academia Sinica Grid Computing, Institute of Physics, Academia Sinica, Taipei, Taiwan
- ^a Also at Department of Physics, King's College London, London, United Kingdom
- ^b Also at Institute of Physics, Azerbaijan Academy of Sciences, Baku, Azerbaijan
- ^c Also at Novosibirsk State University, Novosibirsk, Russia
- ^d Also at TRIUMF, Vancouver BC, Canada
- ^e Also at Department of Physics & Astronomy, University of Louisville, Louisville, KY, United States of America
- ^f Also at Physics Department, An-Najah National University, Nablus, Palestine
- ^g Also at Department of Physics, California State University, Fresno CA, United States of America
- ^h Also at Department of Physics, University of Fribourg, Fribourg, Switzerland
- ⁱ Also at II Physikalisches Institut, Georg-August-Universität, Göttingen, Germany
- ^j Also at Departament de Fisica de la Universitat Autònoma de Barcelona, Barcelona, Spain
- ^k Also at Tomsk State University, Tomsk, and Moscow Institute of Physics and Technology State University, Dolgoprudny, Russia
- ^l Also at The Collaborative Innovation Center of Quantum Matter (CICQM), Beijing, China
- ^m Also at Università di Napoli Parthenope, Napoli, Italy
- ⁿ Also at Institute of Particle Physics (IPP), Canada
- ^o Also at Horia Hulubei National Institute of Physics and Nuclear Engineering, Bucharest, Romania
- ^p Also at CPPM, Aix-Marseille Université and CNRS/IN2P3, Marseille, France
- ^q Also at Department of Physics, St. Petersburg State Polytechnical University, St. Petersburg, Russia
- ^r Also at Borough of Manhattan Community College, City University of New York, New York City, United States of America
- ^s Also at Department of Financial and Management Engineering, University of the Aegean, Chios, Greece
- ^t Also at Centre for High Performance Computing, CSIR Campus, Rosebank, Cape Town, South Africa
- ^u Also at Louisiana Tech University, Ruston LA, United States of America
- ^v Also at Institutio Catalana de Recerca i Estudis Avancats, ICREA, Barcelona, Spain
- ^w Also at Department of Physics, The University of Michigan, Ann Arbor MI, United States of America
- ^x Also at LAL, Univ. Paris-Sud, CNRS/IN2P3, Université Paris-Saclay, Orsay, France
- ^y Also at Graduate School of Science, Osaka University, Osaka, Japan
- ^z Also at Fakultät für Mathematik und Physik, Albert-Ludwigs-Universität, Freiburg, Germany
- ^{aa} Also at Institute for Mathematics, Astrophysics and Particle Physics, Radboud University

Nijmegen/Nikhef, Nijmegen, Netherlands

^{ab} Also at Department of Physics, The University of Texas at Austin, Austin TX, United States of America

^{ac} Also at Institute of Theoretical Physics, Ilia State University, Tbilisi, Georgia

^{ad} Also at CERN, Geneva, Switzerland

^{ae} Also at Georgian Technical University (GTU), Tbilisi, Georgia

^{af} Also at Ochadai Academic Production, Ochanomizu University, Tokyo, Japan

^{ag} Also at Manhattan College, New York NY, United States of America

^{ah} Also at The City College of New York, New York NY, United States of America

^{ai} Also at Departamento de Física Teórica y del Cosmos, Universidad de Granada, Granada, Portugal

^{aj} Also at Department of Physics, California State University, Sacramento CA, United States of America

^{ak} Also at Moscow Institute of Physics and Technology State University, Dolgoprudny, Russia

^{al} Also at Departement de Physique Nucleaire et Corpusculaire, Université de Genève, Geneva, Switzerland

^{am} Also at Institut de Física d'Altes Energies (IFAE), The Barcelona Institute of Science and Technology, Barcelona, Spain

^{an} Also at School of Physics, Sun Yat-sen University, Guangzhou, China

^{ao} Also at Institute for Nuclear Research and Nuclear Energy (INRNE) of the Bulgarian Academy of Sciences, Sofia, Bulgaria

^{ap} Also at Faculty of Physics, M.V.Lomonosov Moscow State University, Moscow, Russia

^{aq} Also at National Research Nuclear University MEPhI, Moscow, Russia

^{ar} Also at Department of Physics, Stanford University, Stanford CA, United States of America

^{as} Also at Institute for Particle and Nuclear Physics, Wigner Research Centre for Physics, Budapest, Hungary

^{at} Also at Giresun University, Faculty of Engineering, Turkey

^{au} Also at Department of Physics, Nanjing University, Jiangsu, China

^{av} Also at Institute of Physics, Academia Sinica, Taipei, Taiwan

^{aw} Also at University of Malaya, Department of Physics, Kuala Lumpur, Malaysia

* Deceased